Self-Assembling Peptide Fibres as Candidates for Bio-Inspired Nanowires: A study of GFDFDFD and GFKFKFK, and the Effect of N-terminus Modification with Biphenyl-Carboxylic Acid and Ferrocene-Carboxylic Acid

Nanobioengineering

Master Thesis

Allan Aagaard Christensen
Jacob Aunstrup Larsen

Aalborg University
School of Engineering and Science
Nanobiotechnology

Nanotechnology
Aalborg University
http://www.aau.dk

AALBORG UNIVERSITY
STUDENT REPORT

Title:
Self-Assembling Peptide Fibres as Candidates for Bio-Inspired Nanowires: A study of GFDFDFD and GFKFKFK, and the Effect of N-terminus Modification with Biphenyl-Carboxylic Acid and Ferrocene-Carboxylic Acid

Theme:
Nanobioengineering

Project Period:
2018/2019

Participants:
Allan Aagaard Christensen
Jacob Aunstrup Larsen

Supervisors:
Leonid Gurevich
Peter Fojan

Appendices: 5

Page Numbers: 73

Date of Completion:
June 10th 2019

Abstract:

DNA has stirred great interest within the field of molecular electronics. Contradicting conductivity experiments give rise for investigations into alternative biological, self-assembling wires. Self-assembling super-structures from aromatic peptides have shown semi-conductive optical properties, and the internal molecular organisation is ideal for protein electron transport mechanisms, which makes self-assembling peptide fibres ideal candidates as bio-inspired molecular wires. In this project, a set of self-assembling peptides have been designed. Fibril-formation of each peptide has been investigated through CD-spectroscopy, Fluorescence Spectroscopy and AFM, which have led to the identification of peptide fibre backbone conformation. Fibres have been imaged by ESFM and investigated by Voltage Sweep across platinum wires after adsorption. Four distinct fibres were formed, two of which formed hydrogel at high concentrations (<3mM). One fibre-type has been proven polarizable, but no fibres were proven conductive. A single peptide formed ringlike superstructures.

Contents

Abbreviations

DNA	Deoxyribonucleic acid
SPPS	Solid Phase Peptide Synthesis
Fmoc	Fluoren-9-ylmethyloxycarbonyl
DMF	N,N-Dimethylformamide
DCM	Dichloromethane
Oxyma	ethyl 2-cyano-2-(hydroxyimino)acetate
HBTU	(N-[(1H-Benzotriazol-1-yl)(dimethylamino)methylene]-N-methylmethanaminiumhexafluorophosphate N-oxide)
TFA	Trifluoroacetic acid
TIS	Triisopropylsilane
CD	Circular Dichroism
UV	Ultraviolet
MD	Molecular Dynamics
CG	Coarse-graining
DMPC	1,2-Dimyristoyl-sn-glycero-3-phosphocholine
AFM	Atomic Force Microscopy
ESFM	Electrostatic Force Microscopy
PME	Particle Mesh Ewald
GFD3	Gly-Phe-Asp-Phe-Asp-Phe-Asp
GFK3	Gly-Phe-Lys-Phe-Lys-Phe-Lys
B-GFD3	Biphenyl-Gly-Phe-Asp-Phe-Asp-Phe-Asp
B-GFK3	Biphenyl-Gly-Phe-Lys-Phe-Lys-Phe-Lys
F-GFD3	Ferrocene-Gly-Phe-Asp-Phe-Asp-Phe-Asp
F-GFK3	Ferrocene-Gly-Phe-Lys-Phe-Lys-Phe-Lys
GFX3-Mix	Mixed GFD3 and GFK3
B-GFX3-Mix	Mixed B-GFD3 and B-GFK3
F-GFX3-Mix	Mixed F-GFD3 and F-GFK3

Chapter 1

Introduction

Deoxyribonucleic acid (DNA) has recently attracted a tremendous amount of interest within the field of molecular electronics [1]. Due to its size and self-assembling properties, DNA could allow for significant downscaling of electrical components. Also, DNA is a biological material, which could be used as a charge carrier within biotechnological and medical fields, where potential biological semiconductors could allow for the development of new in vivo bio-machines [2]. However, DNA has proven difficult to probe for conductive properties, and several contradicting results have been produced [3].
Supramolecular organic organizations, such as the self-assembly of phthalocyanines have been recognised as potential organic self-assembling semiconductors [4, 5, 6].
However, the non-biological nature is an obstacle concerning interfacing electronic devices with living systems, electroactive tissue engineering and development of imaging agents [7].
Some proteins are known to be very effective electron transporters [8, 9, 10]. Two mechanisms are accepted as responsible for the electron transfer – coherent tunnelling [8, 11] and charge hopping [12]. These mechanisms can occur concurrently. Amide-to-amide systems are considered hopping sites, and hydrogen bond networks aid in this coupling [10]. Furthermore, aromatic amino acids also facilitate hopping sites through delocalized pi-orbitals [13]. Self-assembling aromatic peptides have been observed to form fibres, which exhibit amide-to-amide hydrogen bonding and well organised aromatic amino acid stacking in a stable network [14]. Self-assembling superstructures formed by di-phenylalanine has also revealed to have intrinsic semiconductive optical properties [2].
Self-organised peptide fibres could, due to their bio-derived nature, bridge the gap between inorganic electronics and biological systems [2]. The potential conductive mechanisms of the fibre could function in a “dry” state, which allows applications in solid-state electronics as well [1].
This project seeks to design a set of self-assembling peptide fibres, and demonstrate the potential for charge transport.

1.1 Peptide Design for β-Sheet forming peptide Fibrillation

Among peptides with certain sequences of amino acids, a self-assembling property allows the peptides in solution to assemble in an ordered manner to form structures of multiple peptides, and can further extend to form fibre structures. Among observed motifs for the peptide, fibrillation is α-helix, β-sheet, β-hairpin and coil structures [15]. This paper focuses on β-sheet forming peptides. In these structures, the peptides act as β-strands that are laterally connected forming β-sheets stabilized by hydrogen bonding. These β-sheet structures can then extend in length forming a tape structure, and interface with other tapes increasing in thickness as they form ribbon structures, which can assemble into fibrils and eventually fibres [14, 15]. This behaviour is described by a theoretical model for the formation of chiral rod-like β-sheet fibrils can be seen in Figure 1.1.

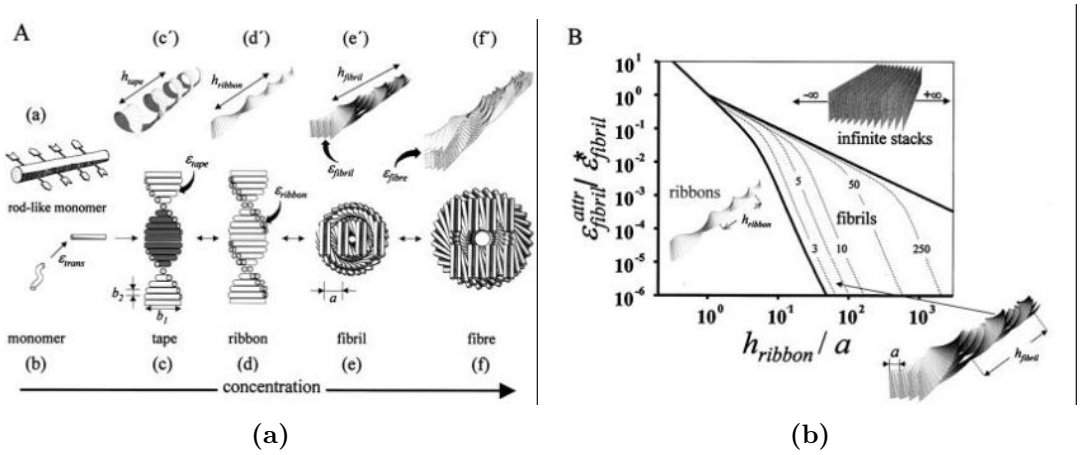

Figure 1.1: Model of hierarchical self-assembly of amphiphatic peptides. (A) Local arrangements (c–f) and the corresponding global equilibrium conformations (c'–f') for the hierarchical self-assembling structures formed in solutions of chiral molecules (a), which conform tapes (c). For clarity one side of tapes (c) have been shaded, which is visible on both ribbon(d), fibrils(e) and fibre-formation (f). (B) indicates the relation between tape/ribbon-formation and fibril-formation. Infinite stacks can be correlated with structures such as crystals. [16]

For the design of peptides self-assembling to form β-sheet structures in solution the following criteria were formulated by Boden et al. 1: cross-strand attractive forces between side chains, such as hydrophobic, electrostatic or hydrogen bonding attractive forces. 2: lateral recognition between adjacent β-strands to constrain their self-assembly to one dimension. 3: strong adhesion of the solvent to the surface of the tapes to control solubility [17, 14]. To create cross-strand attractive forces the side chains of the peptide are typically arranged to produce a peptide with one side being predominantly hydrophobic and the other side being predominantly hydrophilic [16, 15]. Having these two different sides means that it is favourable in aqueous solution for the peptides to arrange themselves with their hydrophobic sides interfacing

with each other to reduce interaction between hydrophobic groups and the solution.

Charged groups in the peptide can inhibit self-assembly as the like charges will repel each other but can be used to favour certain conformations. By using opposite charges at either end of the peptide, an anti-parallel β-sheet structure becomes more favourable [15]. In addition, the inhibiting effect of charged groups can produce a pH-dependence for the self-assembling process, where the pH-dependency correlates to the pKa value of the charged amino acid side chains [15]. Peptides with charged groups have in addition been observed to better self-assemble in ionic solutions, which is attributed to the ionic shield surrounding the charge limiting the repulsive Coulombic interaction between the peptides [15]. The self-assembly operates according to a balance between attractive- and frustration forces. As such, if the attractive force from the hydrophobic interaction, is stronger than the frustrating force provided by the presence of like charges on the peptide, the self-assembly will still occur.

The tendency to self-assemble has further been observed to be promoted by the presence of aromatic groups in the peptide side chains. This effect has been attributed to the $\pi - \pi$ interactions observed in aromatic ring structures.[14] The presence of aromatic ring structures can be used to promote cross-strand recognition, as the ring structures arrange close to each other to allow the $\pi - \pi$ interaction. Aromatic groups have further been observed to form helical twisting tapes, while peptides without aromatic groups only form straight tapes [17, 15, 14].

As peptides self-assemble into fibres, if the concentration is high enough, many fibres will be formed and can get entangled, resulting in gel formation [17, 14]. The time required for self-assembly into gel structures varies greatly, ranging from a few hours to several days [15]. The speed at which the self-assembly process reaches such a point is dependent on the balance of attractive- and frustrating forces, as they determine the rate of self-assembly. This balance has also been shown to affect the length of fibrils, which have been correlated with gel rigidity [15]. Even though many of the tendencies and properties governing the self-assembly of peptides into peptide fibres, the specific relations between the mechanisms, and the self-assembling propensity are not perfectly understood.

1.2 Peptide Design for used Peptides

This section covers the structure and design of the peptides used in this project. Firstly, two main peptide sequences were used for this project, then each of the two peptides was modified at the N-terminus with biphenylalanine or ferrocene.

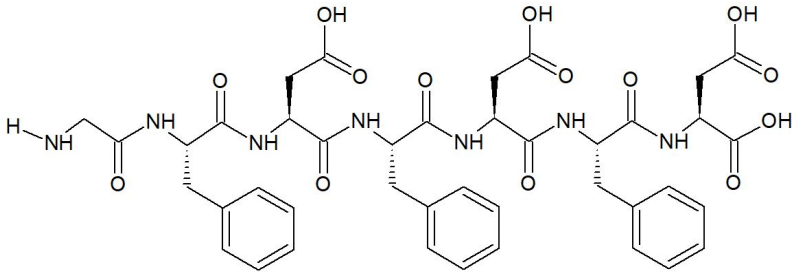

Figure 1.2: Molecular structure of GFDFDFD peptide, made using ChemSketch [18]

The sequence of the first Peptide:
In three letter code:
Gly-Phe-Asp-Phe-Asp-Phe-Asp
In one letter code:
GFDFDFD

GFDFDFD will be abbreviated as GFD3. GFD3 can be seen illustrated in Figure 1.2.

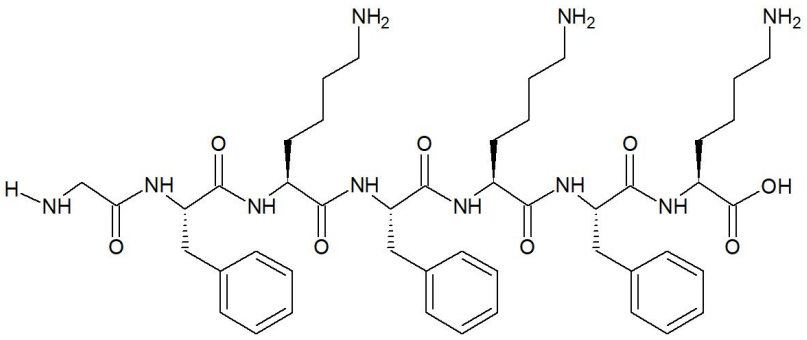

Figure 1.3: Molecular structure of GFKFKFK peptide, made using ChemSketch [18]

In three letter code:
Gly-Phe-Lys-Phe-Lys-Phe-Lys
In one letter code:
GFKFKFK

GFKFKFK will be abbreviated as GFK3. GFK3 can be seen illustrated in Figure 1.3.

GFD3 and GFK3 have structures with alternating phenylalanine groups at positions 2, 4 and 6, providing the peptide with a hydrophobic side and aromatic structures enabling the use of $\pi - \pi$ interactions to provide cross-strand recognition. These peptides further have charged groups at positions 3, 5 and 7.

GFD3 uses aspartic acid, as the charged residue, providing a mostly hydrophilic side, with negatively charged side groups. The hydrophilic side increases the water-solubility of potential peptide tapes. Charged groups will repel each other which could inhibit the self-assembly of the peptide. GFK3 uses lysine to provide similar effects, however with positively charged side groups.
The two differently charged peptides promote self-assembly in mixed solutions where both GFD3 and GFK3 are present, this mix will be referred to as GFX3-Mix. In GFX3-Mix, the charges could aid in bringing the peptides together, enabling the peptides to stack, alternating between the two peptides in an ABABA sequence, neutralizing the net charge, and supporting the formation of the two distinct tape-sides. The use of glycine at position 1 for both these peptides, is to promote anti-parallel stacking of the peptides, as the seventh position charged side group, interfaces with the glycine in the anti-parallel conformation, forming a lower energy state than parallel conformation, paring similarly charged 7th position groups. The anti-parallel conformation is not expected for mixed solutions, as charged group-pairing should be more favourable.

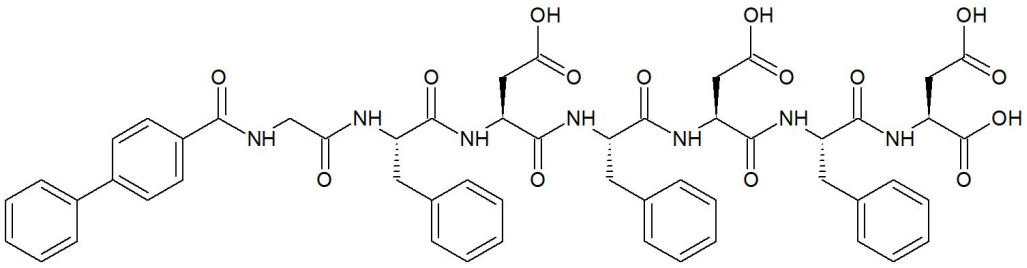

Figure 1.4: Molecular structure of Biphenyl modified GFDFDFD peptide, made using ChemSketch [18]

In three letter code:
Biphe-Gly-Phe-Asp-Phe-Asp-Phe-Asp
In one letter code:
Biphe-GFDFDFD

Biphenyl modified GFDFDFD will be abbreviated as B-GFD3. B-GFD3 can be seen illustrated in Figure 1.4.

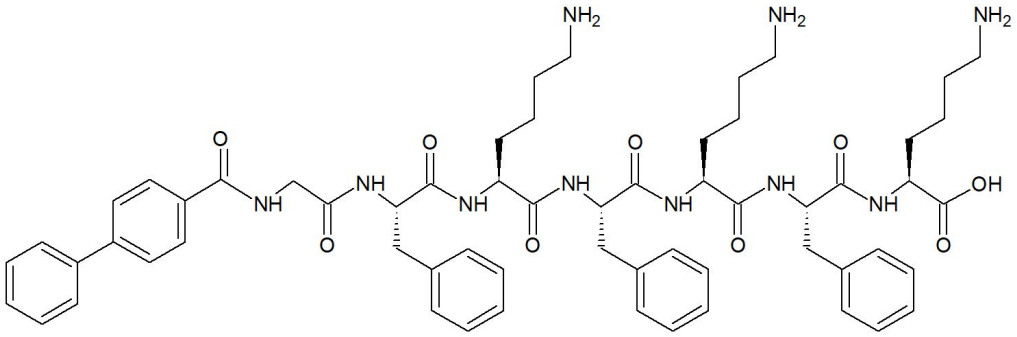

Figure 1.5: Molecular structure of Biphenyl modified GFKFKFK peptide, made using ChemSketch [18]

In three letter code:
Biphe-Gly-Phe-Lys-Phe-Lys-Phe-Lys
In one letter code:
Biphe-GFKFKFK

Biphenyl modified GFKFKFK will be abbreviated as B-GFK3. BGFK3 can be seen illustrated in Figure 1.5.

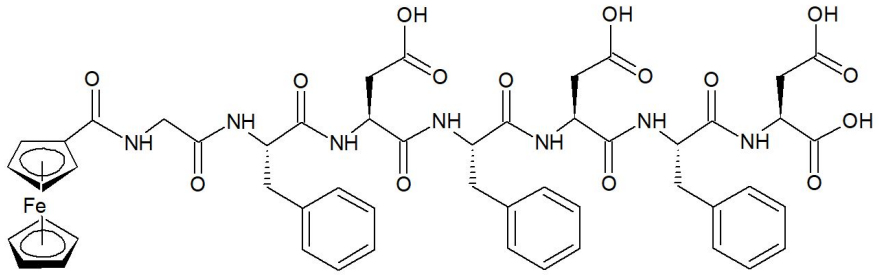

Figure 1.6: Molecular structure of Ferrocene modified GFDFDFD peptide, made using ChemSketch [18]

In three letter code:
Ferro-Gly-Phe-Asp-Phe-Asp-Phe-Asp
In one letter code:
Ferro-GFDFDFD

Ferrocene modified GFDFDFD will be abbreviated as F-GFD3. F-GFD3 can be seen illustrated in Figure 1.6.

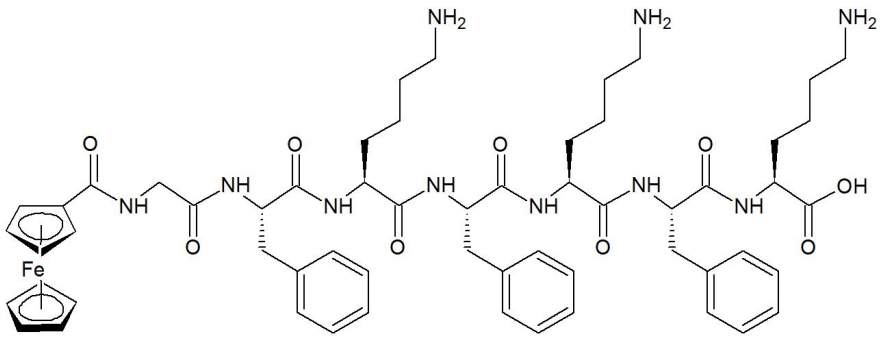

Figure 1.7: Molecular structure of Ferrocene modified GFKFKFK peptide, made using ChemSketch [18]

In three letter code:
Ferro-Gly-Phe-Asp-Phe-Asp-Phe-Asp
In one letter code:
Ferro-GFKFKFK

Ferrocene modified GFKFKFK will be abbreviated as F-GFK3. F-GFK3 can be seen illustrated in Figure 1.7.

Modification with biphenylalanine and ferrocene was performed, assuming improved charge-transport properties of the fibres formed. Biphenylalanine is used to increase the number of $\pi - \pi$ interaction along the fibre. Ferrocene modified fibres would have ferrocene groups along the tape edge. Ferrocene has shown good charge-transfer properties in several complexes, and couples especially well with ferricinium, which is a positively charged ferrocene group [19]. Both these modifications are at the N-terminal. The modifications are hydrophobic and as such increases the hydrophobic effects to aggregate in solution, and makes the peptides less water soluble. The non-symmetrical modifications should increase parallel backbone formation, which could diminish fibre stability. Mixed solutions of B-GFD3 and B-GFK3, will be referred to as B-GFX3-Mix, and Mixed Solutions of F-GFD3 and F-GFK3, will be referred to as F-GFX3-Mix.

1.3 Solid Phase Peptide Synthesis

Solid Phase Peptide Synthesis (SPPS), is an established method for the production of synthetic peptides. This is done by anchoring the backbone of the amino acid at the C-terminus end of the peptide, to a solid support. The amino acids N-terminus is being protected by Fmoc, which during synthesis will be removed, deprotecting the N-terminus to allow the coupling to the next amino acid in the peptide sequence. The synthesis is performed by repeating the process of deprotection and coupling until the desired amino acid sequence is achieved. Following the synthesis, the peptide is released from the solid support and the peptide side chains are deprotected.[20]

The solid support is anchored to the C-terminus of the peptide with 4-alkoxybenzyl Wang linker, and the solid support is a Wang Resin consisting of polystyrene.

Deprotection of Fmoc is done with piperidine in DMF as seen in Figure 1.8.[20]

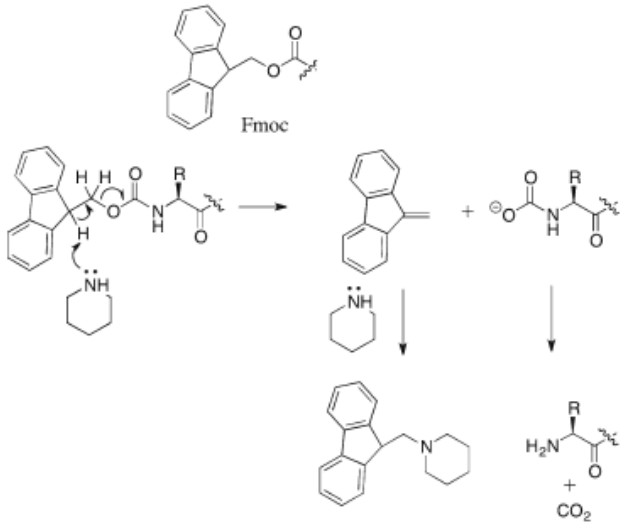

Figure 1.8: Deprotection of Fmoc with Piperidine.[20]

The following step after deprotecting the N-terminus is to couple the next amino acid in the sequence to the amino acid chain on the solid support. To perform this coupling of the amino acid backbones, the C-terminus of the incoming amino acid must first be activated. A Carbodiimide reagent like DCM prevents the occurrence of secondary reactions, such as the formation of anhydride, which leads to epimerisation. Oxyma forms esters that react with bi-products of the reaction, while the addition of HBTU decreases epimerisation and reduces coupling time. The available coupling reagents are shown in Figure 1.9 and the activation of ester in Fmoc synthesis is shown in Figure 1.10.[20]

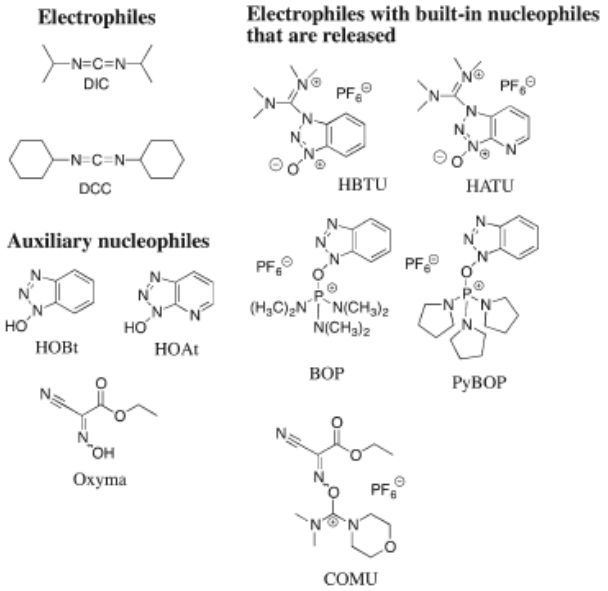

Figure 1.9: Available Coupling Reagents.[20]

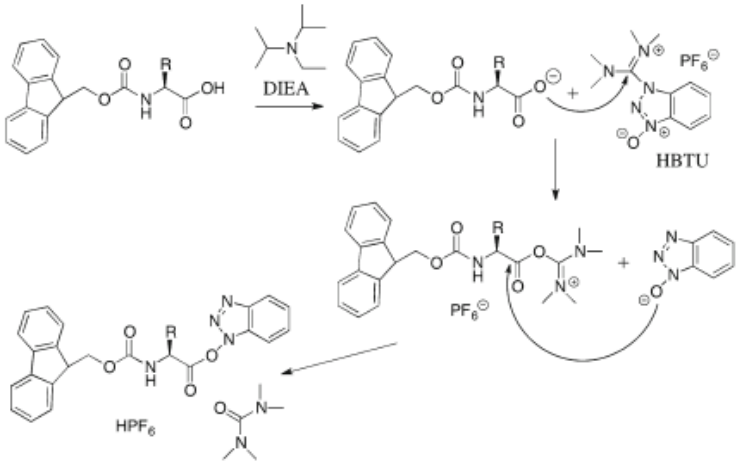

Figure 1.10: Activation of HBTU before coupling.[20]

The side chains of the amino acids are also protected during synthesis to prevent undesired interactions during the process. The amino acid side chains are protected with different semi-permanent protecting groups depending on the functional groups in the side chain. The most common side chain protecting groups for Fmoc SPPS are shown in Figure 1.11. TFA Labile groups are protecting groups which can be cleaved with TFA, while the TFA stabile groups require other conditions for deprotection.[20]

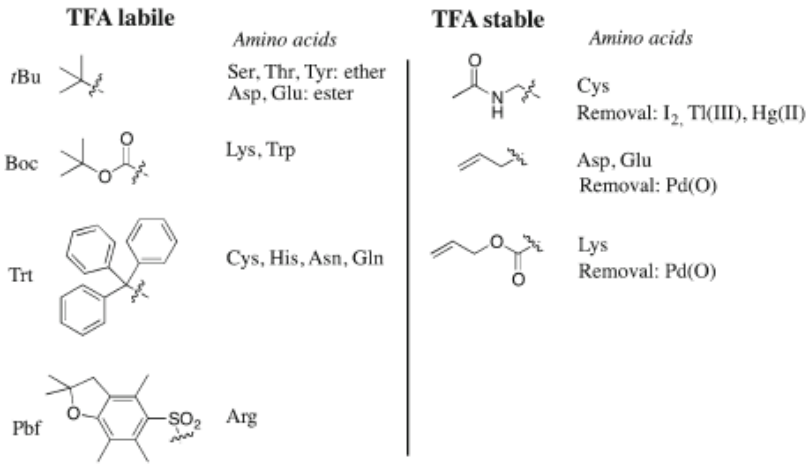

Figure 1.11: Table of protection groups for the functional groups in side chains, used with Fmoc.[20]

In the final steps, the peptide is released from the solid support, by addition of TFA, which if TFA labile side chain protecting groups are used, will simultaneously deprotect the side chains. When the side chains are deprotected, carbocations are formed, which can react with nucleophilic sides. To prevent this, water and TIS is added to react with the cations. [20]

1.4 Circular Dichroism Spectroscopy

Circular dichroism (CD) spectroscopy is a method commonly used for rapid determination of secondary structure and folding properties of proteins and polypeptides [21]. It is a chiroptical spectroscopy method, a field of spectroscopy utilizing the differential interactions of molecules with left-and right-circularly polarised light. A molecule gives rise to the different interaction between the two types of polarised light, only if that molecule is chiral [22].

CD spectroscopy utilises the unequal absorption of the left-and right-circularly polarised light, unlike other chiroptical spectroscopy methods [22].
The measurements are achieved by sending two oppositely circular polarised lightwaves through the sample. The waves are out of phase with each other by 90 degrees. When chiral molecules absorb the two polarised waves to a different extent, the sum of the waves forms an elliptically polarised wave. CD is reported either as degrees of ellipticity or units of ΔE, which is the difference in absorbance of clock-wise and anti-clockwise light [21].

A CD spectra is achieved by measuring across a range of wavelengths. Protein CD spectra are divided into three wavelength ranges, based on the energy of the electronic transitions, which are the cause of light absorption, see Figure 1.12 [22].

These are (1) near UV-visible region (> 300 nm), which are contributed to by extrinsic groups and tertiary structures, (2) near UV (250-300 nm), where aromatic side chains contribute and (3) far UV (<250 nm), where secondary structures dominate.

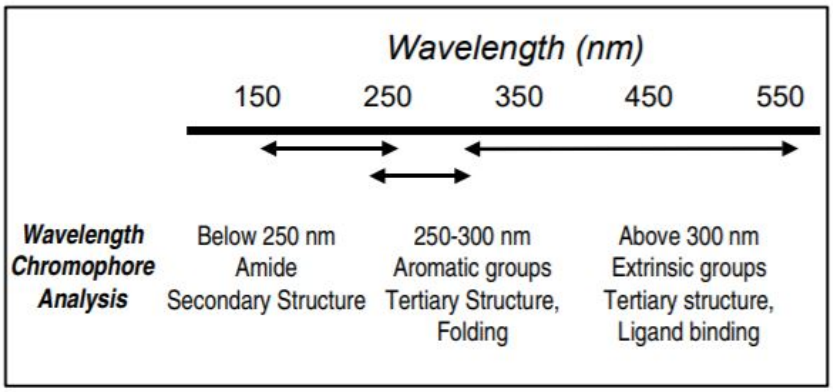

Figure 1.12: CD spectral regions and contributing chromophores in proteins [22]

When the chromophores of the amides of the polypeptide backbone are aligned, their optical transitions are shifted or split into multiple transitions due to excitation interactions. CD spectra for protein structural elements are therefore quite characteristic, as seen in Figure 1.13. α helical proteins have a positive band at 193 nm and two negative bands at 208 nm and 222 nm. Antiparallel β-sheets have a positive band at 195 nm negative band at 218 nm, while poorly organised, or random coil, proteins have a negative band near 195 nm and a small positive band at 210 nm [21]. A protein CD spectra can be approximated as a linear combination of secondary structure spectra, determined by the relative contents within the total structure.

Three fundamental types of interactions between transitions on chromophores drive the rotational strength. While this report will not describe these in detail, a fundamental understanding is necessary to discuss some of the phenomena observed, as well as understanding why CD measurements of the peptide structures investigated, does not necessarily coincide with data from known secondary structures.
1: The coupled-oscillator mechanism, also known as the $\mu - \mu$ mechanism: Describes the Coloumb interactions between two electrically allowed transitions, such as $\pi \rightarrow \pi^*$ transitions of the peptide group. Exciton coupling is a special case of this mechanism [22].
2: The $\mu - m$ mechanism: When an electrically allowed transition on one chromophore mixes with a magnetically allowed transition on another chromophore [22].
3: One electron mechanism, or static-field mixing: The electrically and magnetically allowed transitions on the same chromophore mix in the electrostatic field of the rest of the molecule [22].

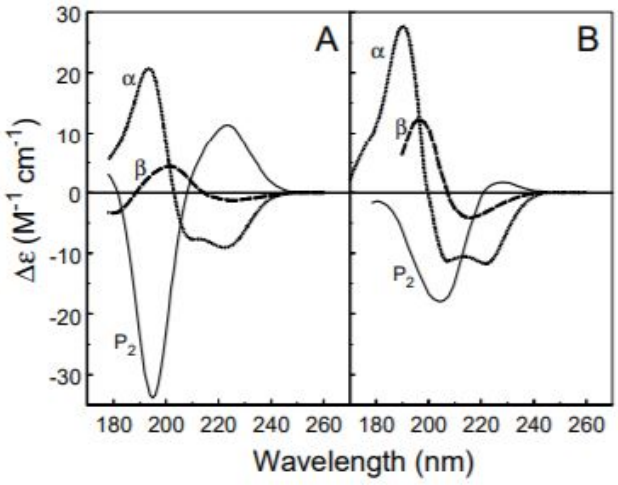

Figure 1.13: (A) CD spectra of α-helix, β-sheet, and P_2 (collagen) structure, deconvoluted from a set of 37 reference proteins. (B) CD spectra of model polypeptides in α-helix, β-sheet and P_2 conformation. [22]

These mechanisms interact between all chromophores within the protein. CD calculations for secondary structures, do often only consider amide chromophores, as they dominate the far-UV CD spectrum. The transitions are best represented as dipoles, which means, that the range and angle between each chromophore plays a role in the determination of the total CD spectrum. Since secondary structures have characteristic and repeating intermolecular distances and dihedral angles, these interactions are set. If these variables are different, the CD spectrum changes as well. This phenomenon can be observed to some extent, in twisting β-sheets, which leads to increased amplitudes of CD bands [22].

1.5 Principle of Fluorescence and Solvent Relaxation

Fluorescence is the emission of light from electron relaxation through a singlet state. The emission rate of fluorescence is typically 10^{-8}s, making a typical fluorescence lifetime near 10 ns. The fluorophore lifetime is the average time between electron excitation and its return to the ground state.
The processes that occur between absorption and emission are usually illustrated through a Jablonski diagram [23].

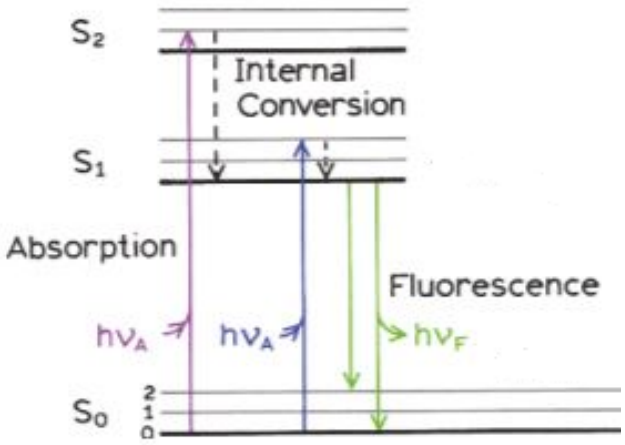

Figure 1.14: A simple Jablonski diagram. Electronic states are noted S_0, S_1 and S_2. Vibrational states are noted 0, 1 and 2. Absorption transitions are lined purple and blue. Fluorescence transitions are lined green.[23]

Figure 1.14 shows a simple Jablonski diagram with three electronic states. S_0, the ground state, S_1, the first excited state and S_2, the second excited state. Each electronic state has several vibrational energies 0, 1, 2 etc. The transition from the ground state to an excited electronic state, by light absorption, usually occurs in about 10^{-15}s, and is generally considered instantaneous [23]. Following light absorption, several processes occur. A fluorophore is usually excited to higher vibrational levels of S_1 or S_2. Relaxation to the lowest S_1 vibrational state through internal conversion occurs within 10^{-12}s. Fluorescence emission is therefore generally from the thermally equilibrated state. Return to the ground state typically occurs to a higher vibrational state, which then relaxes through internal conversion. Fluorescence typically occurs at lower energies and hence longer wavelengths, than the absorption. The shift is referred to as the Stokes shift [23].

Several interactions are omitted from this Jablonski diagram, such as quenching, solvent interaction, energy transfer and phosphorescence. Quenching is a general term for mechanisms, which induce fluorescence intensity drops [23].
Polar solvents generally increase the Stokes shift. Polar solvent molecules stabilise the excited state and shift the fluorescence emission to even lower wavelengths. This occurs due to the larger dipole moment of the excited state, causing solvent dipoles to reorient and relax around the excited fluorophore. Generally, only polar fluorophores display large sensitivity to solvent polarity. Solvent relaxation usually occurs within 10-100·10^{-12}s, and fluorescence emission is representative of the solvent relaxed state [23].

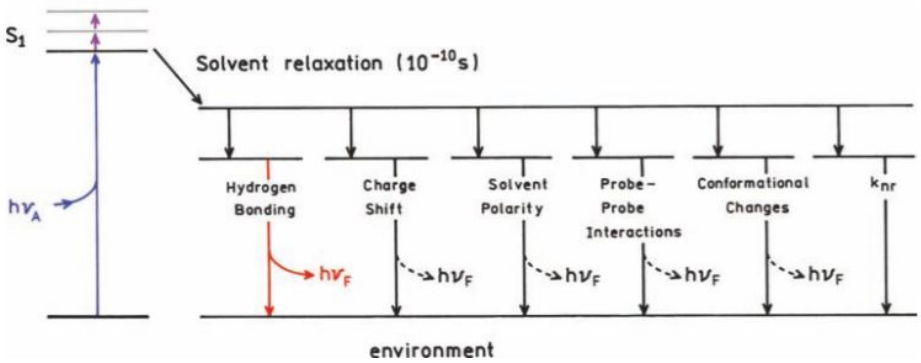

Figure 1.15: Simple Jablonski diagram showing environmental effects on the energy of the excited state. Dashed lines indicate that the fluorophore can be fluorescent or non-fluorescent in the state.[23]

Solvents effects can lower the energy of the excited state through several mechanisms. These will not be described in great detail but represented in Figure 1.15. Solvent-dependent spectra can be rather complex as all mechanisms affect the signal [23].

1.6 Principle of Electrostatic Force Microscopy

Electrostatic force microscopy (ESFM) is an electrical scanning probe microscopy method. The method detects weak, but long-range electrostatic forces [24], and is most commonly used by a two-pass method. The two-pass method involves a typical Atomic Force Microscopy (AFM) topography measurement, followed by a non-contact, second scan with a set probe-surface distance, often referred to as lift-mode [24]. Lift-mode is a retracing of the topography at a higher elevation than the sample. The second scan must be performed with a lift sufficient to detach the probe from short-range interactions with the sample. ESFM is performed using a conductive probe and a metallic sample holder. [24]
During the second scan, an electric bias is established between the probe and the metallic sample holder, creating the equivalent of a capacitor. The interaction between an ESFM sensor and the metallic sample holder is a combination of an attractive Coloumbic force between induced charges on electrodes due to the capacitance C of the probed region, and a Columbic force between local surface charges and the image charge on the tip.
The total tip-sample voltage can be expressed by the externally applied bias, and the tip-to-surface potential difference, V_{CP}. The tip-to-surface potential difference expression contains induced voltages, such as those resulting from polarization, illumination, mechanical stress, etc. Figure 1.16 shows a schematic representation of the tip-sample voltage of an insulating sample possessing a permanent surface charge. [24]

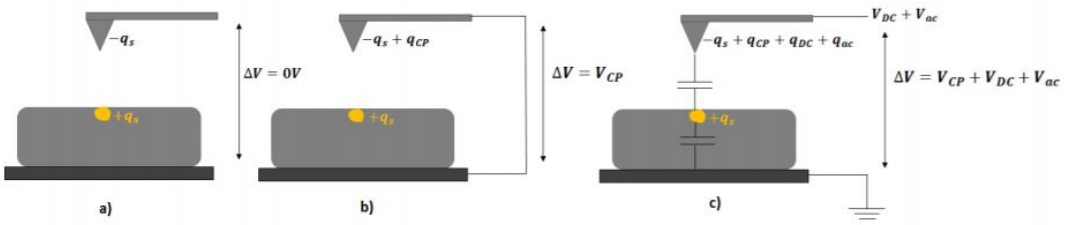

Figure 1.16: electrostatic interactions of an insulating substrate possessing a permanent surface charge when: a) electrodes are disconnected, b) electrodes are connected, and c) electrodes are biased with a DC and AC voltage [24]

A general force expression for these interactions, at large tip-surface distances, is defined as:

$$F = \frac{1}{2}\frac{\delta C}{\delta z}\Delta V^2 + \frac{q_s q_t}{4\pi\epsilon_0 z^2} \tag{1.1}$$

Where z is the distance between the tip apex and the sample surface, q_t is the sum of all charges interacting with the surface charges q_s. The voltage difference is described as

$$\Delta V = V_{DC} + V_{AC} \cdot sin(\omega \cdot t) + V_{CP} \tag{1.2}$$

V_{DC} and $V_{AC} \cdot sin(\omega \cdot t)$ are the externally applied voltages. V_{CP} is the tip-to-surface potential difference.

Due to the long-range forces, electrostatic effects such as surface charges, substrate polarization, illumination, etc. can be identified through ESFM by amplitude, frequency and phase shift detection. [24]

1.7 Molecular Dynamics Simulation of Peptides

Molecular Dynamics (MD) simulation is a method for molecular simulation, that is based on computing equilibrium and transport properties of a classical many-body system. In this case, classical means that the nuclear motion of the constituent particles in the simulation, obey the laws of classical mechanics. MD simulations have been found to give good approximations for a wide range of materials, even though it is based on classical mechanics. [25]

Setting up an MD simulation requires a model system of the desired molecules and solvent, within the simulated space, followed by equilibration of the system. Each particle is given a starting momentum, such that the system will be dynamic, meaning the particles will move. As the simulation is run the momenta and position of each particle is calculated at each time step. The starting conditions for MD simulation includes initial temperature, number of particles, time step and run time.

The initial temperature is important as temperature is linked to molecular movement. The number of particles in the simulation is important, as you want a high concentration of molecules, to be able to see the effect of their interaction. But calculations of momenta and position are made for each particle in the system, and as such increasing the number of particles in the simulation, increases the required amount of computations. The increase in necessary computations means that the simulation will take longer to perform or require more computational power.
The time step length is similarly important, as it determines the amount of time simulated between each time the momenta and position of each particle in the system are calculated. If you need to simulate the changes in solution over a certain amount of simulated time, it will take longer to perform the simulation, the shorter the time step is. The advantage of shorter time steps is, that the system is simulated at a high degree of detail. The problem with using longer time steps is that the simulation becomes more loosely connected to the behaviour of the particles in the system. For instance, at longer time steps the collision of particles might not be calculated properly. The time step should be chosen based on the largest time step, that can deliver on the level detail needed in the simulation.[25, 26]

When inserting model molecules into the simulation space, they must be placed with a minimum overlap of molecular centres. The conditions of density and temperature determine the stability of the starting conformation. If the starting conformation is too tightly packed, the particles will not move, rendering the use of MD simulation pointless.[25]

The process of calculating the forces acting on each particle in the system is typically one of the more time-consuming processes in the simulation. Following this step, the Newtonian laws of motion are integrated through the use of certain algorithms. The choice of which algorithm to use is not always trivial. Fast algorithms are good, but speed is not essential, as this step in the simulation is already much faster than the previous step. Rather the algorithms ability to accurately calculate for larger time steps are preferable, as the use of longer time steps greatly reduces the necessary steps to complete the simulation. The algorithms accomplish this typically by storing information on increasingly higher orders of derivatives of the particle coordinates. Doing this requires more memory storage, which typically only poses a problem when computing larger systems.[25]

1.7.1 Coarse-Grained Molecular Dynamics

When dealing with larger molecules, such as in the case of simulating bio-molecules. Performing MD simulation becomes problematic, because the systems become very large, requiring a lot of computational power. This would mean that it would take a very long time to simulate. In this case, a method for decreasing the computational cost of the simulation is by using coarse-graining (CG), which represents the system

by a simpler model system. Instead of representing each atom as a particle in the simulation, atoms are grouped and represented by a rough representation, consisting of fewer particles. [27]

A versatile CG method is the Martini force field, which uses a 4:1 mapping scheme, grouping four heavy atoms and their associated hydrogen atoms into a single virtual particle. This CG mapping can be seen in Figure 1.17. This 4:1 mapping is insufficient to represent the geometry of small ring structures like benzene and cholesterol. Depending on the chemical nature of the atoms included in the CG particles, the particles are given a particle type varying polarity: Polar (P), non-polar (N), apolar (C), and charged (Q). Particles are further defined by their hydrogen-bonding capabilities with another letter, d = doner, a = acceptor, da = doner and acceptor, 0 = none. Alternatively, the latter can be assigned as a number 1 - 5 indicating their degree of polarity, with 1 being low polarity and 5 being High polarity.[28]

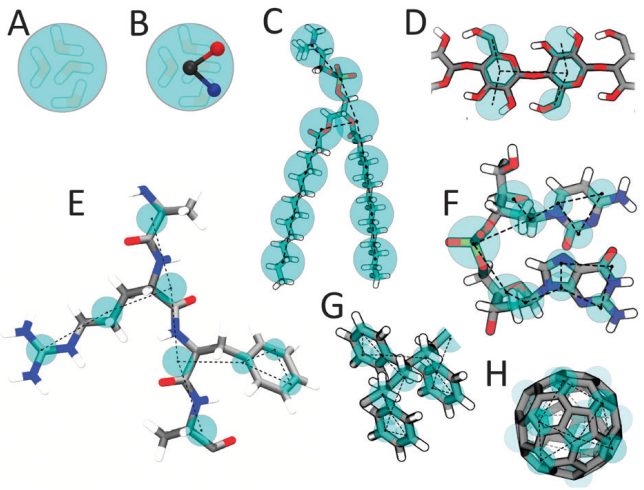

Figure 1.17: Examples of Martini mapping of some molecules. The martini CG beads are shown as cyan overlays the atomistic structures. (A) Standard Martini water representing 4 water molecules. (B) Polarizable Martini water with embedded charges. (C) DMPC lipid. (D) Polysaccharide fragment. (E) Peptide. (F) DNA fragment. (G) Polystyrene fragment. (H) Fullerene molecule.[28]

Chapter 2

Materials and Methods

2.1 Materials

In this section the different materials and instruments used in this project will be listed

Table 2.1: Chemical list

Chemicals	Cas	Description	Supplier
Fmoc-L-Phe-OH	35661-40-6		Activotech
Fmoc-L-Asp(OtBu)-OH	71989-14-5		Activotech
Fmoc-Gly-OH	29022-11-5		Activotech
Fmoc-L-Lys(Boc)-OH	71989-26-9		Activotech
Fmoc-L-Asp(OtBu)-Wang resin	FL-200-0401		Matrix Innovation
Fmoc-Rink-Amid-MBHA resin		Lot# 10K15-20-08-079	Iris Biotech GmbH
DCM	75-09-2		Iris Biotech GmbH
DMF	68-12-2	Lot# 122595G	Iris Biotech GmbH
TFA	76-05-1		Iris Biotech GmbH
Diethylether	60-29-7	Lot# V1I778141L	Iris Biotech GmbH
Acetonitrile	75-05-8		TH Geyer
DMSO	67-68-5		ChemSolute
TIS	6485-79-6		Iris Biotech GmbH
HBTU	94790-37-1		Iris Biotech GmbH
Oxyma	3849-21-6		Iris Biotech GmbH
DIEA	7087-68-5		Sigma Aldrich
Piperidine	110-89-4		Iris Biotech GMbH

2.2 Methods

2.2.1 Peptide Synthesis

Peptide synthesis was performed with an Activo-P11 system from Activotech. The system uses an Azura UVD 2.1 S UV monitor. Before and after synthesis a manual DCM wash of the synthesiser is performed, using a dummy reactor. Synthesis worklists can be found in Appendix B. N_2 is used for all gas pressures. Amino-acids are loaded in 15 mL Greiner tubes. Amino acids are weighed directly in the Greiner within a 5% error margin to minimize synthesis errors. All solutions for the synthesis are loaded with an additional 25% volume compared to worklist recommendations. If the recommended solution volume is less than 120 mL, increase the recommended volume by 30 mL instead. Mixer speed and amplitude is set to 120 cycles/minute and 170 degrees respectively, during both mixing and washing. The system is set to perform the following operations before the synthesis run is initialised: Prime, Clean Machine, Initialise UV Monitor and Initial wash probe/wash through.

The peptide was deprotected using 4mL of a 95% TFA, 2.5% milli-Q water and 2.5% TIS solution. The vial is then shaken at 250rpm for 1 hour to release the peptide. Cooled Diethylether is added to a 50mL Greiner Tube with the peptide to extract and precipitate it. It is centrifuged at 6000 rpm for 30 minutes for collection of the pellet.

2.2.2 Peptide Dissolution

All peptide solutions are 95% water, 5% acetonitrile. The Peptides are first dissolved in 100% acetonitrile, using ultrasound treatment for 1 hour periods and heating to 45 °C. This treatment is repeated until the peptide is properly dissolved. The peptide solution is then diluted to 85% acetonitrile and shaken gently for 1 minute. The solution is then diluted in further steps to 75 %, 50%, 25%, 15%, 10% and 5% acetonitrile. For solutions of less than 1 mM, the appropriate amount of peptide solution from a freshly made higher concentration solution is pipetted into another Greiner tube and diluted to the target concentration with the addition of 5% acetonitrile in water. Samples are stored at 5 degrees Celsius in a dark storage room to protect from light.

2.3 High Pressure Liquid Chromatography

High Pressure Liquid Chromatography (HPLC) was performed using an Acclaim 300 C18 LC Column. Inject volume was set to 20 μL. 40 μL was injected into the injection ring to ensure that the injection ring was full. The flow was directed through the injection ring immediately after the retention timer began. Sample concentration is 1 g/L. The HPLC sequence can be found in Appendix

HPLC was performed on peptide samples, which could be dissolved in 95 % water and 5 % acetonitrile. A.

2.4 Circular Dichroism Spectroscopy

Jasco J-715 is used for CD measurements. The system performs 8 measurements and produces an average of all measurements. Measurements are performed using 1 nm steps from 260 to 180 nm wavelengths. All peptide solutions used are 95% milli-Q water, 5% acetonitrile produced as described earlier. A quartz cuvette with 1 cm path length was used. A range of concentrations from 1 μM to 3 mM was used for CD measurements. The spread of concentrations was 1 μM, 5 μM, 10 μM, 20 μM, 50 μM, 100 μM, 200 μM, 300 μM, 400 μM, 500 μM, 1 mM, 2 mM, and 3mM. For mixed peptide solutions concentrations range from 0,5 μM to 3 mM, having solutions at half concentrations to allow comparison with non-mixed peptide solution. The spread of concentrations for mixed peptide solutions was 0,5 μM, 1 μM, 2,5 μM, 5 μM, 10 μM, 20 μM, 25 μM, 50 μM, 100 μM, 150 μM, 200 μM, 250 μM, 300 μM, 400 μM, 500 μM, 1 mM, 1,5 mM, 2 mM, and 3 mM. This wide spread of concentrations was used to be able to get a rough view of signal changes across concentrations.

CD-spectroscopy was performed on peptide samples, which could be dissolved in 95 % water and 5 % acetonitrile.

2.5 Fluorescence spectroscopy

Chronos DFD ISS model 90021 was used for fluorescent measurements of peptide solutions. Emission wavelength 250 nm, measuring from 260 nm - 400 nm, with the temperature set at 20 °C. Measurements were performed on solution concentrations of one concentration step lower, and one concentration step higher, than concentrations of significant signal changes in CD measurements. Fluorescent measurements on 3mM concentration solutions, of peptides observed to form fibres, was performed across 5 °C temperature steps, ranging from 20 °C to 60 °C. The temperature range was chosen as the Peltier system could safely adjust 40 °C from the water bath stabilizing temperature, which was at around 20 °C. The aperture was adjusted to keep the signal within the range of the sensor system.

2.6 Fibril Deposition

Before deposition of peptide solutions, the SiO substrates are cleaned by 30 minutes of ultrasound in acetone and 30 minutes of ultrasound in water, followed by rinsing with Milli-Q water, ethanol and acetone. The wafer is then dried using compressed N_2 before UV treatment for 30 min. After cleaning, a 3mM peptide solution is deposited onto the substrate by pipetting of 15 μL. The sample is left to dry for

up to 24 hours. This is performed in a dust-free environment. After drying, the peptide coverage on the surface can be reduced by rinsing with Milli-Q water. For deposition on samples with platinum wires, only the area containing the platinum wire, at the centre of the sample, is covered. Deposited solution volume is set to 2 μL. The procedure is otherwise similar. Platinum plate samples need more thorough rinsing to reduce peptide coverage.

2.7 Atomic Force Microscopy

AFM measurements were performed on samples deposited with peptide solutions, to scan the sample for fibre-structures. The instrument used is NT-MDT SOLVER and the cantilever is OMCL-AC160TS, the sample is mounted in the AFM by glueing the sample to a metal disk kept in place by a magnet in the AFM setup. The laser aim is adjusted onto the tip, and areas near structures observed in the optical microscope. After finding structures, settings are adjusted in an attempt to get a clearer measurement of the structures. All AFM data visualization has been performed in Gwyddion 2.53 [29].

2.8 Electrostatic Force Microscopy

To perform ESFM measurements, NT-MDT NTEGRA was used, grounding the sample with a wire attaching the sample to a ground on the apparatus, and a platinum-coated conductive tip was used. The cantilever is ScanSens GmbH ETALON series HA_FM/Pt. The surface of the sample was scanned for an area containing both a platinum wire and multiple distinct fibres. Then the AFM is set to perform a two-pass process, the first pass measuring topography as in conventional AFM, and the second pass moving over the sample at a set lift distance, using the topographical measurement to adjust the lift to achieve a constant lift distance from the sample. During the second pass a potential is applied to the tip at 3 V, 0 V, and -3 V. Each potential was used in a separate measurement. For each of the potential measurements, lift heights of 20 nm, 30 nm, 40 nm, and 50 nm.
ESFM was performed on peptide fibres identified through AFM, produced from 95 % water and 5 % acetonitrile solvents.

2.9 Voltage sweep measurements

For Voltage sweeps a setup from SUSS MicroTec was used. The sample with platinum wires on it as in Figure 2.1 was measured at different electrode points, the main contacts of interest being 1-59, as are connected by a single set of platinum wires. Measurements performed through slowly increasing range of potentials, starting from -0.001 V to 0.001 V, then -0.01 V to 0.01 V, -0.1 V to 0.1 V, followed by -1 V to 1V and finally -7 V to 7 V. This was done for a clean plate as a control, a plate

with GFD3 fibres deposited across the platinum wires, and a plate with GFX3-Mix fibres deposited across the platinum wires. As a further control, the two opposite detached corner contacts were measured. A control sample with silver paint on contacts was tested to ensure that contact needles did not penetrate the SiO layer. A wire control of the wire was performed by coating the platinum wire centre with silver paint, connecting all the platinum wires on the sample, for these measurements, an external resistance of 1 MΩ was used.
Voltage sweep was performed on peptide fibres identified through AFM, produced from 95 % water and 5 % acetonitrile solvents.

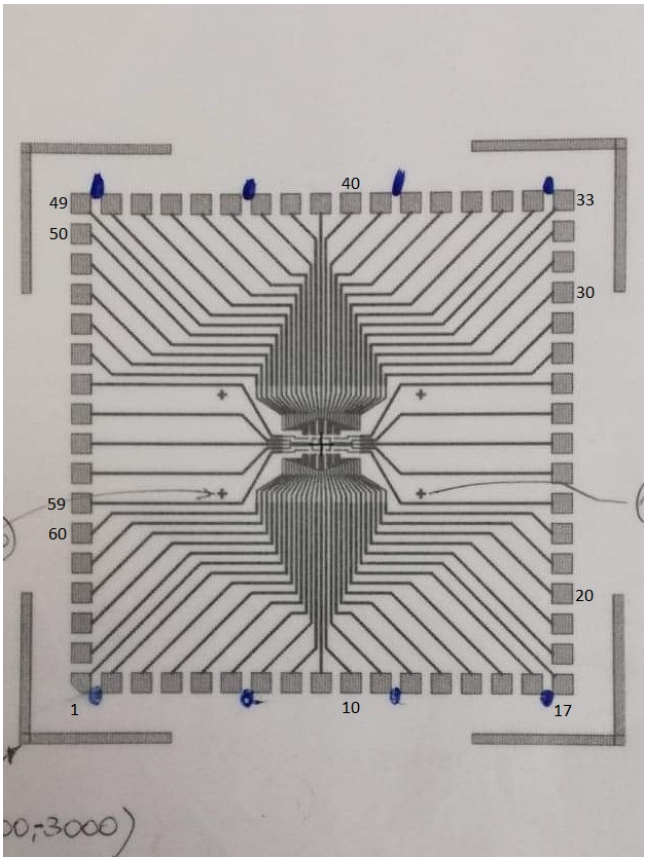

(a)

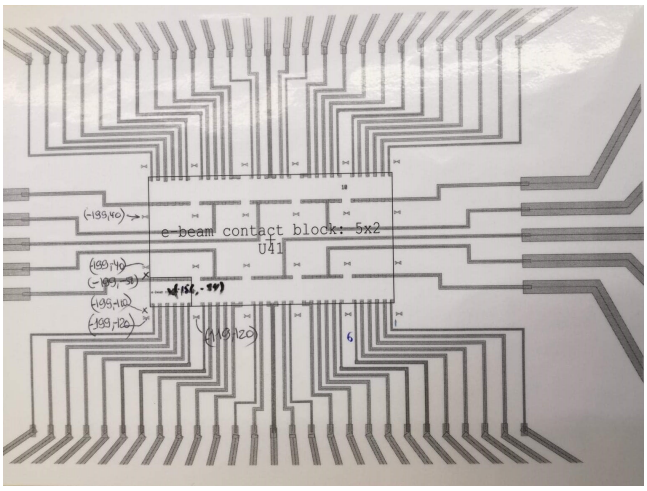

(b)

Figure 2.1: The design of platinum wires on the Si/SiO Sample, with square Gold contacts. a) an overview of the design, b) is a closeup on the centre of the plate. Even thinner platinum wires than depicted in b, in the spaces leading between the visible wires even closer.

2.10 Molecular Dynamics Simulations

For simulation, first .pdb files with atomistic models for GFD3 and GFK3 was prepared. These were made using the protein builder in YASARA, by YASARA Biosciences GbmH. The Files where then coarse-grained by using the martinize.py v2.2 script. The coarse-grain mapping can be seen in Figure 2.2a and 2.2b.

All simulations were performed using GROMACS v5.1.2 [30]. Simulation system was prepared by creating a 7x5x5 nm box and placing 13 GFD3 or GFK3 molecules in the simulation space, before filling the remaining space with polarisable martini water. Then a short simulation run of 10000 steps was performed for energy minimization. Then the simulation was run using Martini v2.2P force field for 200 ns in 10000000 steps, reference pressure is set to 1 bar using the Berendsen algorithm, and at a set temperature of 300 K using the velocity-rescale algorithm. Van der Waals and electrostatic interactions were calculated using Particle Mesh Ewald, PME. Simulations were run with periodic boundary conditions. Specific conditions can be found in .mdp format in Appendix C. For Visualization of simulation products VMD for LINUXAMD64 v1.9.4a12 [31] was used. For visualization of backbones, the native VMD extension Bendix v1.1 [32] was used. For GFX3-Mix simulation 7 GFD3 molecules, and 7 GFK3 molecules were loaded into the simulation space, rather than 13 molecules of either one peptide.

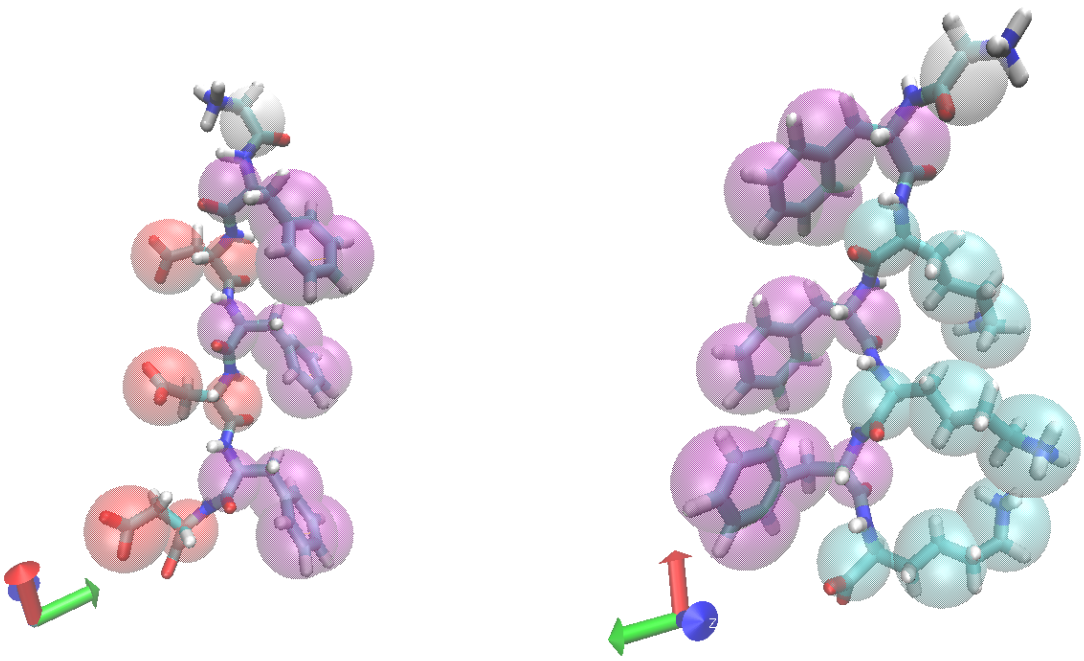

(a) **(b)**

Figure 2.2: a) Atomistic structure of GFD3 using licorice representation, with the coarse-grained mapping overlayed as transparent beads. White beads are Gly, Red beads are Asp, and Purple beads are Phe. As according to the 4:1 Martini mapping; Gly consists of 1 bead, Asp consists of 2 beads, while Phe consists of 4 beads due to the presence of a ring structure. While it can not be seen in this figure, the martinize.py script also added 1 charged dummy bead to the charged residues, Asp, to make it more compatible with the Martini v2.2P force field. b) Atomistic structure of GFK3 using licorice representation, with the coarse-grained mapping overlayed as transparent beads. White beads are Gly, Cyan beads are Lys, and purple beads are Phe. As according to the 4:1 Martini mapping; Gly consists of 1 bead, Lys consists of 3 beads, while Phe consists of 4 beads due to the presence of a ring structure. While it can not be seen in this figure, the martinize.py script also added 1 charged dummy bead to the charged residues, Lys, to make it more compatible with the Martini v2.2P force field.

Chapter 3

Results

In the following chapter, results from all experiments will be shown and described individually.

3.1 High Pressure Liquid Chromatography

Throughout this project, analytical HPLC was performed on the majority of synthesized peptides, as to identify, whether further purification was necessary.

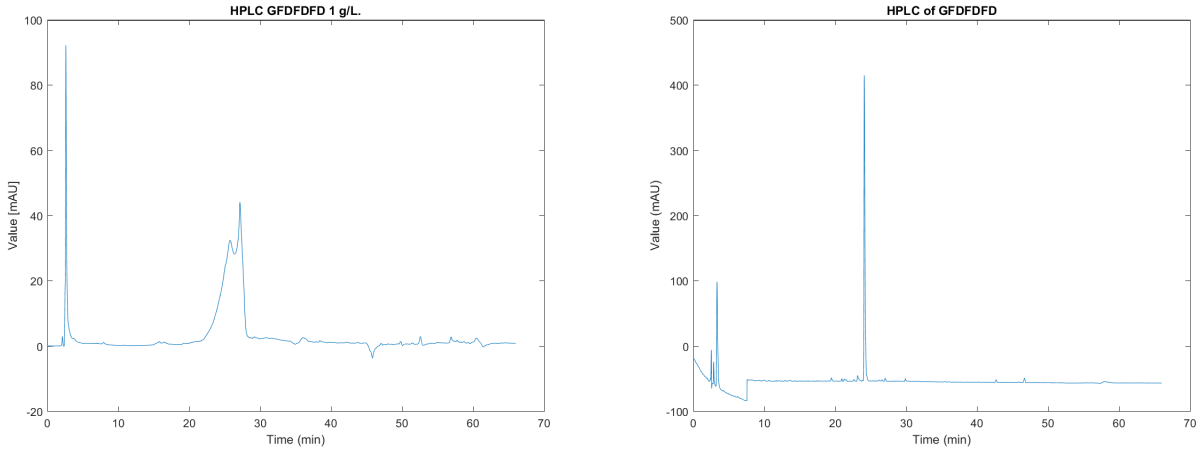

(a) **(b)**

Figure 3.1: HPLC of the two GFD3 syntheses. (a) HPLC analysis of the initial synthesis. Two relevant peaks are noticeable, after 25 and 27 minutes retention time respectively. The bandwidth of these peaks is above 5 minutes. (b) HPLC analysis of the second synthesis. Only a single noteworthy peak appears in this profile. After 24 minutes of retention time. The bandwidth of the peak is less than 30 seconds.

Figure 3.1a has three peaks. The first, and highest peak occurs after 2.5 minutes,

which is considered the flush peak. The following two peaks occur after 25 and 27 minutes respectively. The bandwidth for these signals is several minutes. This is indicative of two quite similar substrates being present in the solution. Figure 3.1b has a similar flush peak and a single well-defined peak after a retention time of 24 minutes. The bandwidth is less than 30 seconds, identifying a very well defined compound band. This shows, that only a single compound is likely to be present within the solution and further purification is not necessary.

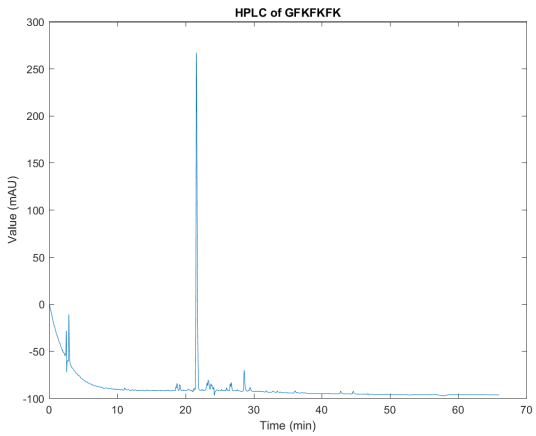

Figure 3.2: HPLC of the GFK3 peptide synthesized. An initial drop in signal occurs, which shows, that no proper baseline has been achieved. Only one significant peak occurs. This peak has a retention time of 21 minutes, and a bandwidth of 1 minute.

Figure 3.2 has a poor baseline, as the baseline seems to drop throughout the entire measurement, which is a noteworthy observation. A single peak is observed at 21 minutes of retention time. The peak is well defined, with a bandwidth of 1 minute. This indicates, that a single compound is present in the solution and further purification is not necessary.

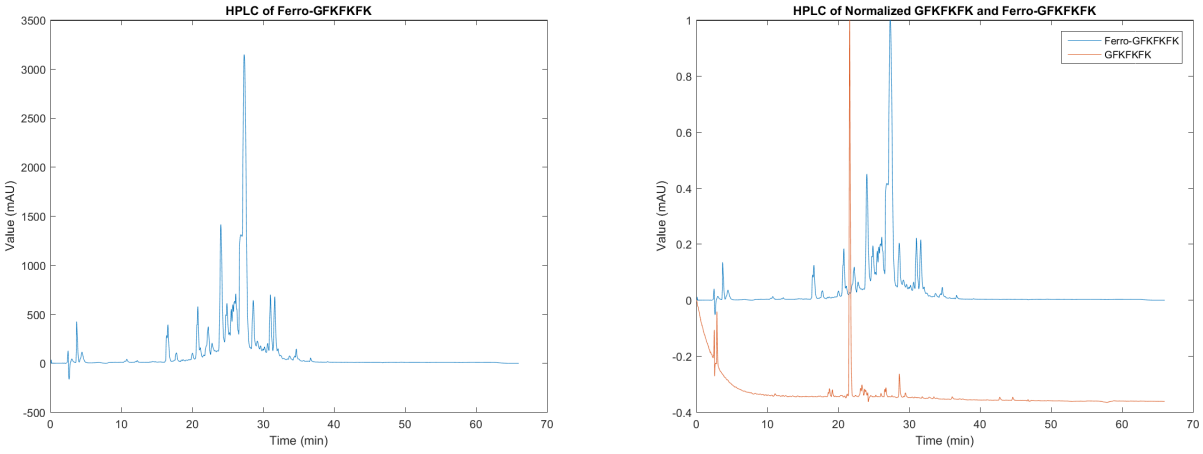

(a) **(b)**

Figure 3.3: (a) HPLC of F-GFK3. Several peaks are observed. A single peak appears after 16 minutes of retention time with a bandwidth of less than a minute. Another significant peak appears with 20 minutes of retention time, and a bandwidth of 30 seconds. A group of peaks occurs between 23 and 29 minutes, defined by two significantly larger peaks. The smaller has a retention time of 24 minutes, and a bandwidth of 1 minute. The largest peak has a retention time of 26.5 minutes, with a bandwidth of almost 2 minutes. The larger peak does have a noticeable shoulder. Two smaller peaks have a retention time of 31 minutes, and 31.5 minutes. (b) HPLC profile of (a), and Figure 3.2, normalized. The profile, shows that the retention time of the main GFK3 peak, does not correlate with the retention time of peaks produced by the ferrocene modified peptide.

Figure 3.3a has several peaks, implying, that several compounds are present within the solution. The two largest peaks, with a retention time of 24 minutes and 26.5 minutes, does not resolve distinctly. The retention period between the two peaks shows a significant signal. Figure 3.3b reveals, that the retention time of the group of peaks, produced by the ferrocene modified peptide, is significantly higher, than that of the original peptide. Such behaviour would be expected, given the hydrophobic nature of ferrocene. As such, the group of peaks can likely be attributed to ferrocene modified variants of the peptide.
Assuming that the primary peptide structure was synthesized correctly, it can be concluded that all peaks, occurring later than the original peptide peak, are caused by either properly modified peptides, or free ferrocene itself. If the peaks are attributed solely to peptide variants, it appears likely, that each peak represents a peptide formation. Likely different aggregate structures, which have different retention times. Such a phenomenon would explain, why baseline is not achieved between two, otherwise, well-defined peaks. No purification steps were deemed necessary.

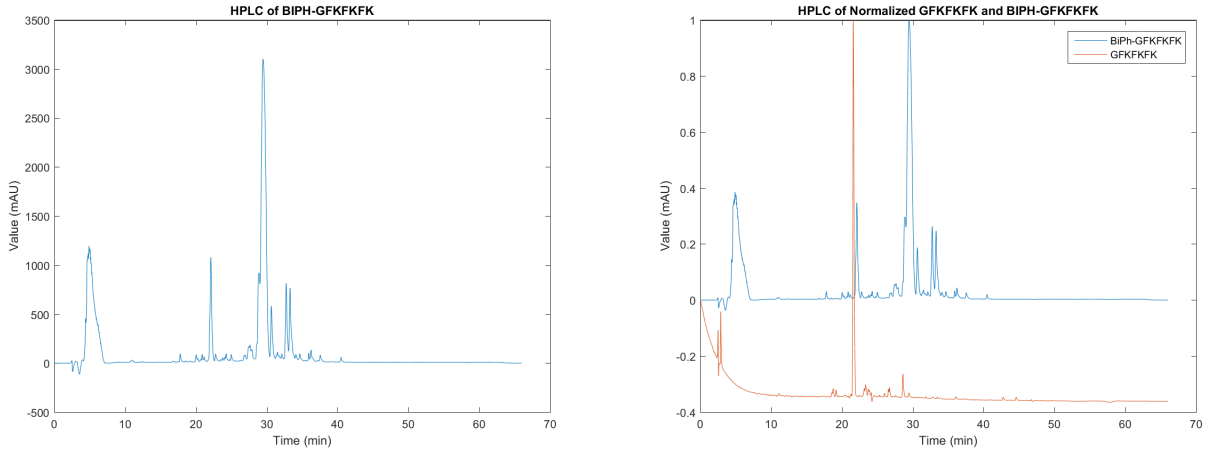

(a) **(b)**

Figure 3.4: (a) HPLC analysis of B-GFK3. An unusually large flush peak is observed, with a bandwidth of 3 minutes. A single peak appears with a retention time of 21 minutes. The largest peak has a retention time of 29 minutes, and a bandwidth of 90 seconds. Two small peaks appear with retention times of 32.5 minutes and 33 minutes. (b) HPLC profile of (a) and Figure 3.2 normalized. The profile shows, that the first peak in (a) correlates well with the main peak of the original peptide.

Figure 3.4a has a distinctly different flush peak than observed in other experiments. This will be considered an artifact, which was likely caused by a pressure drop, which was experienced during the inject step of this measurement. The first peak aligns well with the main peak of the original peptide, which indicates, that some of the peptides have not been properly modified. The largest peak is significantly later, which would be expected with the hydrophobic modification. Comparing the two largest peaks by bandwidth and height, an estimation of the relative compound composition of the solution can be achieved. As the original and modified peptide, should provide equal signal strength per peptide, the composition of the solution, should be proportional to the area of the triangle created by the signal. The peptide composition is calculated below. The peptide composition was deemed acceptable, without further purification steps.

	Signal Height	Band Width	Relative Peptide Concentration
GFK3 Signal	1843 mAu	0.74 min	17.5%
B-GFK3 Signal	3298 mAu	1.95 min	82.5%

3.2 CD Spectroscopy

CD spectroscopy was performed on all water-soluble peptides, produced in this project. Peptide concentrations range between 0.5 μM and 3 mM. Mixed peptide

concentrations are named by single peptide concentrations, as such, a 2mM mixed peptide solution contains 2mM of both GFD3 and GFK3. Hence, mixed samples are produced with intermediate concentration steps, to ensure the comparison between mixed and single peptide solutions can be performed both by total peptide concentration and concentration of the individual peptide. All peptides are dissolved in 95% water and 5 % acetonitrile.

3.2.1 CD spectroscopy of GFDFDFD

Figure 3.5a shows no significant behaviour at concentrations below 50 μM. The peak observed at 183 nm is seemingly independent of concentration, and is observed in all samples. At 50 μM a positive and a negative peak becomes apparent. These peaks, do not correlate with peaks expected from known secondary structures [22]. These peaks are likely attributable to the formation of peptide aggregates or fibres. Figure 3.5b shows, that the negative peak, observed at 232-234 nm, increases with concentration. The positive peak at 220-223 nm, does not increase proportionally to the negative peak. An observation, which is confirmed by Figure 3.5d, which shows a decreasing correlation at concentrations above 200 μM. This suggests that the peaks are attributable to different structures, as the profile should be maintained if only a single structure caused these peaks. It is likely that, the structure creating the positive peak reaches a saturation point, as the signal in Figure 3.5b does not decline, hence the structure concentration remains the same. Figure 3.5c shows the positive peak dissipating with high concentration. It is noteworthy, that all features of the CD profile dissipates at 3mM peptide concentration. It is difficult to evaluate whether the positive peak dissipates as a result of such behaviour. A similar case can be made in regards to the equal negative peak observed between 1mM and 2mM at 236-238 nm.

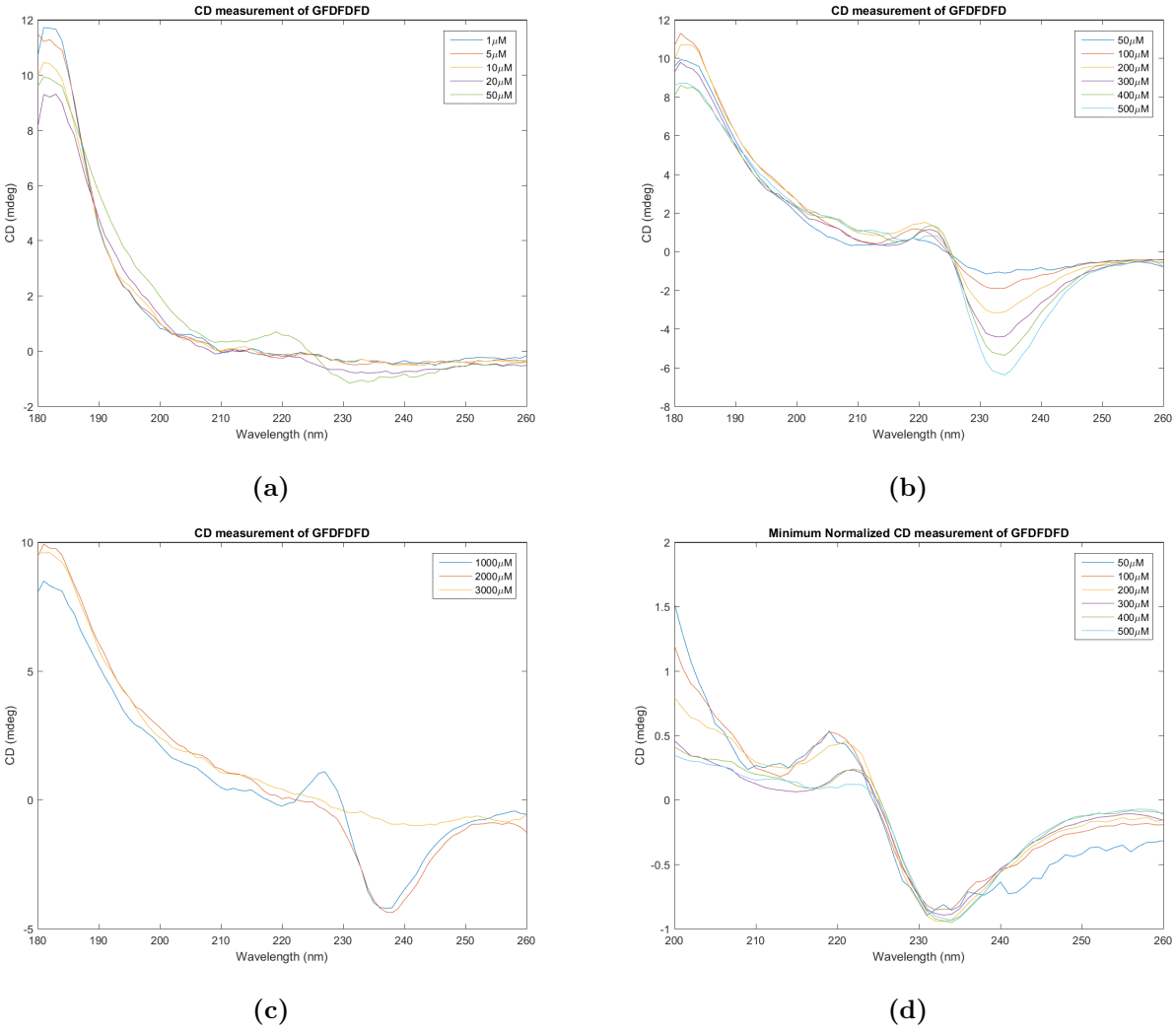

Figure 3.5: (a) CD spectra of GFD3-solutions at concentrations of 50 μM and below. A peak is observed at 183 nm for all concentrations. A positive peak is observed at 220 nm, and a negative peak at 232 nm is seen in the 50 μM sample. (b) CD spectra of GFD3-solutions at concentrations of 50 μM to 500 μM. All solutions have a peak at 183 nm. A positive peak is present at all concentrations at 220-223 nm. A negative peak is observed at 232-234 nm, increasing with concentration. (c) CD spectra of GFD3-solutions at concentrations of 1mM, 2mM and 3mM. A positive peak is present at 183 nm for all concentrations. The 1mM sample has a positive peak at 227 nm. A negative peak is present at 236-238 nm for 1mM and 2mM concentration. (d) CD spectra of GFD3-solutions at concentrations of 50 μM to 500 μM normalized relative to the negative peak at 232-234 nm. Wavelength below 200 nm have been omitted. The peak observed at 220-223 nm, does not increase proportionally to the normalization peak.

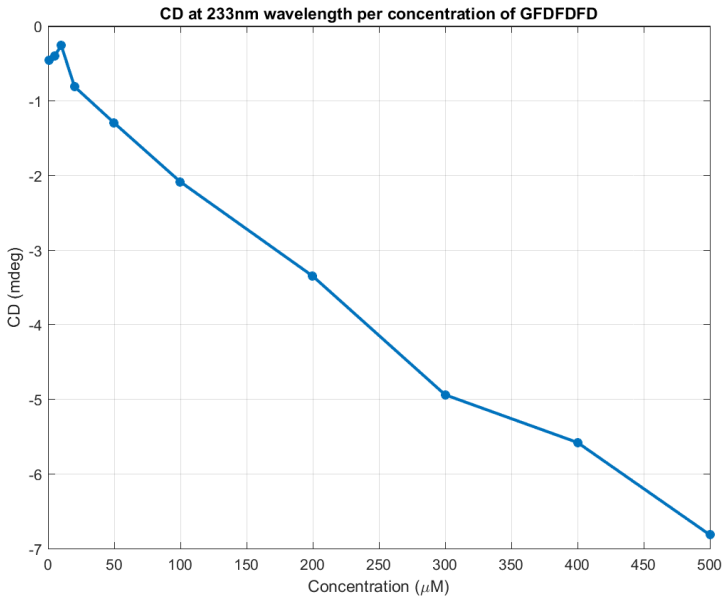

Figure 3.6: CD amplitude at 233 nm for GFD3 peptide solutions of concentration 1 μM to 500 μM. A linear relationship between concentration and amplitude is established for concentrations of 20 μM to 500 μM: $mdeg = -0.0124 \cdot C - 0.765$, $R^2 = 0.99$

Figure 3.6 shows a linear relation between peptide concentration and CD spectra amplitude at 233 nm for 20 μM to 500μM: $mdeg = -0.0124 \cdot C - 0.765$, $R^2 = 0.99$. Such a relation is indicative of a linear increase of a single peptide structure correlated with peptide concentration increase. Since no such relation is observed at concentrations below 20 μM, it can be expected that a critical structure formation concentration exists below 20 μM.

3.2.2 CD Spectroscopy of GFKFKFK

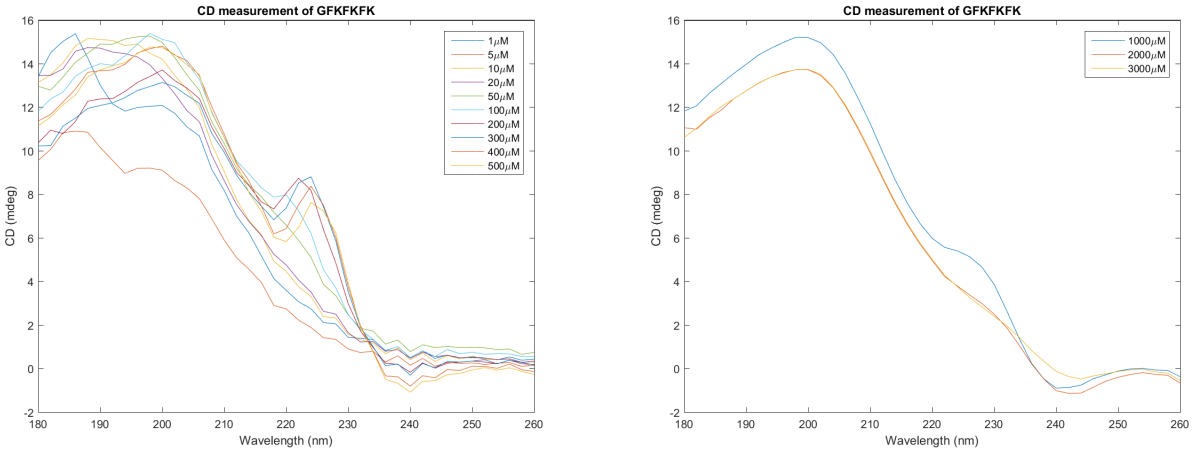

(a) **(b)**

Figure 3.7: (a) CD spectra of GFK3-solutions at 500 μM and below. With increasing concentration a negative peak becomes more significant at 240 nm. A positive peak is observed at 224-227 nm, in concentrations 200 μM and above. The peak is highest at 200 and 300 μM. A positive rotational absorption is observed with decreasing wavelengths below 240 nm. (b) CD spectra of GFK3-solutions 1mM, 2mM and 3mM. A negative peak is observed at 240-245 nm. A positive shoulder is observed around 227 nm in the 1mM concentration. Higher concentrations have less features in the CD profile.

Figure 3.7a show, that increasing concentration creates a negative peak at 240 nm. Increasing concentration also creates a positive peak at 227 nm but maximizes at 300 μM. This observation can also be made in Figure 3.7b. The rotational absorption increases with decreasing wavelengths, which seems independent of peptide concentrations. CD profiles of concentrations above 500 μM appear to lose these features.

3.2.3 CD spectroscopy of mixed GFDFDFD and GFKFKFK

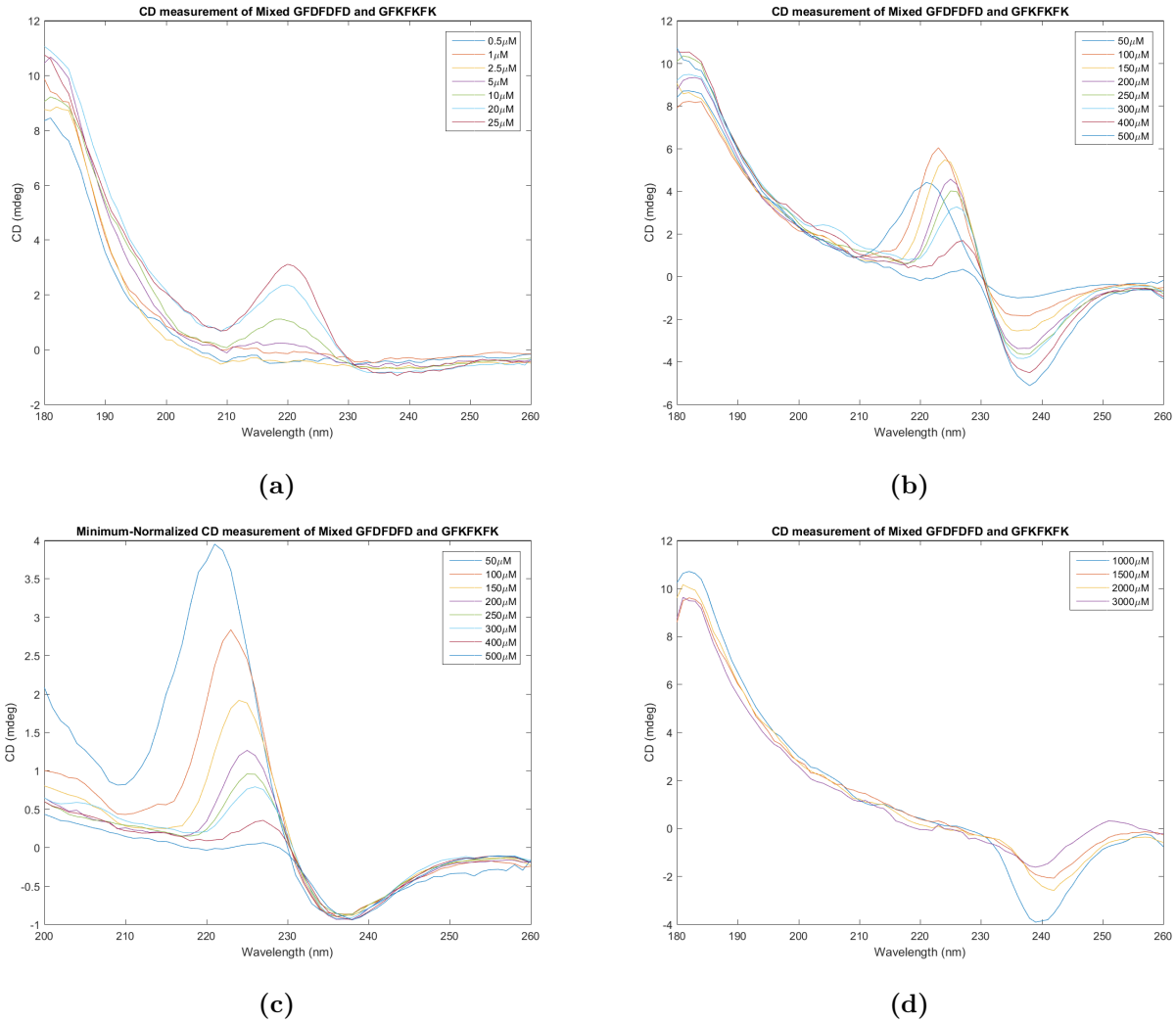

Figure 3.8: (a) CD spectra of GFX3-Mix solutions of concentrations 25μM and below. A positive peak is observed at 180 nm. This peak is independent of concentration. At 220 nm, a positive peak is observed. This peak increases with concentration. (b) CD spectra of GFX3-Mix solutions of concentrations 50 μM to 500 μM. A positive peak is observed at 180 nm. This peak is independent of concentration. A positive peak is observed at 220 nm in 50 μM. This peak red-shifts with increasing concentration. At concentration 100 μM, the peak is decreasing with increasing concentration. A negative peak is observed at 236 nm and increases with concentration. (c) CD spectra of GFX3-Mix solutions of concentrations 50 μM to 500 μM, normalized with respect to the negative peak at 236 nm. Wavelengths below 200 nm have been omitted. The red-shifting positive peak is observed to decrease relative to the negative peak with increasing concentration. The negative peak profile is similar across peptide concentrations. (d) CD spectra of GFX3-Mix solutions of concentrations of 1mM, 1.5mM, 2mM and 3mM. A positive peak is observed at 182 nm. This peak is independent of concentration. A negative peak is observed at 239 nm in the 1mM spectrum. The peak decreases with increasing concentration.

Figure 3.8a shows, increasing concentration creates a positive peak at 230 nm. This peak is observed in Figure 3.8b as well. This peak is red-shifting with increasing peptide concentrations. The peak is decreasing, when 100 μM is reached. This decrease could be due to an overlap with the negative peak observed at 236 nm. This would create a shift in the negative peak profile with increasing peptide concentration, which is not observed in Figure 3.8c, which shows a distinct profile across peptide concentration. It can, therefore, be assumed, that the peak decrease is indicative of a structure concentration diminishing. Suggesting, that such a structure ceases to be favourable with increasing peptide concentration. The well defined negative peak observed in Figure 3.8c is indicative of a consistent structure, which is observed to increase in concentration in Figure 3.8b. As concentrations increase to the mM-range, the negative peak red-shifts and decreases, which can be seen in Figure 3.8d. This behaviour appears consistent across peptide solutions containing GFD3 and GFK3, which all show diminishing CD profiles at high concentrations.

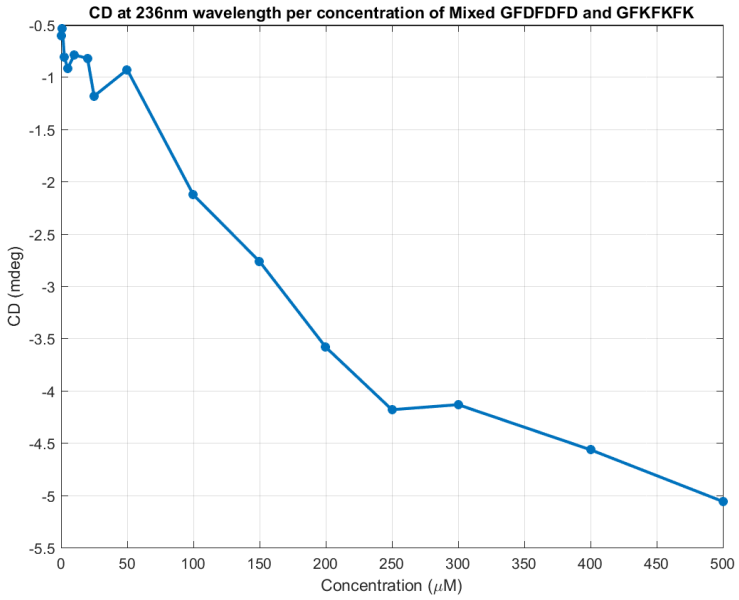

Figure 3.9: CD amplitude at 236 nm for GFX3-Mix solutions of concentrations 0.5 μM to 500 μM. A linear relationship between concentration and amplitude is observed up to 250 μM: $mdeg = -0.0143 \cdot C - 0.6350$, $R^2 = 0.9819$. A linear relation is observed from 300 μM to 500 μM: $mdeg = -0.0046 \cdot C - 2.7343$, $R^2 = 0.9984$

Figure 3.9 shows a linear relationship between CD spectra amplitude and peptide concentration below 250 μM, which can be described as $mdeg = -0.0143 \cdot C - 0.6350$, $R^2 = 0.9819$. From 300 μM to 500 μM a different linear relation is observed, which can be described as $mdeg = -0.0046 \cdot C - 2.7343$, $R^2 = 0.9984$. As such a change in linear dependency occurs, it can be assumed that a change in super structure formation occurs as well. A critical formation concentration can be speculated to

exist between 200 μM and 300 μM.

3.2.4 CD spectroscopy of ferrocene modified GFKFKFK

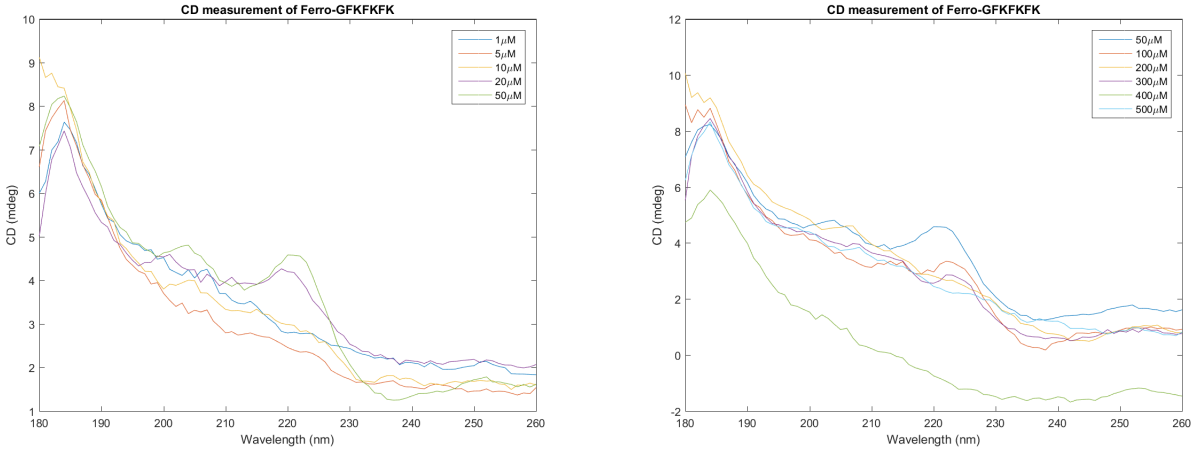

(a) **(b)**

Figure 3.10: (a) CD spectra of F-GFK3 solutions concentration 50 μM and below. A positive peak is observed at 185 nm, which is independent of concentration. A positive peak appears with increasing concentration at 223 nm. A small negative peak is observed at 236 nm in the 50 μM sample. (b) CD spectra of F-GFK3 solutions of concentration 50 μM to 500 μM. The positive peak observed at 223 nm red-shifts and decreases with increasing concentration. The negative peak observed at 236 nm decreases with increasing peptide concentration. The 400 μM solution has a lower baseline than all other measurements.

Figure 3.10a shows an increasing concentration correlated positive peak at 223 nm. It red-shifts and decreases with an increasing concentration above 50 μM, as observed in other peptide solutions. A negative peak at 236 nm appears in concentrations higher than 20 μM. It flattens, in concentrations above 300 μM.

3.2.5 CD spectroscopy of mixed ferrocene modified GFDFDFD and ferrocene modified GFKFKFK

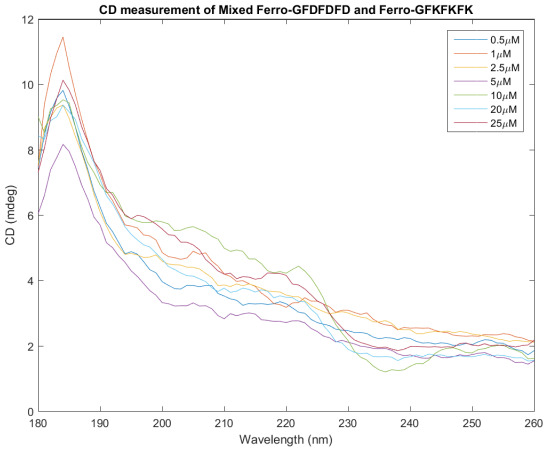

(a)

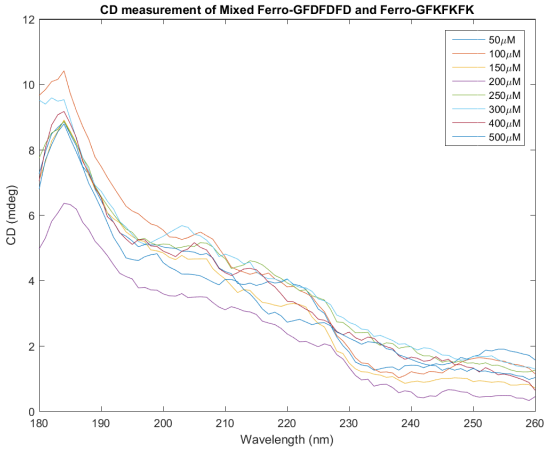

(b)

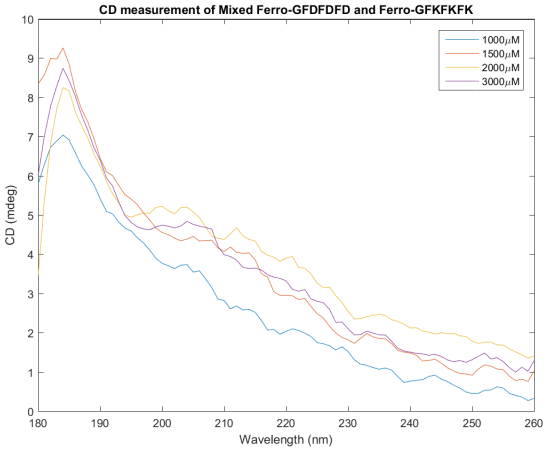

(c)

Figure 3.11: (a) CD spectra of F-GFX3-Mix solutions of concentration 25 μM and below. A positive peak is observed at 184 nm, which is independent of concentration. The 10 μM solution has a positive peak at 223 nm, and a negative peak at 238 nm. These peaks are not as expressed in other concentrations. 20 μM and 25 μM show some similar peaks. Positive rotational absorption increases in wavelengths below 240nm. (b) CD spectra of F-GFX3-Mix solutions of concentration from 50 μM to 500 μM. A positive peak is observed at 184 nm, which is independent of concentration. No well-defined peak is observed between 220 and 240 nm. Positive rotational absorption increases in wavelengths below 240nm. (c) CD spectra of F-GFX3-Mix solutions of concentration 1mM, 1.5mM 2mM, and 3mM. A positive peak is observed at 184 nm, which is independent of concentration. Positive rotational absorption increases in wavelengths below 240nm

Figure 3.11a shows indications of a positive and negative peak at 223 and 238 nm respectively. These indications are also observed in Figure 3.11b. However, no clear signal is observed, and the peak resolution is seemingly independent of concentration above 10 μM. These peak indications are not observed in concentrations above 250 μM as seen in Figure 3.11b and 3.11c.

3.2.6 CD spectroscopy of biphenyl modified GFKFKFK

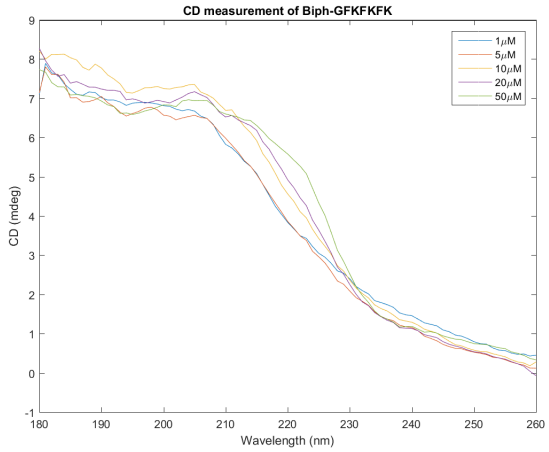

(a)

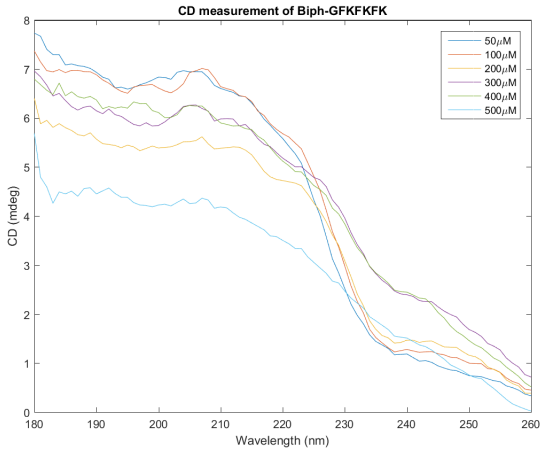

(b)

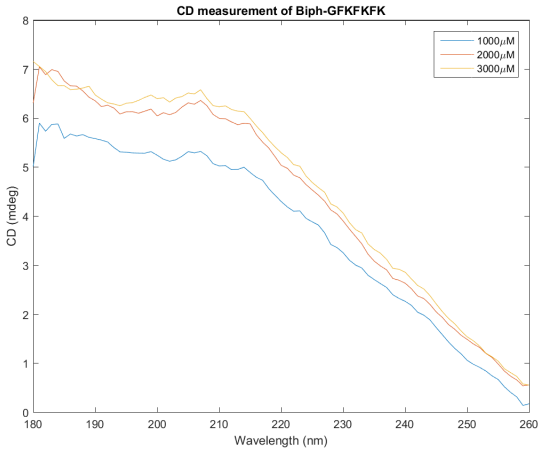

(c)

Figure 3.12: (a) CD spectra of B-GFK3 solutions at concentration 50 μM and below. No distinct peak is observed. Positive rotational absorption increases as wavelength decreases. (b) CD spectra of B-GFK3 solutions at concentrations 50 μM to 500 μM. No distinct peak is observed. Concentrations below 300 μM show lower rotational absorption above 230 nm, but similar absorption below this wavelength. (c) CD spectra of B-GFK3 solutions at concentrations 1mM, 2mM and 3mM. Absorption decreases linearly with increases in wavelength above 215 nm. Below 215 nm a flat CD profile is observed.

Figure 3.12a shows no defined peaks. The rotational absorption decreases with increasing wavelengths. This relationship becomes steeper as peptide concentration increases. This relation ceases at concentrations above 50 μM, where the change in absorption becomes more linear, which is observed in Figure 3.12b and 3.12c. The rotational absorption below 215 nm remains consistent across concentrations.

3.2.7 CD spectroscopy of mixed biphenyl modified GFDFDFD and biphenyl modified GFKFKFK

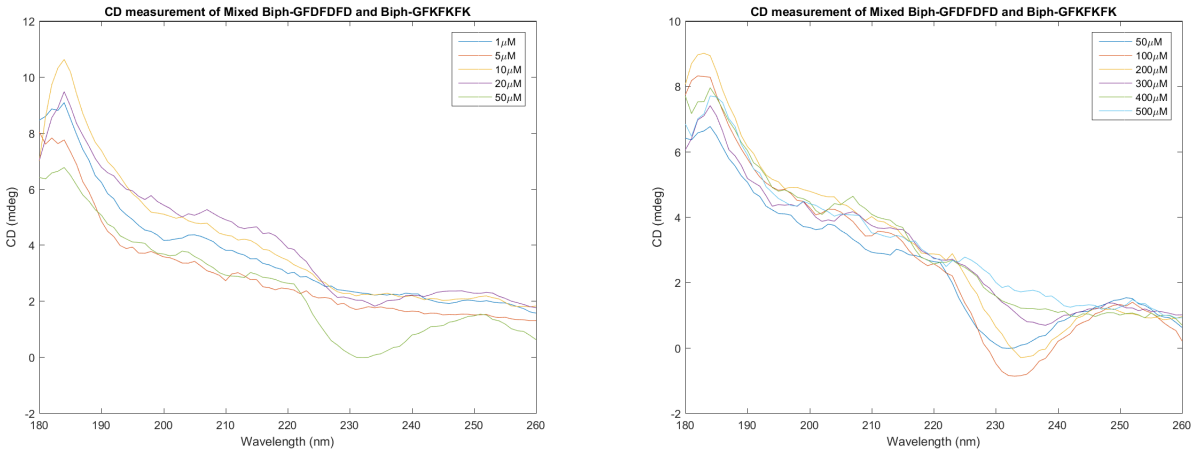

(a) **(b)**

Figure 3.13: (a) CD spectra of B-GFX3-Mix solutions of concentration 50 μM and below. A positive peak is observed at 183 nm, which is independent of concentration. A negative peak is observed at 232 nm in concentration 20 μM and 50 μM, increasing with concentration. A slight positive peak appears at 250 nm. (b) B-GFX3-Mix solutions of concentration 50 μM to 500 μM. A positive peak is observed at 183 nm, which is independent of concentration. A negative peak is observed at 232 nm for 50μM concentration. The peak red-shifts with increasing concentration. Above 100 μM, the peak diminishes with concentration. At 250 nm a positive peak is observed. It is most distinct in the 100 μM sample and decreases with increasing concentration. The 500 μM sample has no distinct peaks above 183 nm.

Figure 3.13a shows two peaks appearing with an increase in concentration. A negative peak at 232 nm and a positive at 250 nm. These peaks are most apparent at 100 μM, but decreases at higher concentrations, as seen in Figure 3.13b. Neither of the peaks appears independently of the other, which likely means, that the same structure is creating both signals.

3.3 Atomic Force Microscopy

AFM was performed on all peptide solutions. Peptides were deposited on silica oxide wafers, using the deposition method described in Section 2.6. All peptide solutions used for deposition are 3 mM concentration, except GFK3. The deposition of GFK3 was performed using a solution of 6 mM concentration. In the following section AFM images for peptides, which were found to form distinct structures, will be presented. F-GFD3 and B-GFK3 were not found to form any structures. AFM images of F-GFD3 aggregates can be found in Appendix D. No structures were identified in

B-GFK3 samples, and no AFM images of B-GFK3 will be presented within this report.

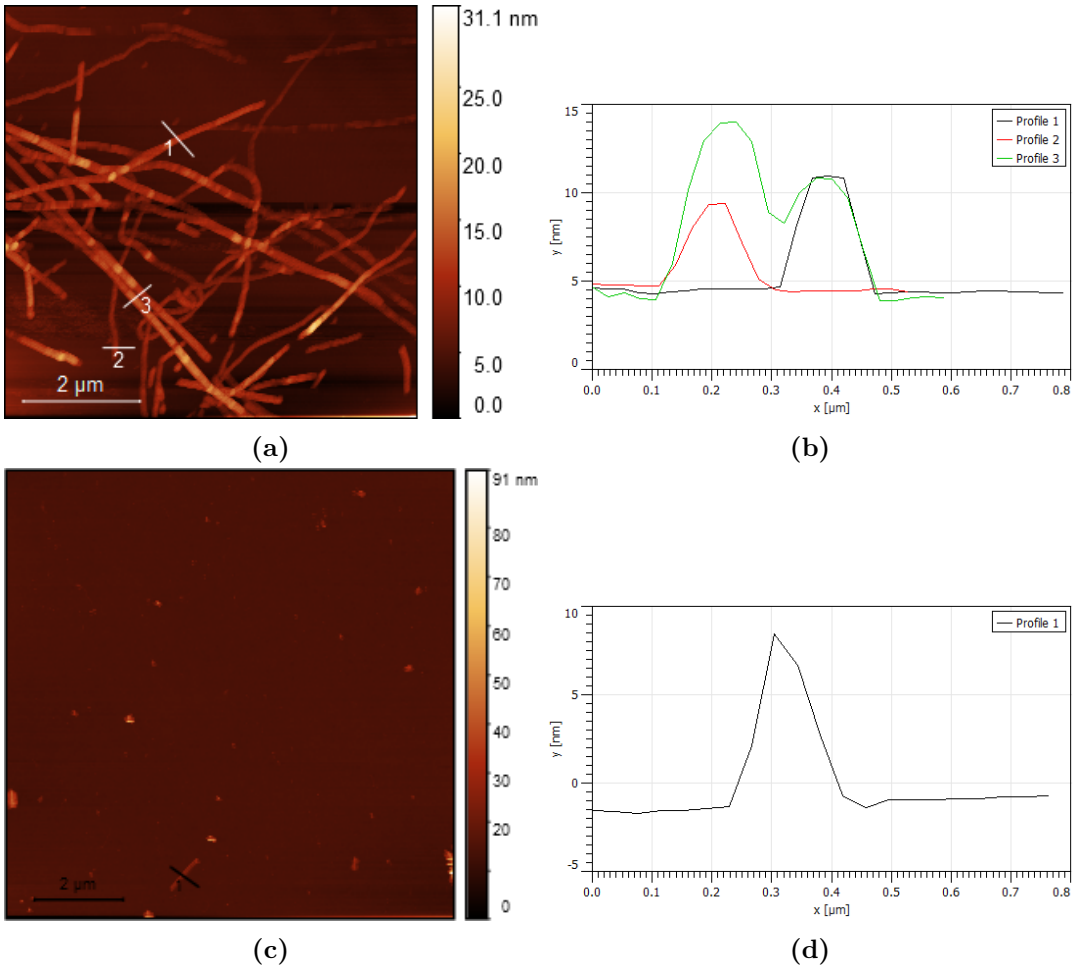

Figure 3.14: (a) A 7 μm x 7 μm AFM image of GFX3-Mix peptide. Well defined, straight, fibres are formed. Profile measurements 1, 2 and 3 can be seen in (b). Profile heights are shown in Table 3.1. (c) A 10 μm x 10 μm AFM image of GFK3. A single fiber have been identified. Several aggregates are observed. Profile measurement 1 can be seen in (d). Profile height is measured in Table 3.1

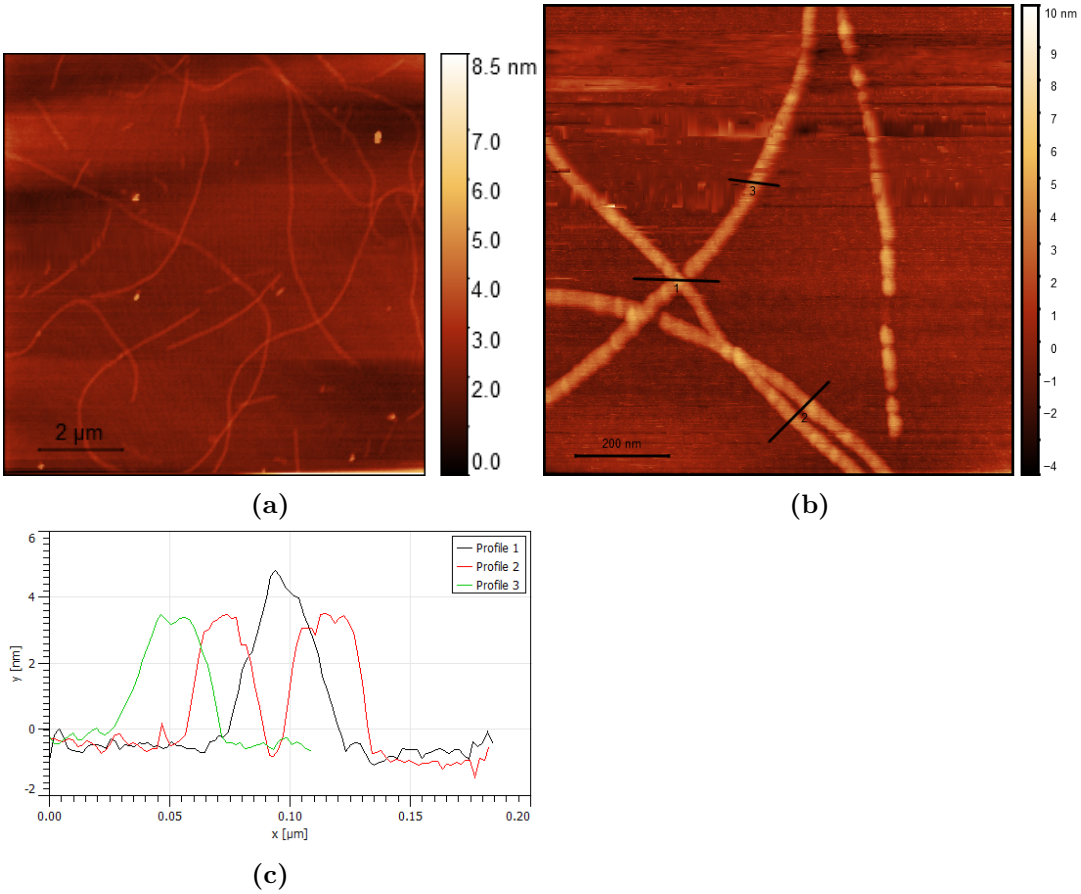

Figure 3.15: (a) A 10 μm x 10 μm AFM image of GFD3. Well defined fibres are formed. The fibres are generally straight, but bends are allowed. (b) A 1 μm x 1 μm AFM image. Profiles 1, 2 and 3 can be seen in (c). Profile heights are measured in Table 3.1.

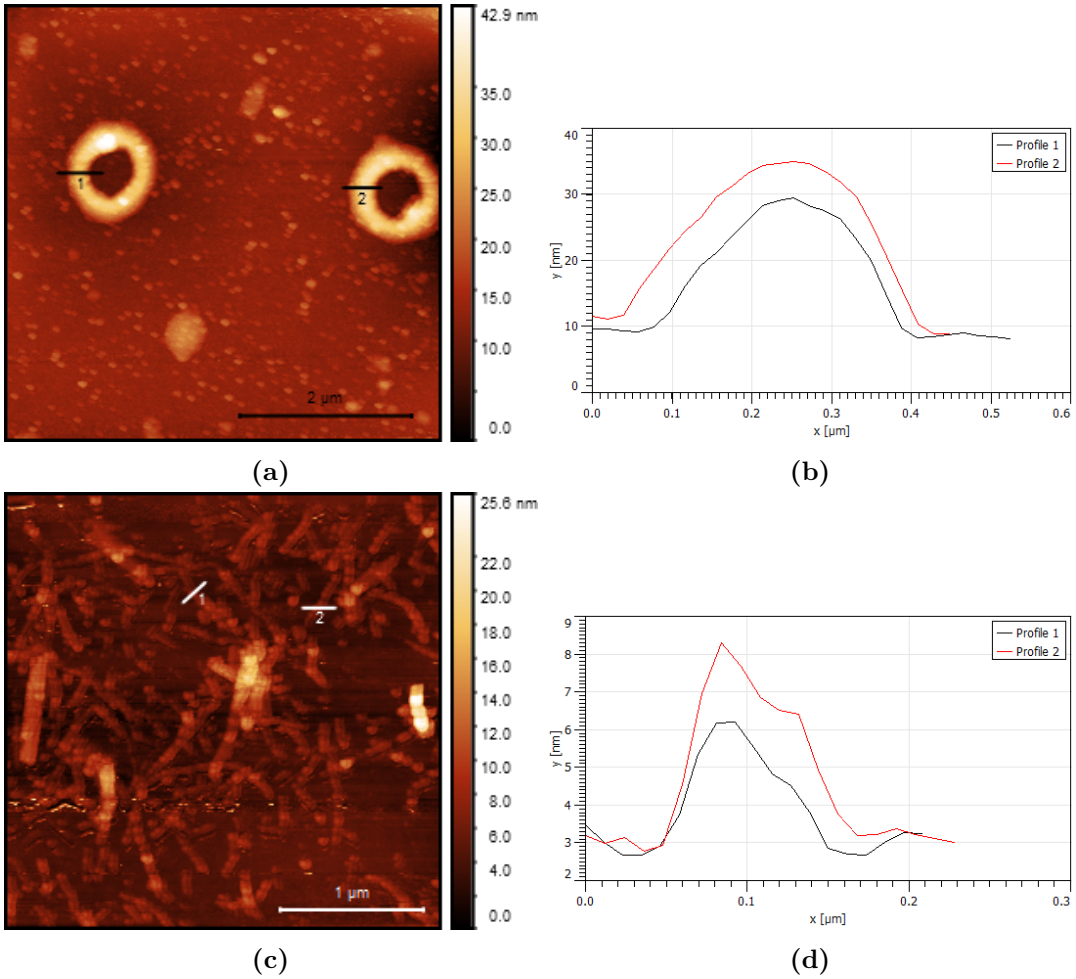

Figure 3.16: (a) A 5 μm x 5 μm AFM image of F-GFK3. Two circular structures are observed. Several aggregates are present. Profiles 1 and 2 can be seen in (b). Profile heights are measured in Table 3.1. (c) A 3 μm x 3 μm AFM image of B-GFX3-Mix. Short fibres are observed. Resolution is poor. Profiles 1 and 2 can be seen in (d). Profile heights are measured in Table 3.1.

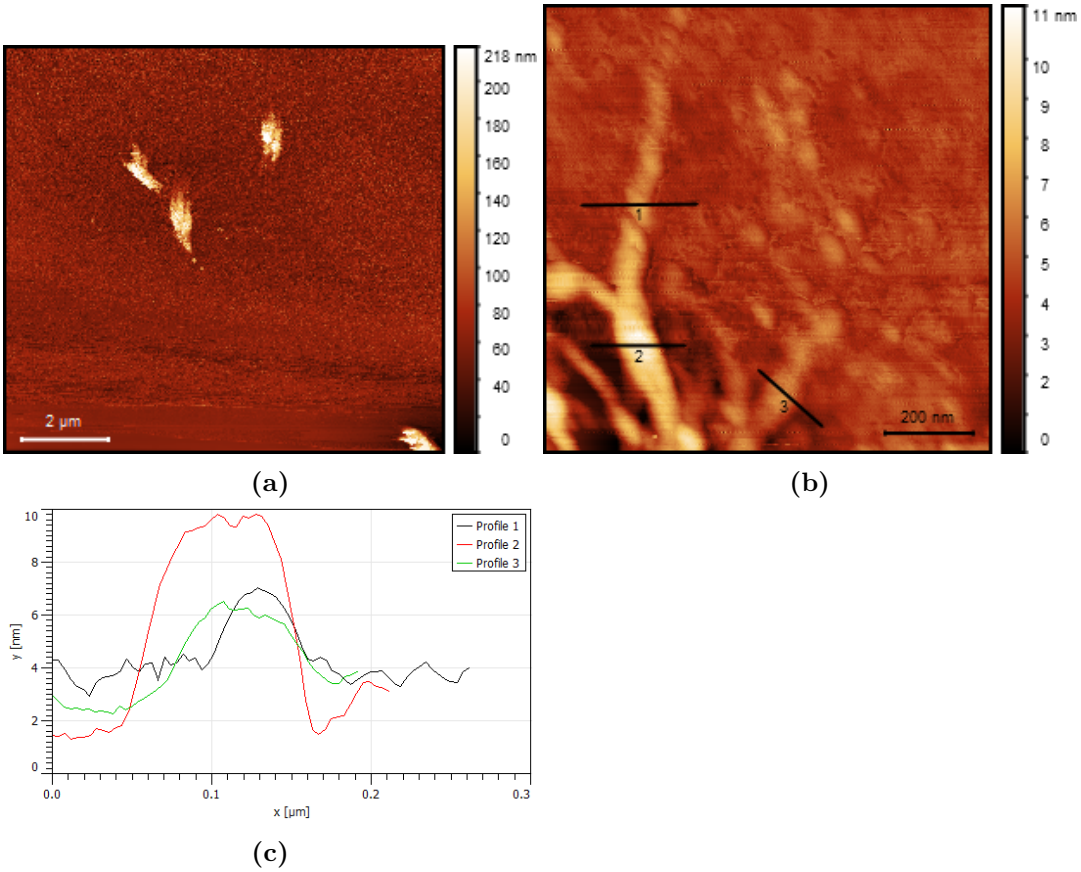

Figure 3.17: (a) A 10 μm x 10 μm AFM image of B-GFD3. Aggregate like structures are observed. (b) A 1 μm x 1 μm AFM image of the fanned part of the aggregate structures in (a). Profiles 1, 2 and 3 can be seen in (c). Profile heights are measured in Table 3.1.

	Profile 1	Profile 2	Profile 3
GFX3-Mix	6.54 nm	4.84 nm	7.89 nm/4.71 nm
GFK3	8.42 nm		
GFD3	4.81 nm	3.47 nm/3.07 nm	3.47 nm
F-GFK3	20.69 nm	24.96 nm	
B-GFX3-Mix	4.13 nm	5.65 nm	
B-GFD3	3.16 nm	8.10 nm	3.96 nm

Table 3.1: Profile heights of AFM images. Heights are noted relative to baseline heights.

	Profile 1	Profile 2	Profile 3
GFX3-Mix	170 nm	180 nm	200 nm/180 nm
GFK3	190 nm		
GFD3	70 nm	40 nm/40 nm	100 nm
F-GFK3	350 nm	390 nm	
B-GFX3-Mix	110 nm	120 nm	
B-GFD3	100 nm	130 nm	130 nm

Table 3.2: Profile widths of AFM images. Measurements are rounded by to nearest 10 nm.

Figure 3.14a show GFX3-Mix forms well-defined fibres up to several micrometers in length. Figure 3.14b and Table 3.1 show varying fibre heights of 4.7 nm to 7.9 nm, showing that fibre height is not uniform across fibres. GFX3-Mix fibres are generally quite straight. It appears that fibres have been cut or broken in several locations, where two short fibres align quite well. Fibre length varies significantly, with some fibres shorter than 1 μm, and larger fibres longer than 5 μm.
Figure 3.14c show a single 1 μm long fibre formed by GFK3. Aggregates are present across the sample. This fibre was the only GFK3 fibre detected during this report, showing that GFK3 has poor fibre forming capabilities. Figure 3.14d and Table 3.1 show the fibre to be more than 8 nm tall, forming the tallest fibre-structure observed in this report.
Figure 3.15a show GFD3 forms well defined fibers, ranging from 1 μm to over 10 μm in length. The fibres formed are generally straight, but bends significantly more than fibres formed by the GFX3-Mix solution. Figure 3.15b shows a peptide overlap. Profiles across these fibres, seen in Figure 3.15c, reveal uniform fibre heights across fibres of 3-4 nm. Profile 1 of the GFD3 fibres shows that the fibres do not overlap well, as this should produce a double height profile. However, the profile is only 40 % taller than each of the two fibres crossing. This suggests, that the estimated fibre height is too large or that the fibre height does not increase in an additive manner during fibre overlap.
Figure 3.16a show that F-GFK3 forms large ring structures, about 1 μm in diameter. The circumferential structure is 20 to 24 nm tall, seen in Figure 3.16b and Table 3.1, which is larger than any fibres identified in this report. Several small aggregates are present on the surface.
Figure 3.16c show that B-GFX3-Mix forms fibres. These are shorter than fibres produced by GFD3 and GFX3-Mix samples. The poor resolution makes distinct statements of fibre behaviour difficult. The fibres are estimated to be between 4 and 6 nm in height, as shown in Figure 3.16d and Table 3.1.
Figure 3.17a and 3.17b show that B-GFD3 forms bundled fiber structures, which fans into 3-4 nm high single fibers. The fibres do not cover the surface as the other fibres observed, but aggregate into local structures. The bundles are 1 μm wide and 2 μm long.

3.4 Fluorescence

Fluorescence spectroscopy measurements were performed on all peptides, to have shown fibril forming properties in AFM experiments, produced from 95 % water, 5 % acetonitrile solvent. GFK3 have been investigated using fluorescence as a non-fibrillating peptide comparison. Measurements have been performed for selected concentrations, which have shown interesting behaviour in CD spectroscopy and could indicate structure critical concentrations. Temperature step fluorescence spectroscopy measurements have been performed on fibril-forming peptides. 3 mM peptide concentrations were used for these measurements, ranging from 20 °C to 60 °C. All measurements were performed using 250 nm excitation wavelength.

3.4.1 Fluorescence spectroscopy of GFDFDFD

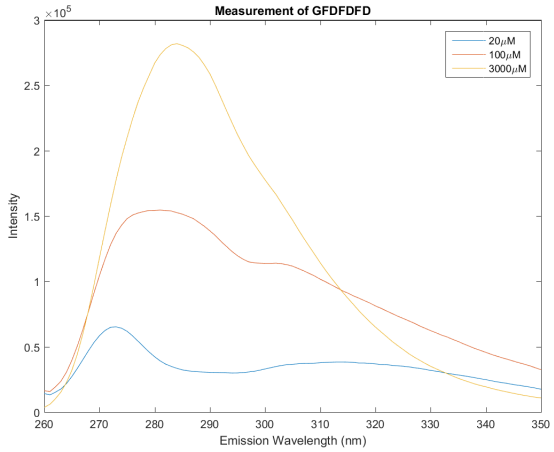

(a)

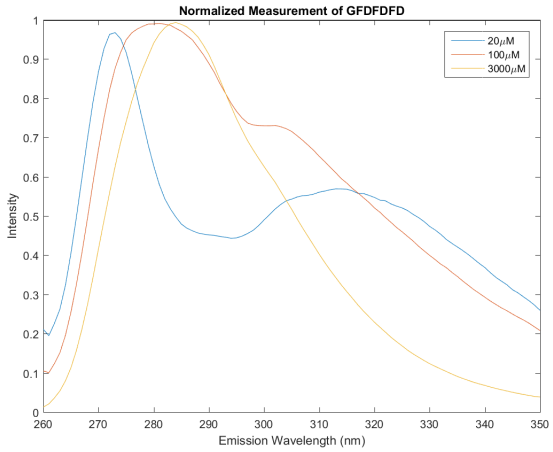

(b)

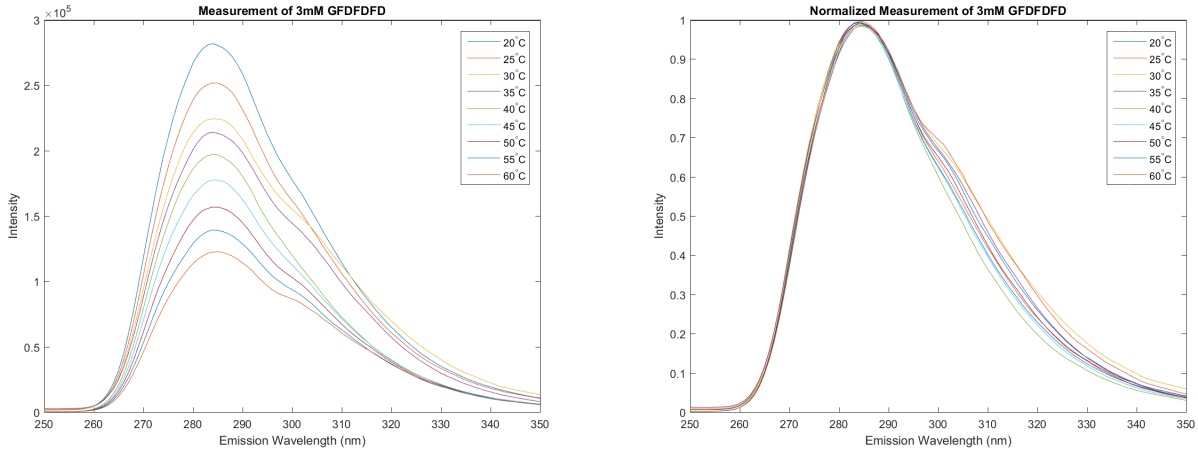

(c) **(d)**

Figure 3.18: (a) Fluorescence spectroscopy measurements of GFD3 peptide solution concentration 20 μM, 100 μM and 3 mM. 20 μM concentration has maximum peak at 273nm. 100 μM concentration has maximum peak at 281 nm. 3mM has maximum peak at 284 nm. A signal is observed above 300 nm. (b) Normalized fluorescence spectroscopy measurements of GFD3 peptide solution concentration 20 μM, 100 μM and 3 mM. The maximum peak of 20 μM, 100 μM and 3 mM is at 273 nm, 281 nm and 284 nm respectively. 20 μM has a second peak at 314nm. 100 μM has a shoulder at 301nm. (c) Temperature step fluorescence spectroscopy measurements of GFD3 peptide solution concentration 3 mM. The main peak at all temperatures is 284 nm. The signal strength decreases with increasing temperature. (d) Normalized temperature step fluorescence spectroscopy measurements of GFD3 peptide solution concentration 3 mM. The right hand shoulder of the signal appears independent of temperature.

Figure 3.18a shows an increasing intensity with concentration. The peak wavelength red-shifts with concentration, as seen in Figure 3.18b, suggesting solvent exposure at higher concentrations. It is noteworthy that 20 μM sample has a peak wavelength significantly below 280 nm since 282 nm is commonly the peak wavelength of phenylalanine fluorescence. The peak observed at 314 nm blue-shifts with increasing peptide concentration, suggesting that a fluorophore becomes buried from the solvent as concentration increases. Figure 3.18c shows a fluorescence signal, which decreases with increasing temperature. No change in peak wavelength is observed with increasing temperature, which is shown in Figure 3.18d. The temperature-intensity relation is linear as described by Figure 3.19.

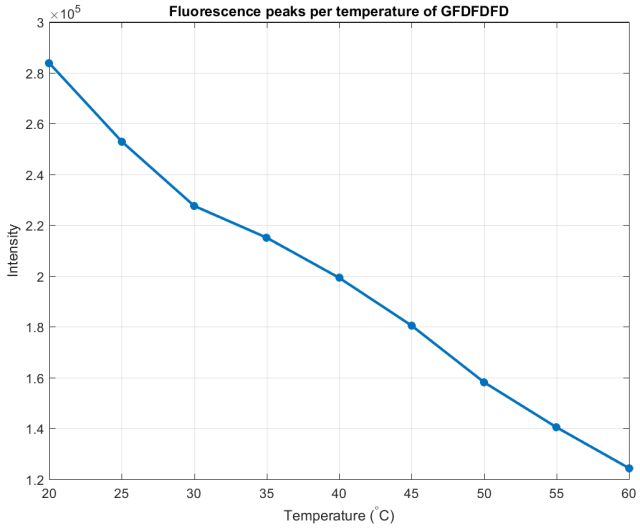

Figure 3.19: Peak fluorescence value of 3 mM GFD3 across temperature steps, 20 ˚C to 60 ˚C. Intensity drops linearly with temperature: $int = -3827.1T + 1.39 \cdot 10^6$, $R^2 = 0.9916$. T is temperature in Kelvin.

3.4.2 Fluorescence spectroscopy of mixed GFDFDFD and GFKFKFK peptide solution

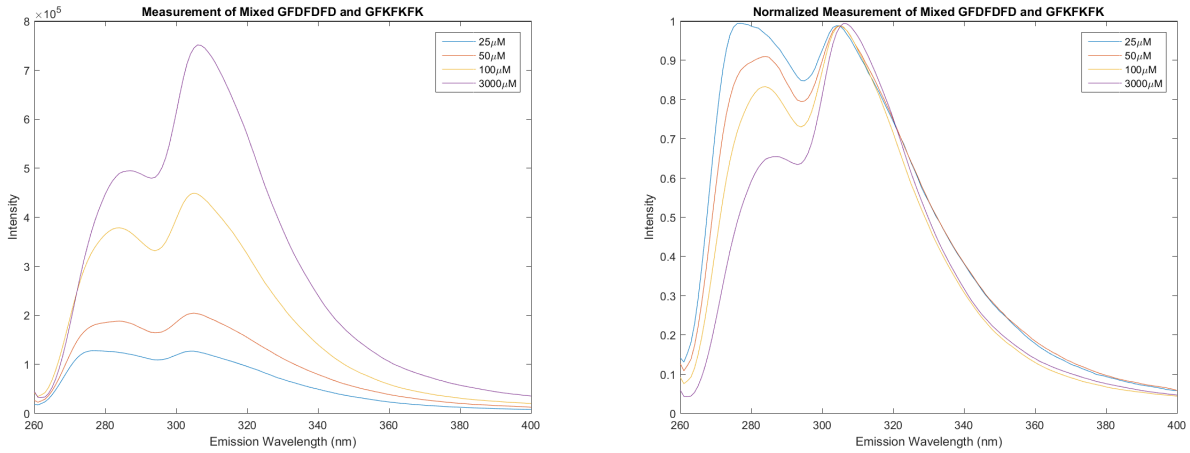

(a) **(b)**

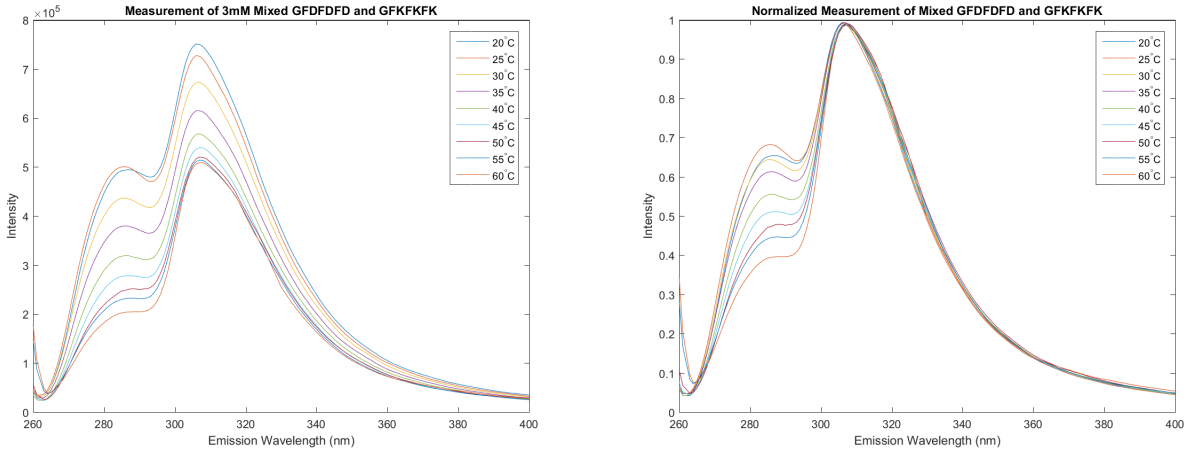

(c) **(d)**

Figure 3.20: (a) Fluorescence spectroscopy measurements of GFX3-Mix peptide solution of concentration 25 μM, 50 μM, 100 μM and 3 mM. 25 μM has two peaks at 304 nm and 275 nm. 50 μM has two peaks at 305 nm and 283 nm. 100 μM has two peaks at 304 nm and 284 nm. 3 mM has two peaks at 306 nm and 286 nm. The peak amplitude increases with temperature. (b) Normalized fluorescence spectroscopy measurements of GFX3-Mix peptide solution of concentration 25 μM, 50 μM, 100 μM and 3 mM. The low wavelength peak is decreasing relative to the main peak as peptide concentration increases. (c) Temperature step fluorescence spectroscopy measurements of GFX3-Mix peptide solution of concentration 3 mM. The signal intensity decreases as temperature decreases. (d) Normalized temperature step fluorescence spectroscopy measurements of GFX3-Mix peptide solution of concentration 3 mM. The low wavelength peak decreases relative to the main peak as temperature increases.

Figure 3.20a shows an increasing signal strength with increasing concentration. Two peaks are observed. The shorter wavelength peak correlates well with the peak observed in the GFD3 measurements. The largest peak is observed at above 300 nm wavelengths. The smallest peak red-shifts with increasing concentration, see Figure 3.20b, similarly to what is observed for GFD3. Figure 3.20c shows decreasing signal intensity with increasing temperature. The signal does not drop linearly with temperature, as seen in Figure 3.21. Figure 3.20d shows that the shorter wavelength peak decreases faster with increasing temperature than the high wavelength peak.

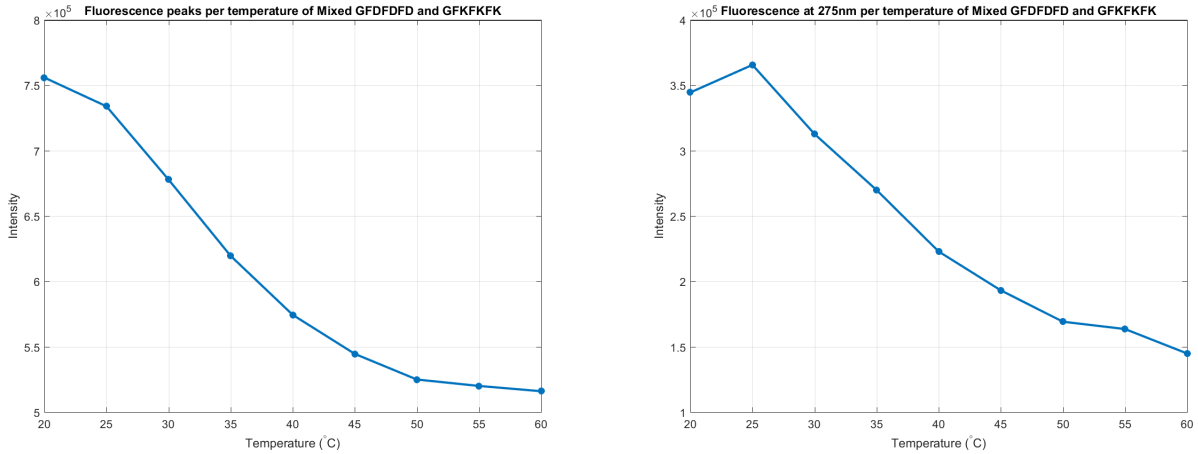

(a) **(b)**

Figure 3.21: (a) Peak fluorescence intensity of 3 mM GFX3-Mix across temperature steps, 20 ˚C to 60 ˚C. Intensity does not drop linearly with temperature $-6606.3T + 2.67 \cdot 10^6$ $R^2 = 0.9222$. T is temperature in Kelvin. (b) Fluorescence intensity at 275 nm of 3 mM GFX3-Mix across temperature steps, 20 ˚C to 60 ˚C. Intensity does not drop linearly with temperature $-5893.9T + 2.08 \cdot 10^6$, $R^2 = 0.9443$. T is temperature in Kelvin

3.4.3 Fluorescence spectroscopy of mixed biphenyl modified GFDFDFD and biphenyl modified GFKFKFK

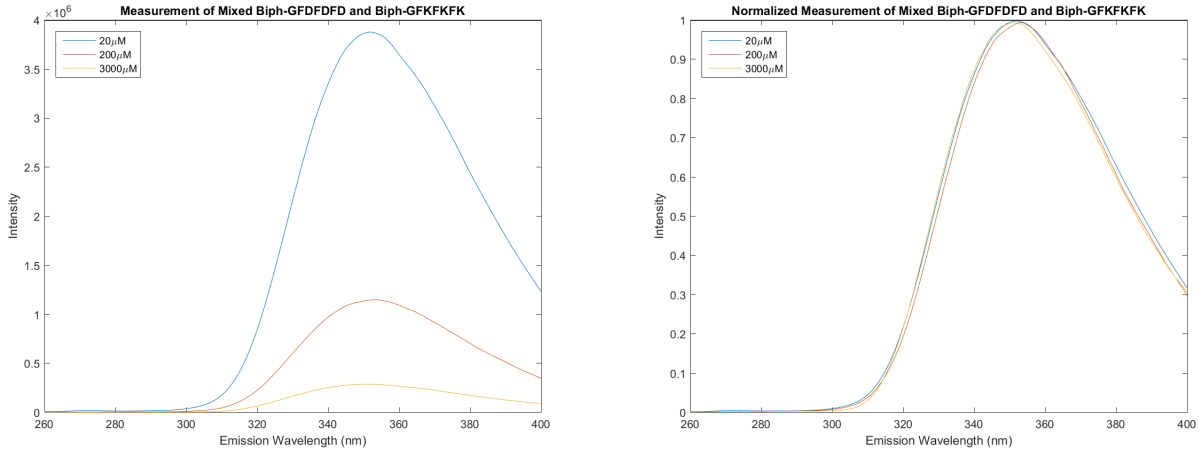

(a) **(b)**

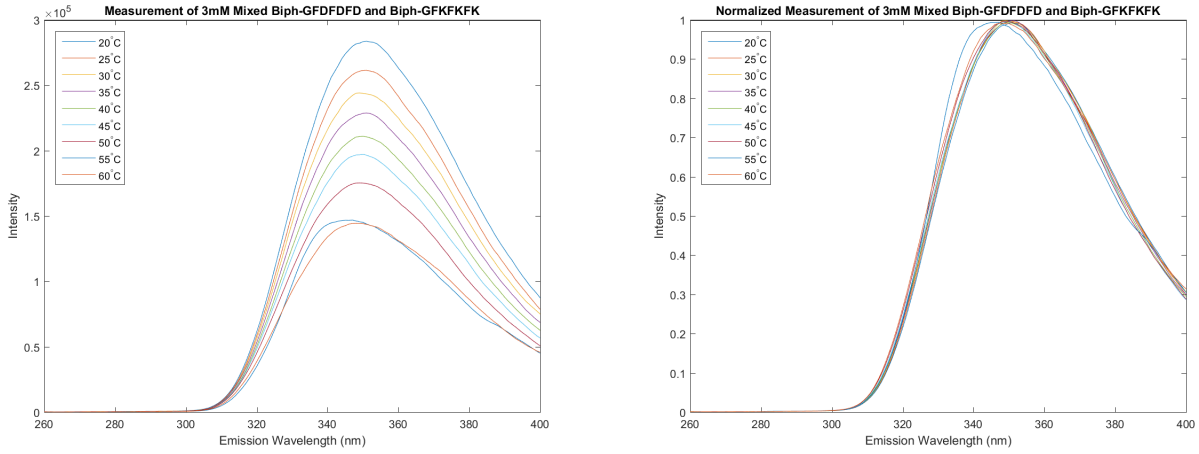

(c) **(d)**

Figure 3.22: (a) Fluorescence spectroscopy measurements of B-GFX3-Mix peptide solution of concentration 20 μM, 200 μM and 3 mM. All peaks are centered at 352. The intensity is proportional to concentration. (b) Normalized fluorescence spectroscopy measurements of B-GFX3-Mix peptide solution of concentration 20 μM, 200 μM and 3 mM. The signals are identical across peptide concentrations. (c) Temperature step fluorescence spectroscopy measurements of B-GFX3-Mix peptide solution of concentration 3 mM. The signal intensity is inversely proportional to temperature. A small blue-shift is observed at 55 °C, but not at other temperatures. (d) Normalized temperature step fluorescence spectroscopy measurements of B-GFX3-Mix peptide solution of concentration 3 mM. Fluorescence profiles are identical across temperature. A small blue-shift is observed at 55 °C.

Figure 3.22a and 3.22b shows a fluorescence signal which increases with peptide concentration, but sustains the same profile. Which suggests that the signal observed is originating from a fluorophore which does not change its environment across concentration. Figure 3.22c and 3.22d shows a fluorescence signal, which decreases with temperature, but sustains the signal profile. Suggesting that increasing temperature does not change the environment of the primary fluorophore. The intensity drops linearly with temperature, which can be seen in Figure 3.23.

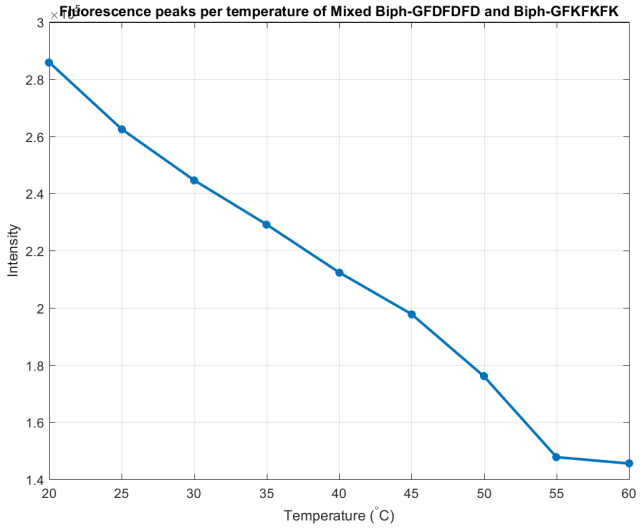

Figure 3.23: Peak fluorescence intensity of 3 mM B-GFX3-Mix across temperature steps, 20 ˚C to 60 ˚C. Intensity drops linearly with temperature $-3579T + 1.33 \cdot 10^6$, $R^2 = 0.9911$. T is temperature in Kelvin

3.4.4 Fluorescence spectroscopy of GFKFKFK

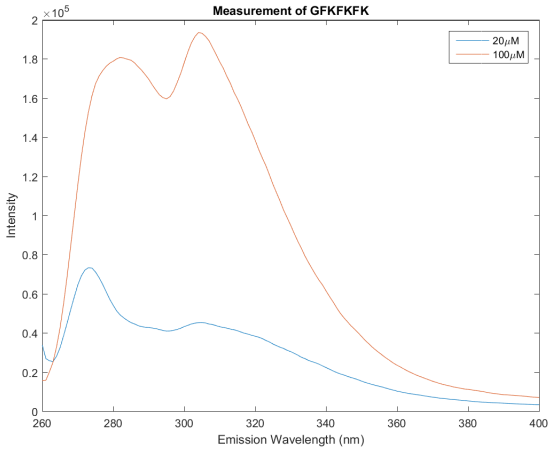

(a)

Figure 3.24: (a) Fluorescence spectroscopy measurements of GFK3 concentration 20 μM and 100 μM. 20 μM has two peaks. The largest at 273 nm, and the smaller at 304 nm. 100 μM has two peaks. The smallest at 283 nm, and the largest at 304 nm.

Figure 3.24 has two peaks. The short wavelength peak red-shifts from 273 nm to 283 as concentration increases. This behaviour is similar to that observed in GFD3 and

GFX3-Mix measurements. The short wavelength peak increases less with increased peptide concentration, similarly to GFX3-Mix. The long wavelength peak does not shift as peptide concentration increases, similar to what is observed in GFX3-Mix.

3.5 Electrostatic Force Microscopy

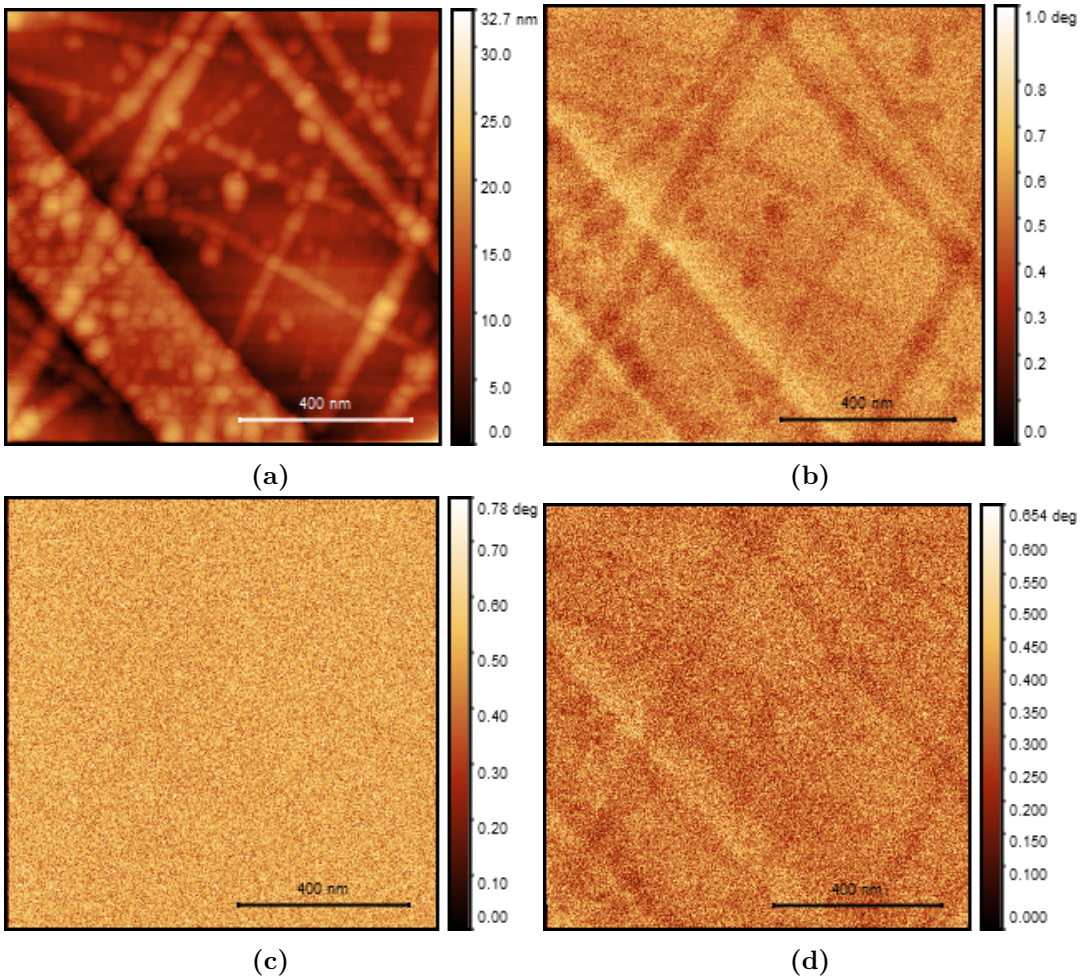

Figure 3.25: ESFM images obtained by two pass technique of GFD3 peptide fibers, on a SiO/Si substrate, and a platinum wire. (a) Height image. Contrast covers structures in the 0-30 nm range. (b) Phase image obtained 20 nm above the sample with a 3V potential. The contrast covers 0-1 degrees range. (c) Phase image obtained 20 nm above the sample with a 0V potential. The contrast covers 0-0.8 degrees range. (d) Phase image obtained 50 nm above the sample with a 3V potential. The contrast covers 0-0.65 degrees range.

Figure 3.25b shows phase contrasts, which correlates well with the structures seen in Figure 3.25a. The contrasts correlate with Figure 3.25d but decrease with height,

which is expected. Figure 3.25c shows no correlation with the observed height structures, which identifies that no crosstalk occurs between the height and phase measurements. The correlation between Figure 3.25b and 3.25a shows that the GFD3 fibres are polarisable across the entire fibre and do not appear to have any charged centres.

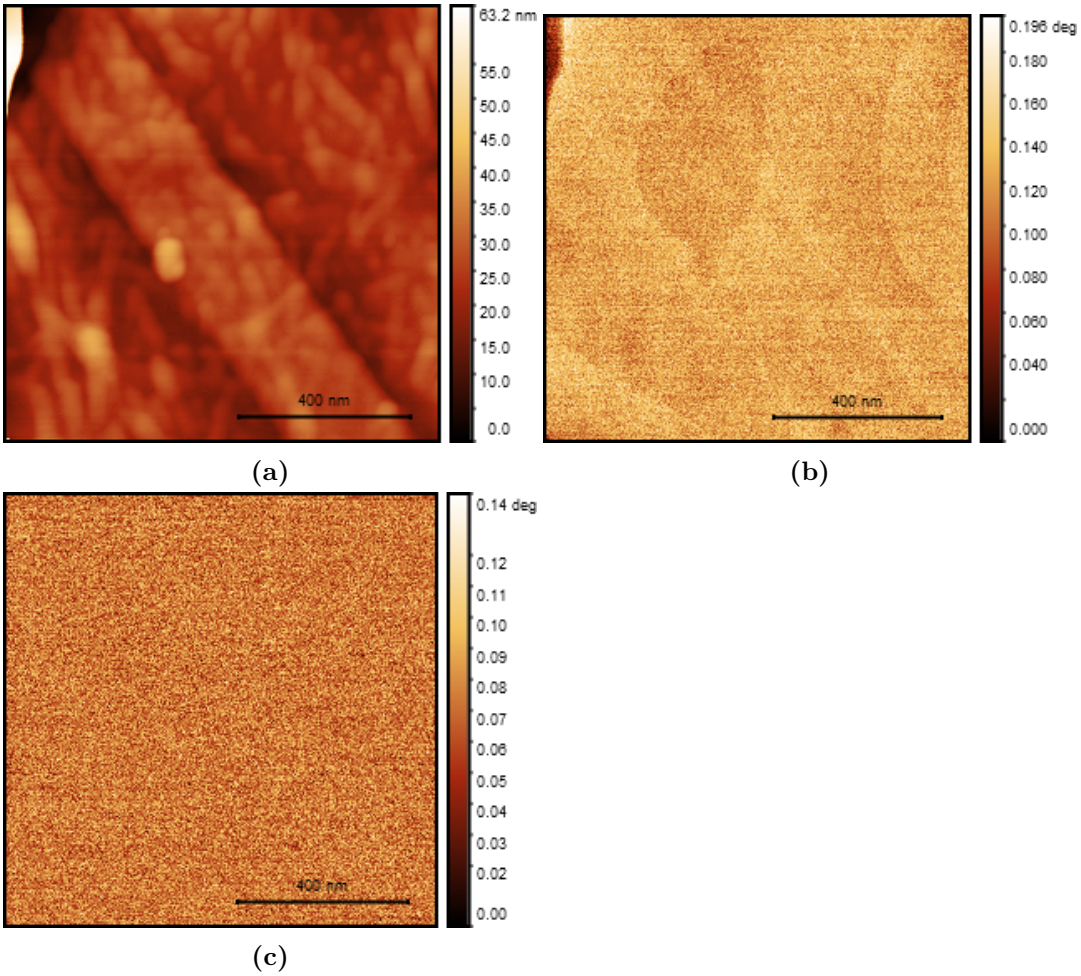

Figure 3.26: ESFM images obtained by two pass technique of GFX3-Mix peptide fibers, on a SiO/Si substrate, and a platinum wire. (a) Height image. Contrast covers structures in the 0-40 nm range. (b) Phase image obtained 20 nm above the sample with a 3V potential. The contrast covers 0-0.2 degrees range. (c) Phase image obtained 20 nm above the sample with a 0V potential. The contrast covers 0-0.14 degrees range.

Figure 3.26b shows phase contrasts, which correlate with the platinum wire seen in Figure 3.26a. Some phase correlation can be seen in the lower left of the image, where large peptide structures are visible. Figure 3.26c show no indication of crosstalk between phase and height measurements. The low resolution of the phase image makes it difficult to identify the polarizability of the fibres. The phase contrast

of the platinum wire is significantly smaller than what is observed in Figure 3.26, which demonstrates, that comparison between ESFM measurements is problematic due to noise.

3.6 Voltage Sweep

Voltage sweeps were performed across a SiO/Si substrate plate with platinum wires with gold contacts, depicted in Section 2.9. In this section only sweeps from -7V to 7V will be revealed. Fibres were deposited locally in the plate centre using the deposition method described in Section 2.6.

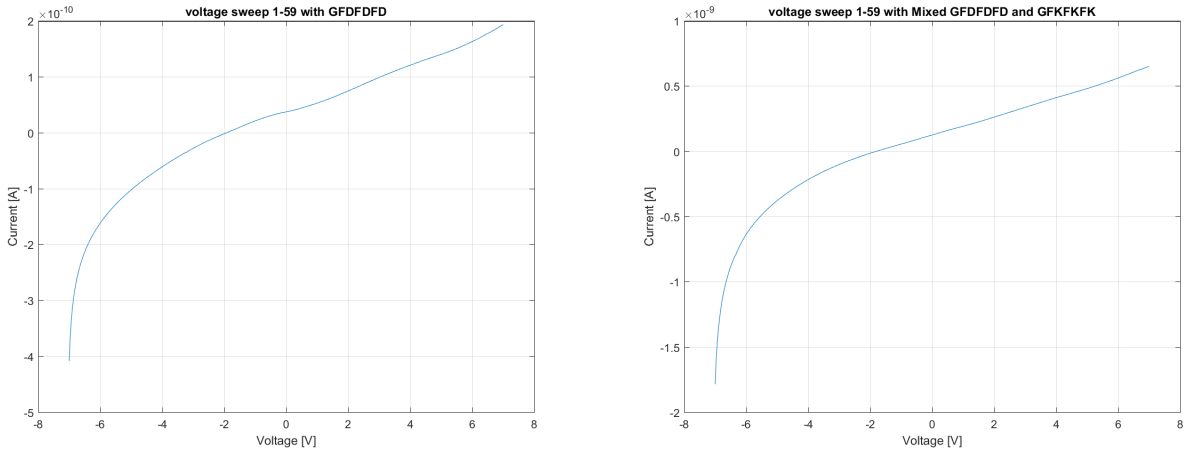

(a) **(b)**

Figure 3.27: (a) Voltage sweep across GFD3 coated platinum wire plate connecting to contacts 1 and 59. The current ranges from -408 pA to 193 pA. (b) Voltage sweep across GFX3-Mix coated platinum wire plate connecting to contacts 1 and 59. The current ranges from -1.78 nA to 650 pA.

Figure 3.27 shows an exponentially decreasing current to voltage relation at currents below 0 A. Currents of 0 A and higher behaves linearly in relation to voltage. The maximum and minimum currents are larger for GFX3-Mix peptide fibres compared to GFD3 fibres.

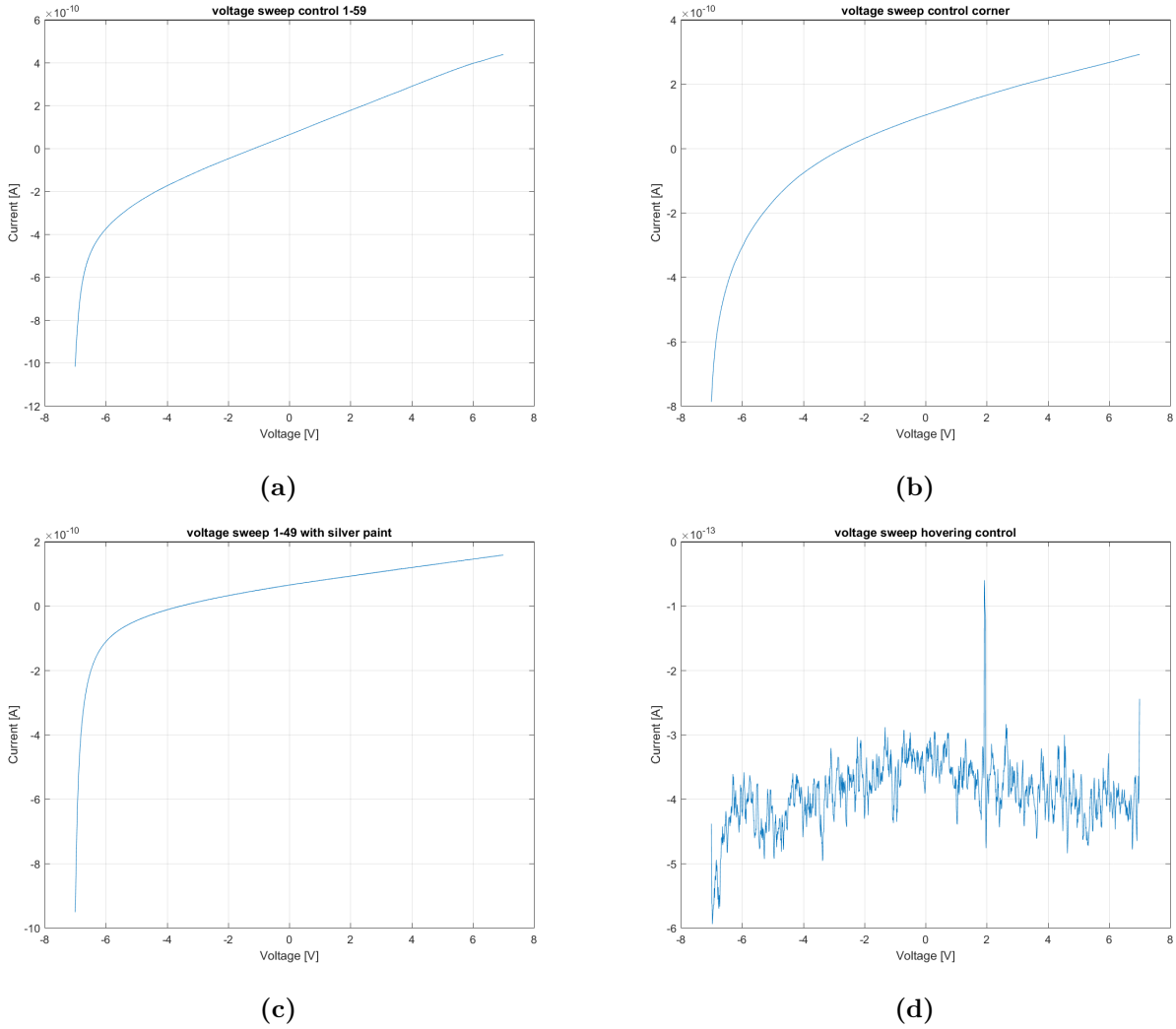

Figure 3.28: (a) Voltage sweep across empty platinum wire plate connecting to contacts 1 and 59. The current ranges from -1.02 nA to 436 pA. (b) Voltage sweep across empty platinum wire plate connecting to gold corners. The current ranges from -787 pA to 291 pA. (c) Voltage sweep across empty platinum wire plate connecting to silver-paint coated contacts 1 and 59. The current ranges from -951 pA to 157 pA. (d) Voltage sweep across empty platinum wire plate with no contact connection. The current is in the femto-Ampere range.

Figure 3.28 shows that empty platinum wire plates are equally conductive to peptide coated plates within a single order of magnitude. The current-voltage relation behaves similarly to peptide coated plates. The relationship is exponential for currents below 0 A, and linear above 0 A. Figure 3.28d shows that no significant current is observed, when the plate is not connected. As such, we can evaluate, that the current observed is not caused by an internal connection error. Figure 3.28b reveals that the current is travelling through the silica plate and not the platinum

wires. Figure 3.28c shows that the current is observed in coated contacts, which ensures that the contact needles are not penetrating the gold contact and SiO layer, indicating that the current is tunnelling through the insulating SiO layer.

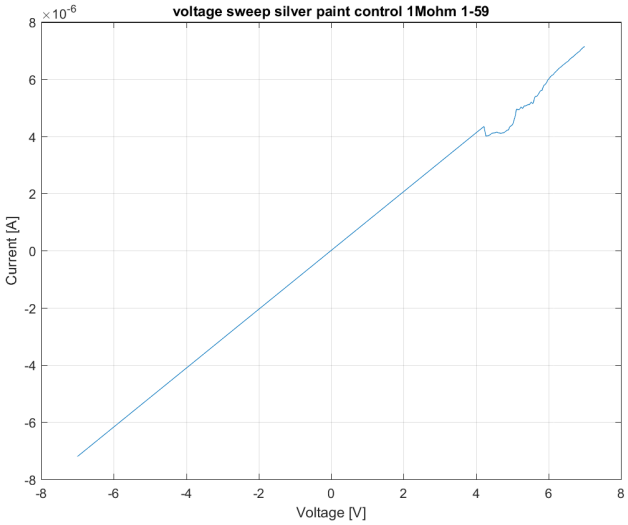

Figure 3.29: Votlage sweep across silver paint covered platinum wire plate connecting to contacts 1 and 59, 1 MΩ external resistance. The current ranges from -7.20 μA to 7.14 μA. The current is linear dependent on voltage. Above 4 V a noise element appears to be introduced.

Figure 3.29 show a linear relationship between current and voltage proportional to the external resistance. This is indicative of no effective resistance comparable to the external resistance. The conduction reveals that the platinum wires and gold contact are not damaged as to affect the conduction across the plate.

3.7 Simulation

In the following section, MD simulations will be presented for non-modified peptides. Water molecules are hidden and peptide side groups transparent for simplification. The reference pressure is set to 1 bar. Simulations presented span 200 ns. Simulations are performed with a set temperature of 300 K.

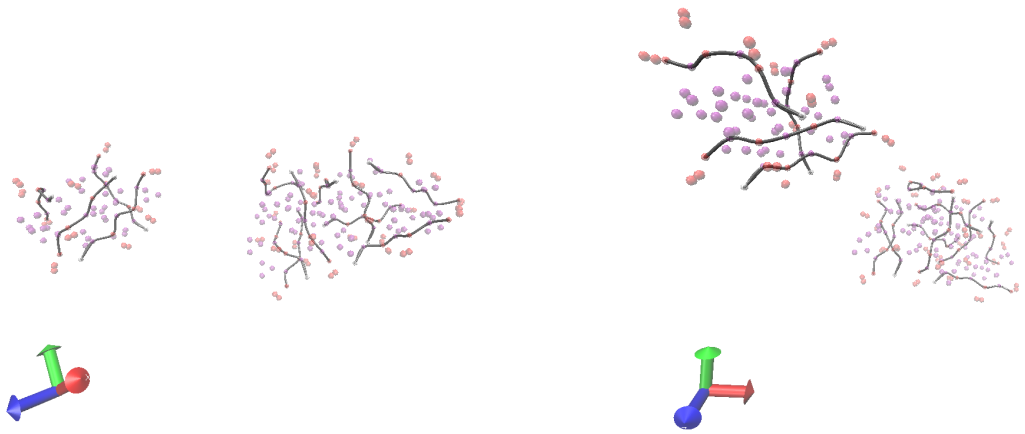

(a) **(b)**

Figure 3.30: CG MD simulation of 13 GFD3 molecules in polarized water, constrained by a 7 nm x 5 nm x 5 nm box. Simulation time 200 ns. white beads are Gly, purple beads are Phe, and red beads are Asp. The peptide forms two distinct clusters. Some backbone alignment is observed in the smallest cluster.

MD simulations of GFD3, seen in Figure 3.30, do not appear to form β-amyloid fibrils, but forms peptide clusters. A few peptides align backbones in a manner expected to form β-amyloid fibrils, but such behaviour is limited to 2 monomer structures. The primary drive for cluster formation appears to be hydrophobicity of phenylalanine. The aligned backbones are ordered antiparallel.

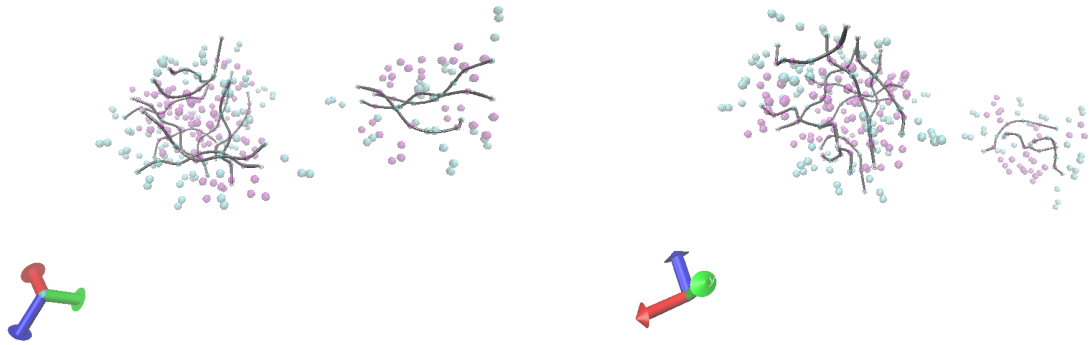

(a) **(b)**

Figure 3.31: CG MD simulation of 13 GFK3 molecules in polarized water, constrained by a 7 nm x 5 nm x 5 nm box. Simulation time 200 ns. white beads are Gly, purple beads are Phe, and cyan beads are Lys. The peptide forms two distinct clusters. Ordered backbones are observed in both clusters. The smaller cluster forms aligned backbones. The larger cluster forms a hydrophobic core.

Figure 3.31a reveals an ordered tubular cluster structure. The driving force for this structure appears to be hydrophobicity of phenylalanine, as a well defined hydrophobic core is formed. The smallest cluster appears to align peptide backbones in a fibril-like manner in Figure 3.31a, but Figure 3.31b reveals that no such ordering occurs.

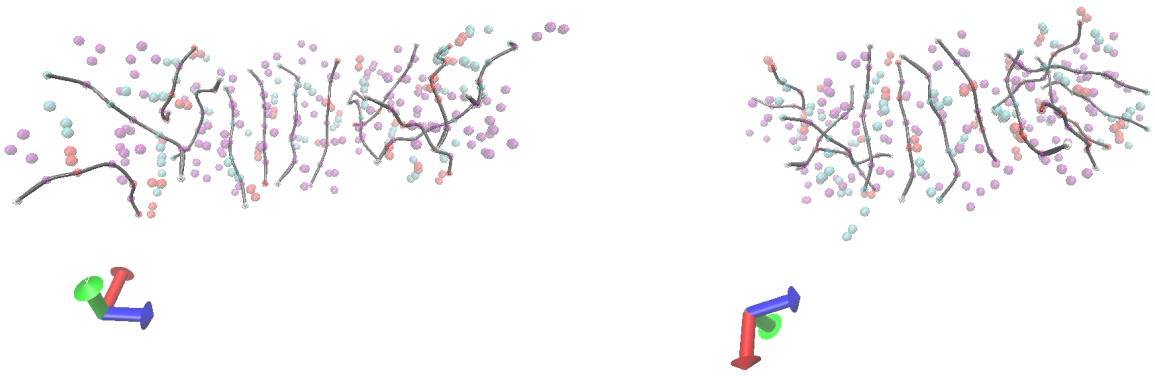

(a) (b)

Figure 3.32: CG MD simulation of 7 GFD3 and 7 GFK3 molecules in water, constrained by a 7 nm x 5 nm x 5 nm box. Simulation time 200 ns. white beads are Gly, purple beads are Phe, red beads are Asp, and cyan beads are Lys. A single elongated structure is formed with some degree of ordered backbones.

Figure 3.32 shows an elongated structure, which has some peptide backbone alignment. This alignment is prevalent in the centre of the structure but appears to break down at the structure termini. The structure, while not well ordered, behaves such, that peptide fibres are expected to be formed by this peptide combination. Aligned backbones do not order specifically parallel or antiparallel.

3.8 Peptide Hydrogellation

Peptide solutions of GFD3 and GFX3-Mix formed hydrogels at concentrations of 3 mM and 2 mM respectively. These gels are not extremely rigid but can sustain their form in Greiner tubes, as shown in Figure 3.33, where gels formed in Greiner tubes are turned upside down. Gels formed within 12 hours after dissolution. These gels liquify upon stress, such as shaking, impact or pipetting, but will reform to a gel overnight.

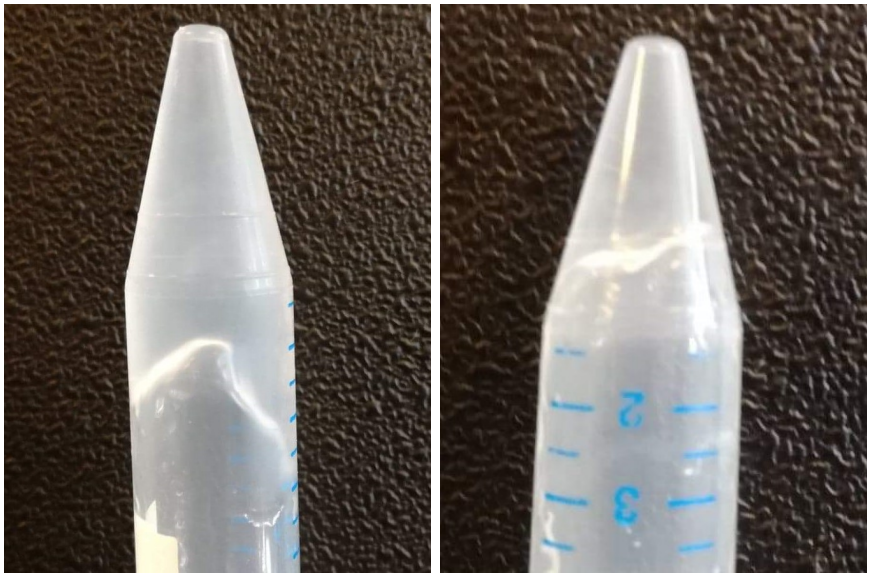

(a) **(b)**

Figure 3.33: (a) Hydrogel formed by 3 mM GFD3 peptide solution. (b) Hydrogel formed by 3 mM GFX3-Mix peptide solution.

Chapter 4

Discussion

This chapter will be divided into two main sections. The first section will be discussing specific methods, limitations and problems regarding the specific setup. The second section will be discussing results regarding each peptide.

4.1 Setup review

Peptide solutions used in this project are not freshly made, but extracted from stock solutions. The age of the sample can be affecting the results obtained in each experiment. While fresh samples are likely ideal to test, dissolving the peptide proved a tedious task involving several hours of ultrasound treatment. The procedure used in this report proved to have a non-zero failure rate for producing high concentration peptide solutions. As such, making new solutions for each experiment was impractical.

Throughout this project, the solvent used for peptide solutions is 95 % water, 5 % acetonitrile. Acetonitrile was used due to its low absorption in the UV range (180 nm - 300 nm). Acetonitrile concentrations above 5 % were not used in order to maximize the hydrophobic driving force for fibre self-assembly. Higher acetonitrile concentrations could allow higher peptide concentrations than investigated in this report, which could allow increased fibrillation rates. However, within the 5 % acetonitrile limitation, peptide concentrations above 3 mM could not be consistently produced, and have not been investigated.

4.1.1 CD

Circular Dichroism is most commonly used to evaluate secondary protein structure composition. However, as secondary protein structures are not present in the peptide super structures produced in this report, using known secondary structure CD spectra for data analysis is not appropriate. Evaluating which structure is observed by CD spectroscopy can be extremely difficult without complex CD-spectrum modelling.

As this is not within the scope of this project, any evaluations concerning structure formation through this method are inconclusive. Correlation between CD-spectra and AFM imaging can provide qualitative evaluations of CD-spectra characteristics, which are indicative of fibril formation.

CD spectroscopy was performed using a predetermined set of peptide concentrations. This set of sample concentrations was chosen as a suitable scan set to identify structure formation tendencies. This concentration set is not suitable for investigation of a precise critical fibrillation concentration, and therefore no such property will be determined with accuracy.

4.1.2 AFM

AFM measurements were performed on SiO surfaces, after sample deposition using the method described in Chapter 2.6. This deposition method is dependent on solvent evaporation, which induced an elevated effective peptide concentration across the surface. As such, structures observed in this report originate from samples with higher effective concentrations than used in CD-spectrometry and fluorescence spectrometry experiments. It should, however, be noted, that concentrations larger than deposition concentrations are not easily achieved, even though heating and ultrasound treatment. As such, this criticism does not incriminate the results obtained. However, if structures produced at lower concentrations are investigated, another deposition method is essential.

In this project, the fibres produced were not statistically investigated. Counting and evaluating a significant sample to achieve such is time-consuming and would significantly limit the set of peptides used. Evaluations of peptide sizes are based on a limited data set and do not hold high statistical validity. If fibre-formation and fibre behaviour are highly prioritized in further studies, a statistical analysis of fibre height, width and length should be performed.

4.1.3 ESFM

Electrostatic force microscopy images achieved in this report are poorly resolved, compared to atomic force microscopy images. During these measurements, high-resolution AFM images were achieved, however, upon mode shift height image resolution drops drastically. As such, the quality of the analysis is significantly lower, than what has been achieved in the literature. Whether this phenomenon is a system error or user error has yet not been identified.

4.1.4 Fluorescence

During all temperature gradient fluorescence spectroscopy, the signal intensity has been observed to drop as temperature increases. The quenching observed in each

peptide can either be static or dynamic. The current data does not allow for the identification of quenching type. However, absorption data across the temperature gradient could provide further insight. Such measurements should have been performed. The quenching observed in all temperature gradient experiment is continuous rather than abrupt. This fact, along with no apparent shift in peak fluorescent wavelength suggests that no drastic conformational change has been observed in these experiments. The structures appear stable across the temperature gradient. The decreasing fluorescent intensity can be speculated to be caused by solvent-fluorophore interactions already present within the structure. Phenylalanine has been observed to sustain weak hydrogen bonds with water [33], which are likely strengthened in the excited state induced by the emission wave. A quenching mechanism of water is the rupture of hydrogen bonds with the excited fluorophore [34]. Increased temperature leads to increased water mobility, which could cause an increase in replacement ratios of water molecules to form new hydrogen bonds with the fluorophore after hydrogen bond rupture. This would lead to increased quenching and could explain the results observed.

4.1.5 Simulation

Molecular dynamics simulations have been criticized for not implementing π-π interactions properly, which have caused inaccurate simulations of structures formed predominantly due to these interactions. After explicitly implementing such interactions in simulations, increased accuracy of structures, such as Trp-zippers, has been achieved [35]. These interactions have not been implemented in this report, as these have yet to be incorporated in Martini force fields. As such, the structures simulated in this report are not accurately considering the influence of π-stacking on the peptide superstructure formation. The proportional influence of hydrophobic interactions is likely to be overemphasized in these simulations. Further, theoretical work regarding peptide fibrillation, by π-stacking, should implement π-π-interaction terms in MD-simulations for accurate predictions.

MD-simulations have not been performed above 400 ns. Longer simulations could produce more accurate data and should be investigated. An increase in molecule number could provide significantly different simulation results, as a minimum peptide number could exist for stable fibre formation. If such a number is larger than 13, these simulations cannot accurately predict fibre formation in a real system. A larger simulation could prove fruitful regarding such considerations.

4.2 Evaluation of results

GFD3 and GFX3-Mix solutions were observed to form hydrogels in this report. Each of these peptides formed peptide fibres observed through AFM measurements. The literature on peptide hydrogels attributes the gel formation to peptide fibre networks.

These solutions will act as models for peptide fibre formation throughout this section.

GFD3 solutions of 50 μM and above forms a negative peak in CD-spectra at 236-238 nm. The same is observed in GFX3-Mix solutions of 50 μM. This energy is low for amide bond transitions and is usually only inhabited by the $n \rightarrow \pi^*$ transition in apolar solvents [22]. This measurement is performed in water, which eludes to the signal arising from amide groups in hydrophobic cores with no hydrogen bonds to other peptide groups in the ground state. This could be explained by the formation of aggregates, driven by π-stacking, forming cores with low degrees of hydrogen bonding. Upon fibre formation, known to occur at high concentrations, the signal diminishes since these cores are no longer present. Increased water exposure upon fibre formation correlates well with the fluorescence signal observed for GFD3, in the which phenylalanine signal red-shifts with increasing peptide concentration. The red-shifting is most likely caused by exposure to the polar solvent upon fibrillation. However, the red-shifting is observed even at low peptide concentrations, where the negative CD maxima are still increasing linearly with concentration, which should not be allowed alongside increasing solvent exposure. The fluorescence data from GFX3-Mix does not reveal a significant red-shift with increasing peptide concentration. The main fluorescence peak is, however, already at long wavelengths, suggesting that the phenylalanine is already exposed to water or another dipole, which decreases the energy of the S_1-state.
Assigning an amide transition to the negative maxima observed in these CD-spectra is not a trivial exercise, which could allude to the peak being induced by a transition found in phenylalanine. However, aromatic transitions are most often found at higher wavelengths [22]. Understanding what is inducing this signal could prove interesting, as the negative maximum at 230-240 nm is most profound in GFD3, GFX3-Mix and B-GFX3-Mix, which are fibre-forming peptides, suggesting a relation between the peak and fibre formation. No literature correlating a negative maximum in this range with peptide fibre-formation have been found.

A positive peak is observed at 220-230 nm for GFD3. $n \rightarrow \pi^*$ transition typically occurs in this range, however, self-assembling peptide studies have assigned peaks at these wavelengths to $\pi \rightarrow \pi^*$ transitions [1]. Positive bands in this wavelength have been observed for β-turn forming aromatic peptides, but attributing this peak to the formation of β-sheet-like structures does not correlate with our data since the same peak is observed in GFK3, F-GFK3 and GFX3-Mix, which do not all form fibre structures.
No repeating superstructure is found in samples, producing these signals. In GFD3, F-GFK3 and GFX3-Mix, the signal red-shifts with increasing concentration, which is indicative of stabilization of the transition, resulting in the decreased transition energy. Each of these three samples produces ordered structures in AFM-imaging, suggesting that, while structures formed are different, the driving inter-molecular structure is similar. Which eludes to red-shifting of $\pi \rightarrow \pi^*$ transition energies, be-

ing indicative of superstructure formation.
As such, speculations can be made, whether the internal molecular structure of fibres formed by B-GFX3-Mix is significantly different than fibres formed by the original peptide variants, as this positive peak is not observed.

Biphenyl modified peptides are probably more prone to forming parallel β-strand-like structures due to the aromatic biphenyl group at the N-terminus. An antiparallel alignment will not allow π-stacking of biphenyl residues, while parallel alignment will. Antiparallel backbone alignment is more energetically favourable in β-sheet structures and is assumed to be the most likely backbone alignment in non-modified fibres, which correlates with MD simulations, where short sequences of antiparallel backbone alignments can be seen.
The positive CD-spectra peak at 220-230 nm, could be a phenomenon correlated specifically to antiparallel peptide backbone formation.
Studies, which observe this peak in β-structure forming aromatic peptides, are investigating antiparallel backbone structures. A less energetically favourable backbone formation could explain, why the biphenyl modified peptide fibres produced are generally shorter than the fibres produced by the original peptide structure.
The B-GFX3-Mix sample shows a significantly different fluorescence spectrum than other samples. The long wavelength peak is very broad, and quite intense, which forced the aperture to be almost fully closed for proper data sampling to be achieved. No other samples had the aperture closed to this extent. This leads the group to believe, that the signal observed does not originate from phenylalanine, but an aromatic group with higher quantum yield and a longer wavelength fluorescence signal. Biphenyl fits these parameters [23, 36, 23] and the observed signal is likely drowning the phenylalanine signal. As such, little can be deduced regarding the phenylalanine environment through these fluorescence measurements. A cutoff could be utilized to address this issue, but due to the broad signal of biphenyl, the signal bleed into the phenylalanine range is likely to be disruptive, despite the cutoff. Biphenyl modified peptides are not suitable for fluorescence investigations through phenylalanine excitation.

AFM imaging of peptide fibres shows wide flat structures. The wide structures are expected to arise from cylindrical fibres flattening during deposition to increase surface-substrate area. Peptide fibre widths are likely slightly overestimated, which is a common error in AFM-measurements. The fibre widths measured are between 40 nm and 200 nm, which is significantly larger than the expected inaccuracy. Fibre circumference can be evaluated, by assuming an elliptical structure using fibre height and width as diameters. GFD3 fibres measure from 178 nm to 444 nm in circumference. GFX3-Mix fibres measure from 755 nm to 889 nm. B-GFX3-Mix fibres measure from 489 nm to 533 nm. While these measurements carry no statistical value, they provide insight into the general fibril thickness in solution. GFD3 fibres are significantly thinner than the other fibres formed, which can be explained

by the positive-charged residue. Peptide-ribbons formed by GFD3 will have net positively charged surfaces, which will increase the energy of fibrils and fibres, causing decreased fibril widths. Peptide ribbons formed by GFX3-Mix will likely alternate charged groups in an ABAB sequencing, producing a net zero surface charge. These fibrils would be expected to be wider than mono-peptide fibrils. Mixed biphenyl modified peptide fibrils are thinner than the mixed non-modified fibril, which can be explained by the parallel backbone formation, which increases strain in the peptide tape, creating more rigid ribbons, which limits the fibril width.

Fluorescence emission of phenylalanine is located around 282 nm, which makes the emission signal at 300-315 nm observed for non-modified peptide samples quite interesting. Some literature has attributed this emission signal to π-stacking [37]. However, for GFD3, the signal blue-shifts and decreases, relative to the 275 nm peak, with fibre-forming concentrations, which does not fit with that conclusion. The peak is maintained by the GFX3-Mix sample, which defines a fundamental structural difference related to this peak. The peak could be induced by local e-fields, produced by charged residues, which stabilize the S_1-state and red-shifts the fluorescence signal. Tryptophan is prone to red and blue-shifting induced by local charges from charged residues, however, this phenomenon is caused by shifting of the electron cloud density between aromatic rings [38], and does not explain, why such a phenomenon could be observed in phenylalanine.
If the high-wavelength signal is produced by charge-induced stabilization, the loss of the signal with increasing concentrations of GFD3 could correlate with tape-ribbon transitions. The ribbon structure would place the fluorophore between two equal point charges and removing the effective E-field.
The maintained signal observed in GFX3-Mix could be caused by the ABAB structure, in which local dipoles are formed between charged residues. These aligned dipoles could form local E-fields causing a coherent field parallel with the fibre, which maintains the S_1-state stabilization. These speculations could be further investigated, by introducing mutations in the peptides, to further investigate the effect of charged groups.

However, as phenylalanine is a non-polar fluorophore, it is not very sensitive towards dipole relaxation in the surrounding environment [23], which is coherent with the low degree of red-shift found at 280 nm. It is significantly more likely, that the >300 nm peaks are caused by inter-phenylalanine angles, relaxing the S_1 state. The changed intermolecular angles could be caused by antiparallel backbone formation.
GFD3 is observed in MD-simulations to form antiparallel backbone alignments, while GFX3-Mix forms both antiparallel and parallel backbone alignment. When longer peptide tapes are formed, one alignment can be expected to become more prevalent. At low peptide concentrations, short tapes are formed in all peptide solutions. Short peptide tapes are likely to not be well structured, and equal distribution of backbone alignment is expected.

As concentration increases, tapes become more ordered, and GFD3 will form more antiparallel backbone structures, while GFX3-mix will still form both, but this group expects parallel backbone structures to be more energetically favourable and dominant in high peptide concentrations.
If the 280 nm peak is associated with antiparallel backbone structures and the >300 nm peak is associated with parallel structures, one would expect fluorescence spectra similar to those observed in this report. This is in agreement with the CD-data, which correlates the positive band at 220-230 nm with antiparallel backbone formation. The signal is observed for GFX3-mix but decreases with concentration, indicating diminishing antiparallel backbones, as speculated from fluorescence spectroscopy.
As such we can argue that a positive CD-spectra at 220-230 nm is indicative of antiparallel peptide tape formation and a phenylalanine fluorescence emission at >300 nm is indicative of parallel peptide tape formation.
Additionally, it appears quite clear, that GFD3 is prone to antiparallel backbone formation, and GFX3-Mix forms both parallel and antiparallel backbone formations, but parallel backbones are more prevalent at high peptide concentrations. B-GFX3-Mix forms parallel backbone-conformations as well.

AFM imaging of B-GFD3 shows fibre development. These fibres are produced in an 85 % acetonitrile, 15 % water solution, which makes a comparison to other fibres skewed, as the environmental effects are significantly different. Development of these fibres reveals, that interaction with polar solvent are unlikely to constitute a main driving force for structure formation, as indicated by MD-simulations.

F-GFK3 forms circular structures as well as dispersed aggregates. Circular structures are not commonly observed in studies of self-assembling aromatic peptides. Other ferrocene modified peptide samples did not form any organized structures, relating these structures to the GFK3 variant specifically. CD spectroscopy of the sample reveals a positive and negative peak at 223 nm and 236 nm, respectively. These peaks correlate well with the peaks, which have been associated with fibrillation in this report. Suggesting that the internal peptide organisation of the rings is similar to the fibres. The ring structures are significantly larger than produced peptide fibres, and curves significantly more than fibres produced in this report. If the internal peptide organisation is similar to peptide fibres, tape-like structures form the building blocks of these structures. As such different self-assembling mechanisms could be the driving the formation of these structures. These structures warrant further investigation, but this has not been performed in this project.

ESFM images show a negative phase shift above GFD3 fibres, which is induced by the polarization of the fibre [39]. Polarizability of DNA-wires has been used as a qualitative evaluation of intermolecular charge mobility. These measurements indicate that charge transport is possible. Whether longitudinal charge transport is

possible, demands further study. Such an experimental setup could be inspired by [40], which uses a metal coated AFM-tip to form a capacitor between the tip and DNA-molecule, which is connected to a gold contact. The group has developed clever methods for contact-less detection of conductive properties as well [40]. A double tip AFM could also be utilized to identify charge transfer across a peptide wire, by applying a tip-bias voltage.

GFX3-Mix fibres do not show the same degree of polarization. But a comparison between the platinum wires in each measurement reveals a significantly lower resolution. Small indications of fibre polarization can be found on the sample, which indicates that better resolution imaging might provide similar results to GFD3 fibres.

Biphenyl modified peptide fibres have not been investigated through ESFM. ESFM measurements are timeconsuming and modified fibres were produced late in the project. These measurements were cut due to time constraints. This is not ideal as the modifications were introduced to increase charge transport properties.

Other groups have used E-fields to order polarizable peptide fibres [2]. It is safe to assume, that GFD3 fibres can be ordered in a similar manner.

No fibres have been shown to carry charges between platinum wires. This does not disqualify the fibres as potential molecular wires. Contact types can greatly alter the charge transport potential of DNA-molecules, and it could be argued that such could be the case in these experiments. Conductivity across the contact-fibre interface is not known, and low electron tunnelling between the platinum wire and peptide fibre could be inhibiting of electron transport. Different contacts could allow electron transport.
DNA-molecules have been speculated to loose conductivity when adsorbed on a surface due to loss of structural integrity. The fibres measured in AFM-imaging have deformed compared to the expected structure in solution, which can have affected fibre conductivity. These measurements are inconclusive of peptide fibres as conductive molecular wires. Adsorbed fibre-structures on platinum wires have not shown conductivity in this report.

Biphenyl modified peptide fibres have not been investigated through voltage-sweep experiments due to poor fibril location control.

Voltage sweep measurement shows differing currents passing through the silica plate. It is worth noting, that between measurements, the silica plate was cleaned, using ultra-sound treatment. The charge transport across the SiO-layer indicates damage within the layer. Ultrasound treatment of the plate is likely to increase any damage to the insulating, crystalline, layer, which is likely to have caused the increasing current. Voltage sweep measurements were performed in the following order of GFD3-coating,

GFX3-Mix-coating and empty control sample, which show increasing currents, correlating well with the aforementioned hypothesis.
If the SiO-layer is damaged, electronic noise may have been affecting the ESFM-measurements. GFD3 fibres were studied by ESFM before any voltage sweep measurements were performed, and hence before much ultrasound treatment of the plate had occurred. ESFM study of GFX3-Mix fibres was performed after all voltage-sweep measurements, and the silica plate had been exposed to significant ultrasound treatment. A "leaking" SiO layer is a possible explanation for poor ESFM measurements, and a new SiO/Si wafer should have been used.

Chapter 5

Conclusion

Two primary peptide designs were investigated in this project. The peptides were designed to fibrillate alone and fibrillate in an ABAB conformation when in solution together. GFD3 formed well-defined peptide fibrils. GFK3 did not form fibrils to the same extent, but some fibre formation has been identified. The peptides form fibres, when in solution together. B-GFX3-Mix forms defined peptide fibres as well, while some fibrillation is observed by B-GFD3. GFD3 forms antiparallel backbone conformations, while GFX3-Mix forms primarily parallel backbone conformations. B-GFX3-Mix forms parallel backbone conformations as well.
High concentration GFD3 and GFX3-Mix peptide fibres form hydrogels, which liquify upon stress. Biphenyl modified peptide fibres were not observed to form hydrogels.
Peptide fibres are up to several μm long and generally straight. Charged residues are likely to affect peptide fibre width. Biphenyl modified peptide fibres are shorter than non-modified fibres.
Structures are stable up to 60 °C. Biphenyl-modified peptides cannot be directly investigated through fluorescence spectroscopy, and a fluorescence probe must be utilized.
Adsorbed non-modified peptide fibres are polarizable, but have not shown longitudinal charge transport properties between platinum wires. Further investigation into longitudinal charge transport is encouraged.
F-GFK3 forms ring structures of 1 μm diameter, but no further insight have been achieved.

Bibliography

[1] Morten Slyngborg, Dennis Achton Nielsen, and Peter Fojan. The physical properties and self-assembly potential of the rfffr peptide. *ChemBioChem*, 17(21):2083–2092, sep 2016.

[2] Kai Tao et al. Self-assembling peptide semiconductors. *Science*, 358(6365), nov 2017.

[3] Gideon I. Livshits et al. Long-range charge transport in single g-quadruplex dna molecules. *Nature Nanotechnology*, 9:1040–1046, okt 2014.

[4] Marks TJ. Electrically conductive metallomacrocyclic assemblies. *Science*, 227(4689):881–889, feb 1985.

[5] P. Turek et al. A new series of molecular semiconductors: phthalocyanine radicals. *J. Am. Chem. Soc.*, 109(17):5119–5122, aug 1987.

[6] C. F. Van Nostrum and R. J. M. Nolte. Functional supramolecular materials: self-assembly of phthalocyanines and porphyrazines. *Chemical Communications*, pages 2385–2392, 1996.

[7] T. Aida, E.W. Meijer, and S.I. Stupp. Functional supramolecular polymers. *Science*, 335(6070):813–817, feb 2012.

[8] R.A.Marcus and Norman Sutin. Electron transfers in chemistry and biology. *Biochimica et Biophysica Acta (BBA) - Reviews on Bioenergetics*, 811(3):265–322, aug 1985.

[9] Jay R. Winkler et al. Electron tunneling in biological molecules. *Pure Appl. Chem*, 71(9):1753–1764, 1999.

[10] Heinz-Bernhard Kraatz et al. Electron transfer through h-bonded peptide assemblies. *J. Phys. Chem.*, 108(52):20164–20172, dec 2004.

[11] Michael N. Paddon-Row. Superexchange-mediated charge separation and charge recombination in covalently linked donor–bridge–acceptor systems. *Australian Journal of Chemistry*, 56(8):729–748, jul 2003.

[12] Joshua Jortner et al. Charge transfer and transport in dna. *Proc. Natl. Acad. Sci. USA*, 95(22):12759–12765, oct 1998.

[13] Mohammad R. Seyedsayamdost et al. Site-specific insertion of 3-aminotyrosine into subunit 2 of e. coli ribonucleotide reductase: Direct evidence for involvement of y730 and y731 in radical propagation. *J. Am. Chem. Soc.*, 129(48):15060–15071, nov 2007.

[14] N. Boden et al. Engineering of peptide b-sheet nanotapes. *J. Mater. Chem.*, 7(7):1135–1145, 1997.

[15] Charles J. Bowerman and Bradley L. Nilsson. Review self-assembly of amphipathic b-sheet peptides: Insightsand applications. *Peptide Science - American Peptide Society*, 98(3):169–248, may 2012.

[16] N. Boden et al. Hierarchical self-assembly of chiral rod-like molecules as a model for peptide β-sheet tapes, ribbons, fibrils, and fibers. *Proceedings of the National Academy of Sciences of the United States of America*, 98(21):11857–11862, oct 2001.

[17] Antara Dasgupta, Julfikar Hassan Mondal, and Debapratim Das. Peptide hydrogels. *RSC Advances*, 24:9117–9149, 2013.

[18] ACD/ChemSketch (Freeware). 2018.2.1. Advanced Chemistry Development, Inc., Toronto, On, Canada, www.acdlabs.com, 2018.

[19] Didier Astruc. Why is ferrocene so exceptional? (1), oct 2016.

[20] K. J. Jensen, P. Tofteng Shelton, and S. L. Pedersen. *Peptide Synthesis and Applications*. Humana Press Inc., second edition, 2013. page: 1-18.

[21] Norma J. Greenfield. *Nat protoc.*, 1(6):Nat Protoc., 2006.

[22] Reerama N and Woody RW. *Methods Enzymol.*, 383(3):318–351, 2004.

[23] Joseph R. Lakowicz. *Principles of Fluorescence Spectroscopy*. Springer, third edition, 2006. page: 1-12, 205-212.

[24] Diana El Khoury. Towards the use of electrostatic force microscopy to study interphases in nanodielectric materials, 2017.

[25] D. Frenkel and B. Smit. *Understanding Molecular Simulation*, volume v. 1. Elsevier Science & Technology, second edition, 2001.

[26] D. C. Rapaport. *The Art of Molecular Dynamics Simulation*. Cambridge University Press, second edition, 2004.

[27] J. Barnoud and L. Monticelli. Coarse-grained force fields for molecular simulations. *Methods in molecular biology (Clifton, N.J.)*, 1215:125–149, 2015.

[28] S.J. Marrink and D.P. Tieleman. Perspective on the martini model. *Chemical Society Reviews*, 42(16):6801–6822, 2013.

[29] David Nečas and Petr Klapetek. Gwyddion: an open-source software for SPM data analysis. *Central European Journal of Physics*, 10:181–188, 2012.

[30] S. Pronk, S. Páll, R. Schulz, P. Larsson, P. Bjelkmar, R. Apostolov, M.R. Shirts, J.C. Smith, P.M. Kasson, D. Van Der Spoel, B. Hess, and E. Lindahl. Gromacs 4.5: a high-throughput and highly parallel open source molecular simulation toolkit. *Bioinformatics*, 29(7):845–854, 2013.

[31] W. Humphrey, A. Dalke, and K. Schulten. Vmd: Visual molecular dynamics. *Journal of Molecular Graphics*, 14(1):33–38, 1996.

[32] A.C.E. Dahl, M. Chavent, and M.S.P. Sansom. Bendix: intuitive helix geometry analysis and abstraction. *Bioinformatics*, 28(16):2193–2194, 2012.

[33] Steve Scheiner, Tapas Kar, and J ayasree Pattanayak. Comparison of various types of hydrogen bonds involving aromatic amino acids. *J. Am. Chem. Soc.*, 124(44):13257–13264, oct 2002.

[34] G. E. Dobretsova, T. I. Syrejschikovaa, and N. V. Smolinaa. On mechanisms of fluorescence quenching by water. *Biophysics*, 59(2):183–188, jun 2014.

[35] Hitomi Yuki et al. Implementation of - interactions in molecular dynamics simulation. *Journal of Computational Chemistry*, 28(6):1091–1099, feb 2007.

[36] Masahiko Taniguchi and Jonathan S. Lindsey. Database of absorption and fluorescence spectra of >300 common compounds for use in photochemcad. *Photochemistry and Photobiology*, 94:290–327, jun 2018.

[37] Marta J. Krysmann et al. Self-assembly and hydrogelation of an amyloid peptide fragment. *Biochemistry*, 47:4597–4605, jan 2008.

[38] James T.Vivian and Patrik R.Callis. Mechanisms of tryptophan fluorescence shifts in proteins. *Biophysical Journal*, 80:2093–2109, may 2001.

[39] Hezy Cohen et al. Polarizability of g4-dna observed by electrostatic force microscopy measurements. 7(4):981–986, jan 2007.

[40] C. Gómez-Navarro et al. Contactless experiments on individual dna molecules show no evidence for molecular wire behavior. 99(13):8484–8487, jun 2002.

Appendix A

A.1 HPCL Sequence

```
        Pressure.LowerLimit =   0 [bar]
        Pressure.UpperLimit =   450 [bar]
        MaximumFlowRampDown =   9.998 [ml/minē]
        MaximumFlowRampUp =     1.000 [ml/minē]
        %A.Equate =     "0.1%TFA"
        %B.Equate =     "ACN"
        %C.Equate =     "%C"
        %D.Equate =     "99,9 Iso"
        Pump_Pressure.Step =    0.01 [s]
        Pump_Pressure.Average =         Off
        Data_Collection_Rate =  5.0 [Hz]
        ResponseTime =  2.000 [s]
        ;*****************************************************************
        ;* Definition of triggers for fraction collection starts here.
        ;*****************************************************************
        ; Definitions copied from template HPLC_1\FractionCollectionTemplate!
        Trigger FracStart               FracStartDetected
        AFC.Valve =             Collect
        Log AFC.TubePosition
        Log FractionCollection.TubePosition
        EndTrigger

        Trigger TubeChange              FracTubeChange
        AFC.Valve =             Drain
        AFC.TubePosition =      FractionCollection.TubePosition
        AFC.Valve =             Collect
        Log AFC.TubePosition
        Log FractionCollection.TubePosition
        EndTrigger

        Trigger FracEnd         FracEndDetected
        AFC.Valve =             Drain
        AFC.TubePosition =      FractionCollection.TubePosition
        Log AFC.TubePosition
        Log FractionCollection.TubePosition
        EndTrigger
        ;*****************************************************************
        ;* Definition of triggers for fraction collection ends here.
        ;*****************************************************************



        UV_VIS_1.Wavelength =   214.0 [nm]
        UV_VIS_1.Bandwidth =    4 [nm]
        UV_VIS_1.RefWavelength =        Off
        UV_VIS_1.RefBandwidth =         1 [nm]
        UV_VIS_2.Wavelength =   240.0 [nm]
        UV_VIS_2.Bandwidth =    4 [nm]
        UV_VIS_2.RefWavelength =        Off
        UV_VIS_2.RefBandwidth =         1 [nm]
        UV_VIS_3.Wavelength =   260.0 [nm]
        UV_VIS_3.Bandwidth =    10 [nm]
        UV_VIS_3.RefWavelength =        Off
        UV_VIS_3.RefBandwidth =         1 [nm]
        3DFIELD.RefWavelength =         Off
        3DFIELD.RefBandwidth =  1 [nm]
        3DFIELD.MinWavelength =         190.0 [nm]
        3DFIELD.MaxWavelength =         400.0 [nm]
        3DFIELD.BunchWidth =    1 [nm]



  0.000  Autozero
        Flow =  1.50[ml/min]
        %B =    5.0 [%]
        %C =    0.0 [%]
        %D =    0.0 [%]
        Wait    UV.Ready and Pump.Ready and PumpModule.Ready
```

```
        Inject
        Pump_Pressure.AcqOn
        CollectFractions =      No
        UV_VIS_1.AcqOn
        UV_VIS_2.AcqOn
        UV_VIS_3.AcqOn
        3Dfield.AcqOn
        Flow =  1.50[ml/min]
        %B =    5.0 [%]
        %C =    0.0 [%]
        %D =    0.0 [%]

 4.000  Flow =  1.50[ml/min]
        %B =    5.0 [%]
        %C =    0.0 [%]
        %D =    0.0 [%]
 60.000 Flow =  1.50[ml/min]
        %B =    80.0 [%]
        %C =    0.0 [%]
        %D =    0.0 [%]

 63.500 Flow =  1.50[ml/min]
        %B =    80.0 [%]
        %C =    0.0 [%]
        %D =    0.0 [%]

 66.000 Flow =  1.50[ml/min]
        %B =    5.0 [%]
        %C =    0.0 [%]
        %D =    0.0 [%]

 66.000
        Pump_Pressure.AcqOff

 66.000 UV_VIS_1.AcqOff
        UV_VIS_2.AcqOff
        UV_VIS_3.AcqOff
        3Dfield.AcqOff

 96.000 End
```

Appendix B

B.1 GFDFDFD Synthesis Worklist

Worklist for Synthesis C:\Documents and Settings\User\Desktop\AACJAL\GFDFDFD\GFDFDFD.syn

Thursday, January 31, 2019 13:34:48 Version 1.4.4.31

Sequence: Gly Phe Asp Phe Asp Phe Asp

N-terminal de-protected, C-terminal acid

Monoisotopic molecular weight: 861.318

Theoretical yield: 0.250 millimole

Time for synthesis: 17 Hours 53 Minutes

Maximum reactor contents: 6.0 ml, use 40 ml reactor

PV not used

Maximum amino acid vial contents: 5.0 ml, use 15 ml vials

Multitask mode: Just in time

Simple wizard used: Single coupling, Swell, Final deprotection, Final DCM wash

UV monitoring used

Resin data:

Substitution: 0.590 mmoles/gram, Quantity: 0.424 grams, Preloaded with Asp, Deprotect before first coupling

Fluid Allocation

Bottle	Fluid	Molarity	millilitres
External 1	DMF	na	2178.0
External 2		na	0.0
External 3		na	0.0
Internal 4		na	0.0
Internal 5		na	0.0
Internal 6	DCM	na	21.0
Internal 7	DIEA 1.0 M	1.00	27.0
Internal 8	HBTU 0.48 M	0.48	27.0
Internal 9	Piperidine 25%	na	175.0

(Add allowance for fluid to cover inlet filters in bottles)

When UV monitoring is used fluid usage is calculated for maximum deprotections

Fit vial 0 with new cap for initial probe wash

Sequence Data

Carousel	Vial	Seq	Protected amino acid		Quantity	Protocol
		0	C terminal			initial
1	1	1	Asp attached to resin	No vial	0 mg	-
1	2	2	Fmoc-Phe-OH	powder	484 mg	standard cycle
1	3	3	Fmoc-Asp(OtBu)-OH	powder	514 mg	standard cycle
1	4	4	Fmoc-Phe-OH	powder	484 mg	standard cycle
1	5	5	Fmoc-Asp(OtBu)-OH	powder	514 mg	standard cycle
1	6	6	Fmoc-Phe-OH	powder	484 mg	standard cycle
1	7	7	Fmoc-Gly-OH	powder	372 mg	standard cycle
		8	N terminal			final

Consolidated amino acid vial data

Protected amino acid		Quantity	No. of vials	Carousel 1	Carousel 2
Asp attached to resin	powder	0 mg	1	1	
Fmoc-Phe-OH	powder	484 mg	3	2,4,6	
Fmoc-Asp(OtBu)-OH	powder	514 mg	2	3,5	
Fmoc-Gly-OH	powder	372 mg	1	7	

B.2 GFKFKFK Synthesis Worklist

Worklist for Synthesis C:\Documents and Settings\User\Desktop\AACJAL\GFDFDFD\GFKFKFK.syn

Friday, March 22, 2019 14:01:04 Version 1.4.4.31

Sequence: Gly Phe Lys Phe Lys Phe Lys

N-terminal de-protected, C-terminal acid

Monoisotopic molecular weight: 900.522

Theoretical yield: 0.250 millimole

Time for synthesis: 20 Hours 28 Minutes

Maximum reactor contents: 6.0 ml, use 40 ml reactor

PV not used

Maximum amino acid vial contents: 5.0 ml, use 15 ml vials

Multitask mode: Just in time

Simple wizard used: Single coupling, Swell, Final deprotection, Final DCM wash

UV monitoring used

Resin data:

Substitution: 0.550 mmoles/gram, Quantity: 0.455 grams, Deprotect before first coupling

Fluid Allocation

Bottle	Fluid	Molarity	millilitres
External 1	DMF	na	2510.0
External 2		na	0.0
External 3		na	0.0
Internal 4		na	0.0
Internal 5		na	0.0
Internal 6	DCM	na	21.0
Internal 7	DIEA 1.0 M	1.00	31.5
Internal 8	HBTU 0.48 M	0.48	31.5
Internal 9	Piperidine 25%	na	200.0

(Add allowance for fluid to cover inlet filters in bottles)

When UV monitoring is used fluid usage is calculated for maximum deprotections

Fit vial 0 with new cap for initial probe wash

Sequence Data

Carousel	Vial	Seq	Protected amino acid		Quantity	Protocol
		0	C terminal			initial
1	1	1	Fmoc-Lys(Boc)-OH	powder	586 mg	standard cycle
1	2	2	Fmoc-Phe-OH	powder	484 mg	standard cycle
1	3	3	Fmoc-Lys(Boc)-OH	powder	586 mg	standard cycle
1	4	4	Fmoc-Phe-OH	powder	484 mg	standard cycle
1	5	5	Fmoc-Lys(Boc)-OH	powder	586 mg	standard cycle
1	6	6	Fmoc-Phe-OH	powder	484 mg	standard cycle
1	7	7	Fmoc-Gly-OH	powder	372 mg	standard cycle
		8	N terminal			final

Consolidated amino acid vial data

Protected amino acid		Quantity	No. of vials	Carousel 1	Carousel 2
Fmoc-Lys(Boc)-OH	powder	586 mg	3	1,3,5	
Fmoc-Phe-OH	powder	484 mg	3	2,4,6	
Fmoc-Gly-OH	powder	372 mg	1	7	

B.3 Modified GFDFDFD Synthesis Worklist

Worklist for Synthesis C:\Documents and Settings\User\Desktop\AACJAL\Modified\GGFDFDFD.syn

Friday, April 12, 2019 22:35:46 Version 1.4.4.31

Sequence: Gly Gly Phe Asp Phe Asp Phe Asp

N-terminal de-protected, C-terminal acid

Monoisotopic molecular weight: 918.340

Theoretical yield: 0.250 millimole

Time for synthesis: 20 Hours 28 Minutes

Maximum reactor contents: 6.0 ml, use 40 ml reactor

PV not used

Maximum amino acid vial contents: 5.0 ml, use 15 ml vials

Multitask mode: Just in time

Simple wizard used: Single coupling, Swell, Final deprotection, Final DCM wash

UV monitoring used

Resin data:

Substitution: 0.590 mmoles/gram, Quantity: 0.424 grams, Preloaded with Asp, Deprotect before first coupling

Fluid Allocation

Bottle	Fluid	Molarity	millilitres
External 1	DMF	na	2510.0
External 2		na	0.0
External 3		na	0.0
Internal 4		na	0.0
Internal 5		na	0.0
Internal 6	DCM	na	21.0
Internal 7	DIEA 1.0 M	1.00	31.5
Internal 8	HBTU 0.48 M	0.48	31.5
Internal 9	Piperidine 25%	na	200.0

(Add allowance for fluid to cover inlet filters in bottles)

When UV monitoring is used fluid usage is calculated for maximum deprotections

Fit vial 0 with new cap for initial probe wash

Sequence Data

Carousel	Vial	Seq	Protected amino acid		Quantity	Protocol
		0	C terminal			initial
1	1	1	Asp attached to resin	No vial	0 mg	-
1	2	2	Fmoc-Phe-OH	powder	484 mg	standard cycle
1	3	3	Fmoc-Asp(OtBu)-OH	powder	514 mg	standard cycle
1	4	4	Fmoc-Phe-OH	powder	484 mg	standard cycle
1	5	5	Fmoc-Asp(OtBu)-OH	powder	514 mg	standard cycle
1	6	6	Fmoc-Phe-OH	powder	484 mg	standard cycle
1	7	7	Fmoc-Gly-OH	powder	372 mg	standard cycle
1	8	8	Fmoc-Gly-OH	powder	372 mg	standard cycle
		9	N terminal			final

Consolidated amino acid vial data

Protected amino acid		Quantity	No. of vials	Carousel 1	Carousel 2
Asp attached to resin	powder	0 mg	1	1	
Fmoc-Phe-OH	powder	484 mg	3	2,4,6	
Fmoc-Asp(OtBu)-OH	powder	514 mg	2	3,5	
Fmoc-Gly-OH	powder	372 mg	2	7,8	

B.4 Modified GFKFKFK Synthesis Worklist

Worklist for Synthesis C:\Documents and Settings\User\Desktop\AACJAL\Modified\GGFKFKFK.syn

Wednesday, March 27, 2019 12:38:32 Version 1.4.4.31

Sequence: Gly Gly Phe Lys Phe Lys Phe Lys

N-terminal de-protected, C-terminal acid

Monoisotopic molecular weight: 957.544

Theoretical yield: 0.250 millimole

Time for synthesis: 23 Hours 3 Minutes

Maximum reactor contents: 6.0 ml, use 40 ml reactor

PV not used

Maximum amino acid vial contents: 5.0 ml, use 15 ml vials

Multitask mode: Just in time

Simple wizard used: Single coupling, Swell, Final deprotection, Final DCM wash

UV monitoring used

Resin data:

Substitution: 0.550 mmoles/gram, Quantity: 0.455 grams, Deprotect before first coupling

Fluid Allocation

Bottle	Fluid	Molarity	millilitres
External 1	DMF	na	2842.0
External 2		na	0.0
External 3		na	0.0
Internal 4		na	0.0
Internal 5		na	0.0
Internal 6	DCM	na	21.0
Internal 7	DIEA 1.0 M	1.00	36.0
Internal 8	HBTU 0.48 M	0.48	36.0
Internal 9	Piperidine 25%	na	225.0

(Add allowance for fluid to cover inlet filters in bottles)

When UV monitoring is used fluid usage is calculated for maximum deprotections

Fit vial 0 with new cap for initial probe wash

Sequence Data

Carousel	Vial	Seq	Protected amino acid		Quantity	Protocol
		0	C terminal			initial
1	1	1	Fmoc-Lys(Boc)-OH	powder	586 mg	standard cycle
1	2	2	Fmoc-Phe-OH	powder	484 mg	standard cycle
1	3	3	Fmoc-Lys(Boc)-OH	powder	586 mg	standard cycle
1	4	4	Fmoc-Phe-OH	powder	484 mg	standard cycle
1	5	5	Fmoc-Lys(Boc)-OH	powder	586 mg	standard cycle
1	6	6	Fmoc-Phe-OH	powder	484 mg	standard cycle
1	7	7	Fmoc-Gly-OH	powder	372 mg	standard cycle
1	8	8	Fmoc-Gly-OH	powder	372 mg	standard cycle
		9	N terminal			final

Consolidated amino acid vial data

Protected amino acid		Quantity	No. of vials	Carousel 1	Carousel 2
Fmoc-Lys(Boc)-OH	powder	586 mg	3	1,3,5	
Fmoc-Phe-OH	powder	484 mg	3	2,4,6	
Fmoc-Gly-OH	powder	372 mg	2	7,8	

Appendix C

C.1 MD Parameters

```
; VARIOUS PREPROCESSING OPTIONS =
title = Yo
cpp = /usr/bin/cpp
include =
define =

; RUN CONTROL PARAMETERS =
integrator = md ; leap-frog algorithm for doing molecular dynamics simulations (= steep
for energy minimisation)
tinit = 0.0 ; start time in ps
dt = 0.020 ; time step in ps (should be between 20 - 30 fs for polarisable water)
nsteps = 10000000 ; number of steps 0.02*10000000 ps = 200000 ps = 200 ns (10000
steps for minimisation)

; OUTPUT CONTROL OPTIONS =
; Output frequency for coords (x), velocities (v) and forces (f) =
nstxout = 5000
nstvout = 5000
nstfout = 0
; Output frequency for energies to log file and energy file =
nstlog = 1000
nstenergy = 100
; Output frequency and precision for xtc file =
nstxtcout = 5000
xtc_precision = 100
xtc-grps =
energygrps = PW

; NEIGHBORSEARCHING PARAMETERS =
cutoff-scheme = Verlet
nstlist = 10 ; nblist update frequency
ns_type = grid ; ns algorithm
pbc = xyz ; periodic boundary conditions
rlist = 1.2 ; nblist cut-off

; OPTIONS FOR ELECTROSTATICS AND VDW =
; Method for doing electrostatics =
coulombtype = PME ; method for doing electrostatics (particle mesh Ewald)
rcoulomb = 1.2 ; coulomb cut-off
rcoulomb_switch = 0.0
epsilon_r = 2.5 ; Dielectric constant
vdw_type = PME ; method for doing van der Waals
rvdw = 1.2 ; van der Waals cut-off
DispCorr = No ; No long range disoersion corrections for energy and pressure
fourierspacing = 0.12 ; Spacing for the PME grid
; FFT grid size, when a value is 0 fourierspacing will be used =
fourier_nx = 10
fourier_ny = 10
fourier_nz = 10

; EWALD/PME/PPPM parameters =
pme_order = 4
ewald_rtol = 1e-05
epsilon_surface = 0
optimize_fft = no

; OPTIONS FOR WEAK COUPLING ALGORITHMS =
tcoupl = v-rescale ; temperature coupling algorithm
; Temperature coupling =
tc-grps = Protein Non-Protein ; two coupling groups - more accurate
tau_t = 0.3 0.3 ; time constant, in ps
ref_t = 300 300 ; reference temperature in K (323 in experiments at higher temp)
; Pressure coupling =
Pcoupl = Berendsen ; pressure coupling algorithm
Pcoupltype = isotropic ; pressure coupling type
; isotropic coupling parameters =
tau_p = 2.0 ; time constant in ps
compressibility = 3e-5 ; compressibility in 1/bar
ref_p = 1.0 ; reference pressure in bar
```

```
; GENERATE VELOCITIES FOR STARTUP RUN =
gen_vel = yes ; initial velocities taken from structure file (should be yes to generate
velocities from seed)
gen_temp = 300 ; temperature to generate in K (323 in experiments at higher temp)
gen_seed = -1 ; generate a random seed

; OPTIONS FOR BONDS =
constraints = none
constraint_algorithm = Lincs ; constraint algorithm
unconstrained_start = no ; no unconstrained start
shake_tol = 0.0001 ; relative tolerance of shake
; Highest order in the expansion of the constraint coupling matrix =
lincs_order = 4
lincs_warnangle = 90 ; Lincs will write a warning if bond rotates more than 90 degrees in a
single step
; for polarizable water sometimes Lincs warnings appear for no apparent reason
; with a warnangle of 90 this is largely avoided
```

Appendix D

D.1 Other AFM Images

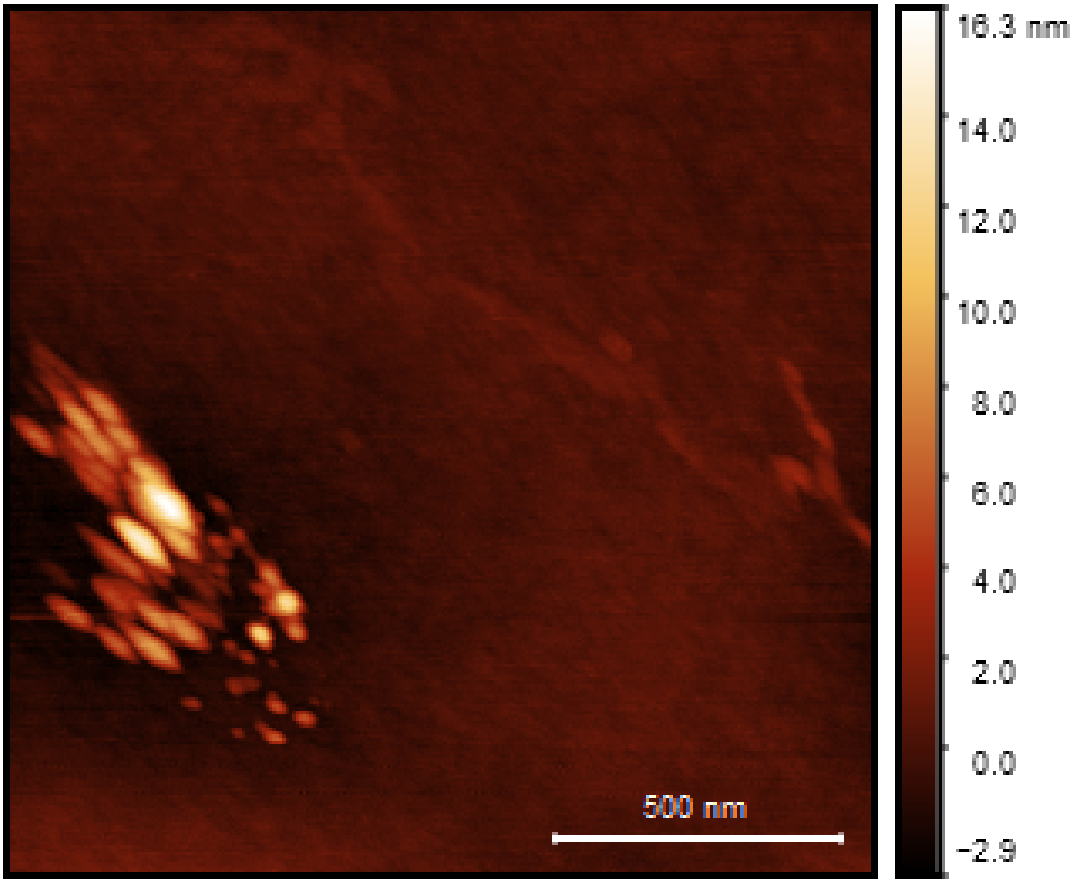

Figure D.1: AFM measurement of Ferrocene modified GFDFDFD.

Appendix E

E.1 Other ESFM Images

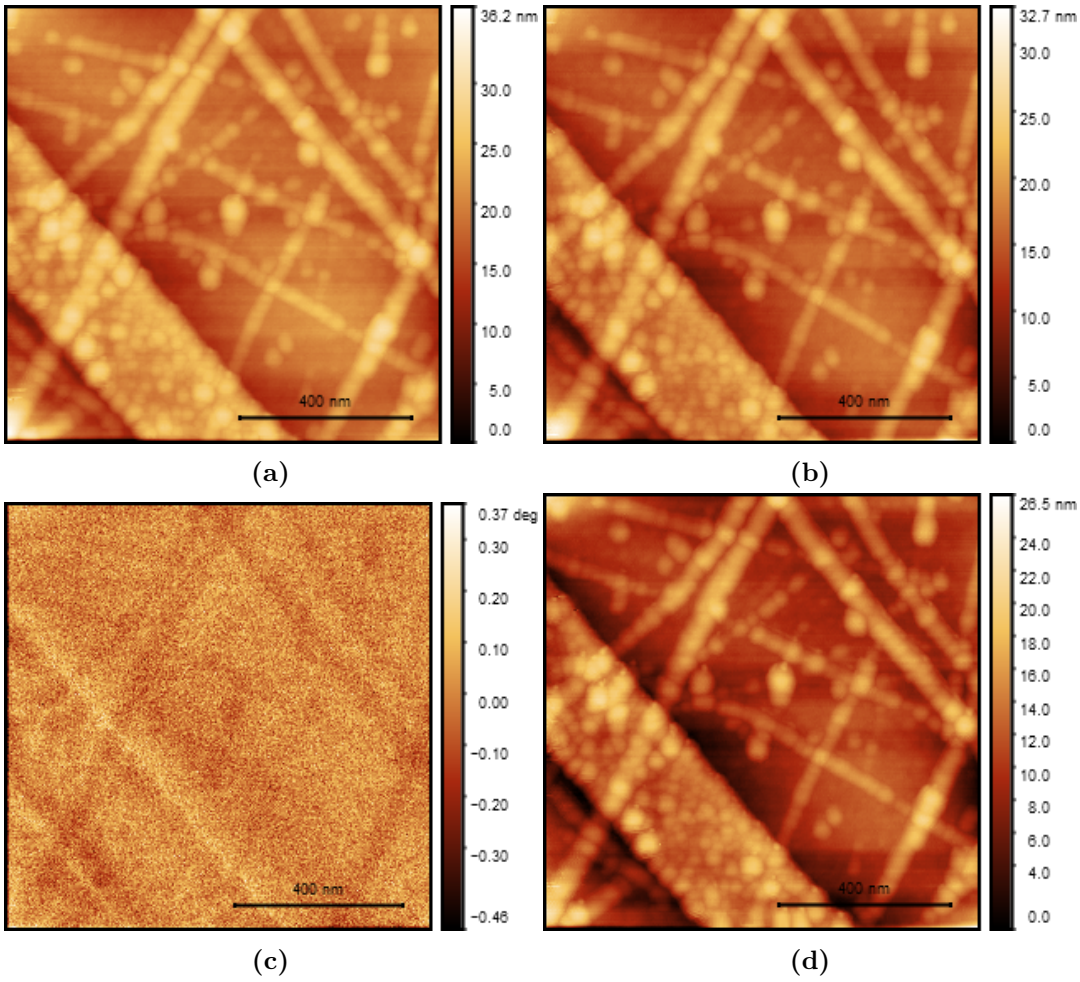

Figure E.1: a) ESFM height measurement of GFDFDFD at 20nm lift, -3 V. b) ESFM height measurement of GFDFDFD at 20nm lift, 3 V. c) ESFM Phase measurement of GFDFDFD at 20nm lift, 3 V. d) ESFM height measurement of GFDFDFD at 30nm lift, -3 V.

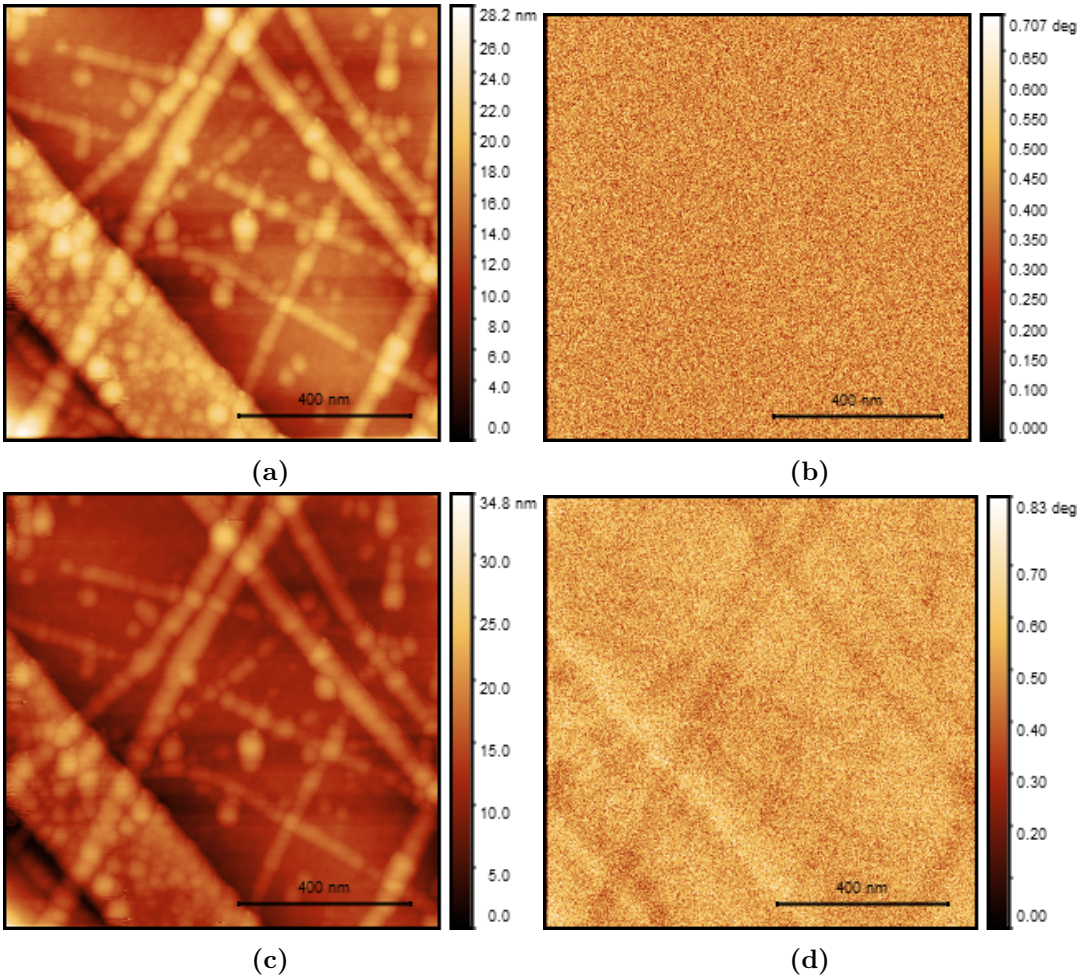

Figure E.2: a) ESFM height measurement of GFDFDFD at 30nm lift, 0 V. b) ESFM Phase measurement of GFDFDFD at 30nm lift, 0 V. c) ESFM height measurement of GFDFDFD at 30nm lift, 3 V. d) ESFM Phase measurement of GFDFDFD at 30nm lift, 3 V.

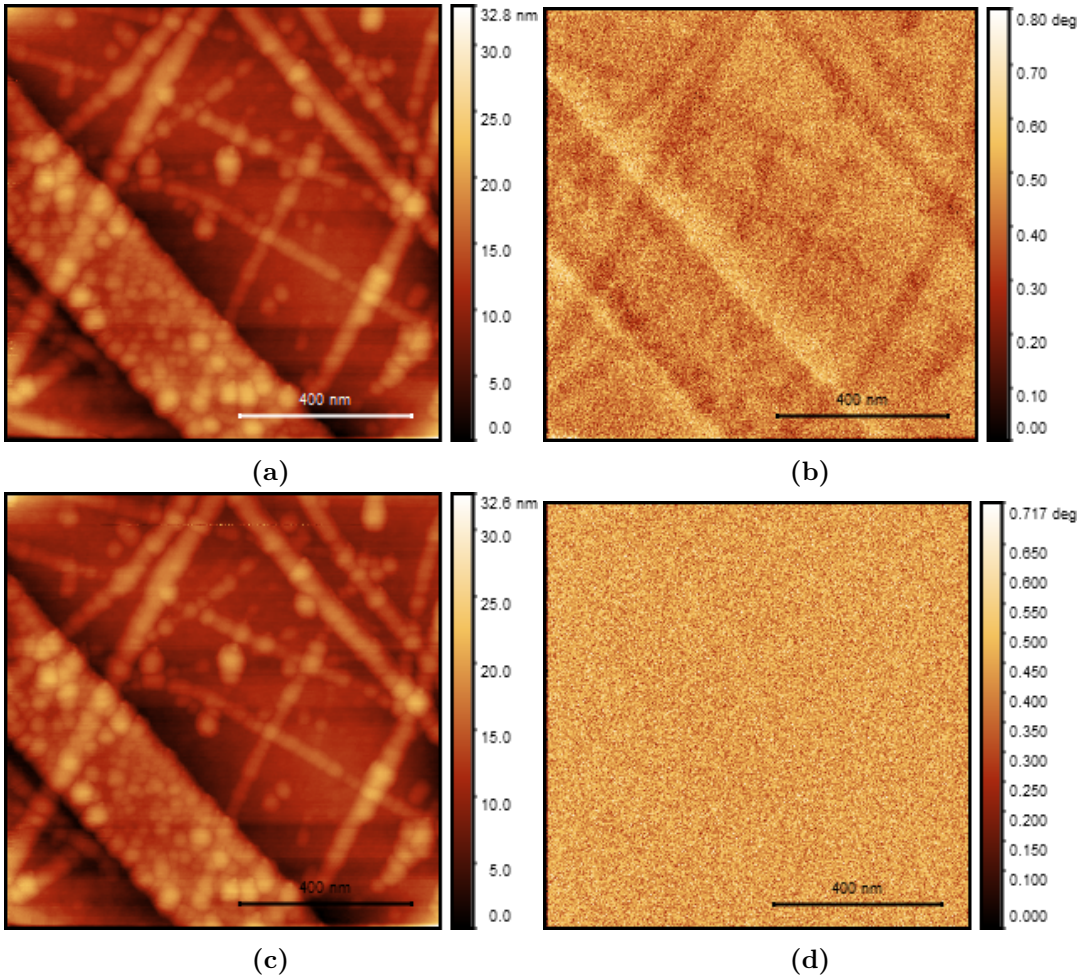

Figure E.3: a) ESFM height measurement of GFDFDFD at 40nm lift, -3 V. b) ESFM Phase measurement of GFDFDFD at 40nm lift, -3 V. c) ESFM height measurement of GFDFDFD at 40nm lift, 0 V. d) ESFM Phase measurement of GFDFDFD at 30nm lift, 0 V.

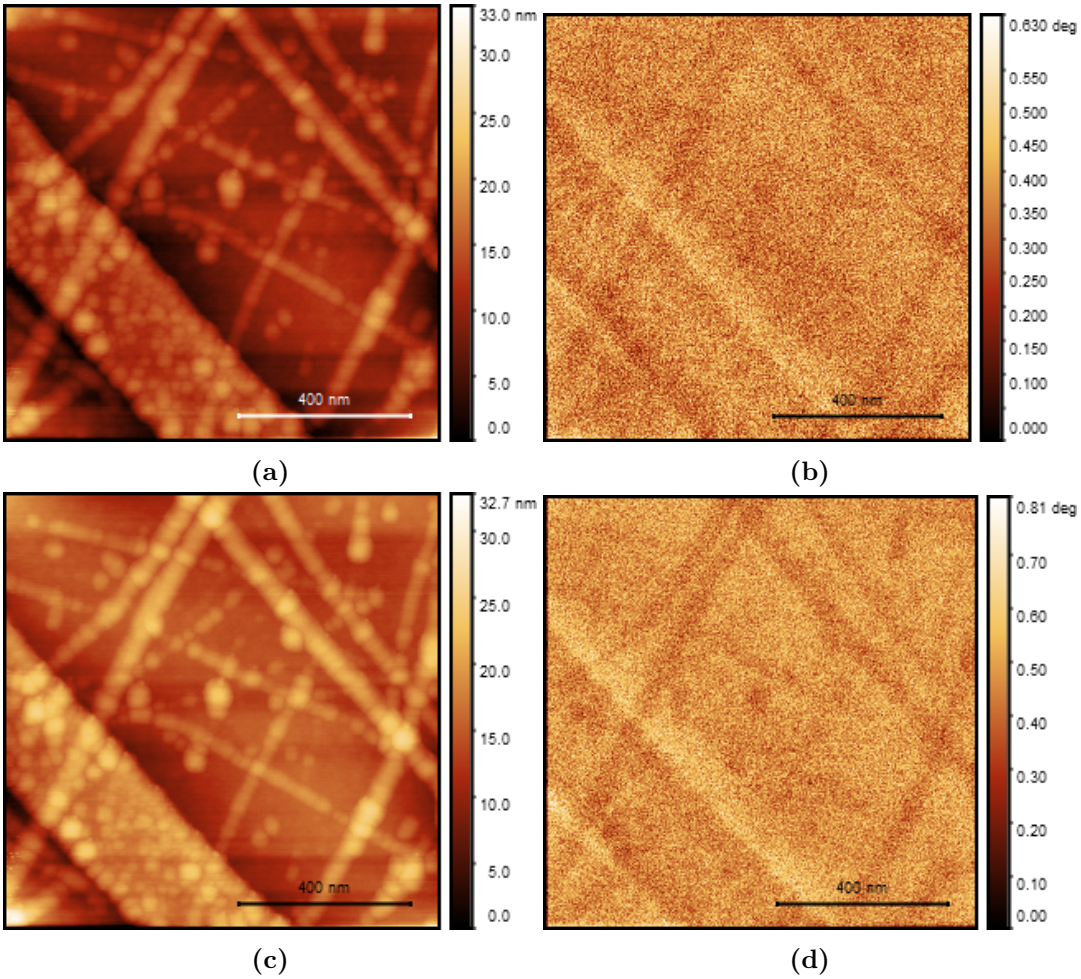

Figure E.4: a) ESFM height measurement of GFDFDFD at 40nm lift, 3 V. b) ESFM Phase measurement of GFDFDFD at 40nm lift, 3 V. c) ESFM height measurement of GFDFDFD at 50nm lift, -3 V. d) ESFM Phase measurement of GFDFDFD at 50nm lift, -3 V.

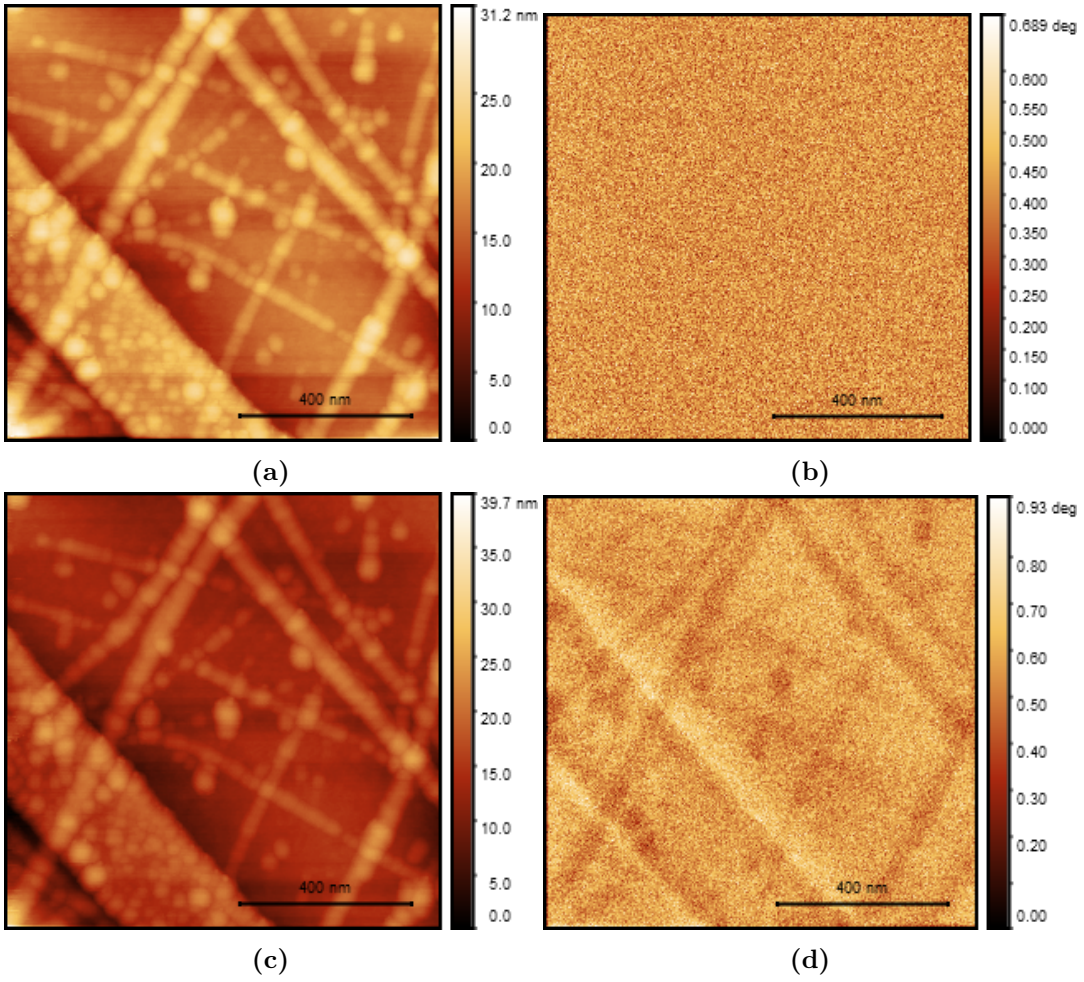

Figure E.5: a) ESFM height measurement of GFDFDFD at 50nm lift, 0 V. b) ESFM Phase measurement of GFDFDFD at 50nm lift, 0 V. c) ESFM height measurement of GFDFDFD at 50nm lift, 3 V. d) ESFM Phase measurement of GFDFDFD at 30nm lift, 3 V.

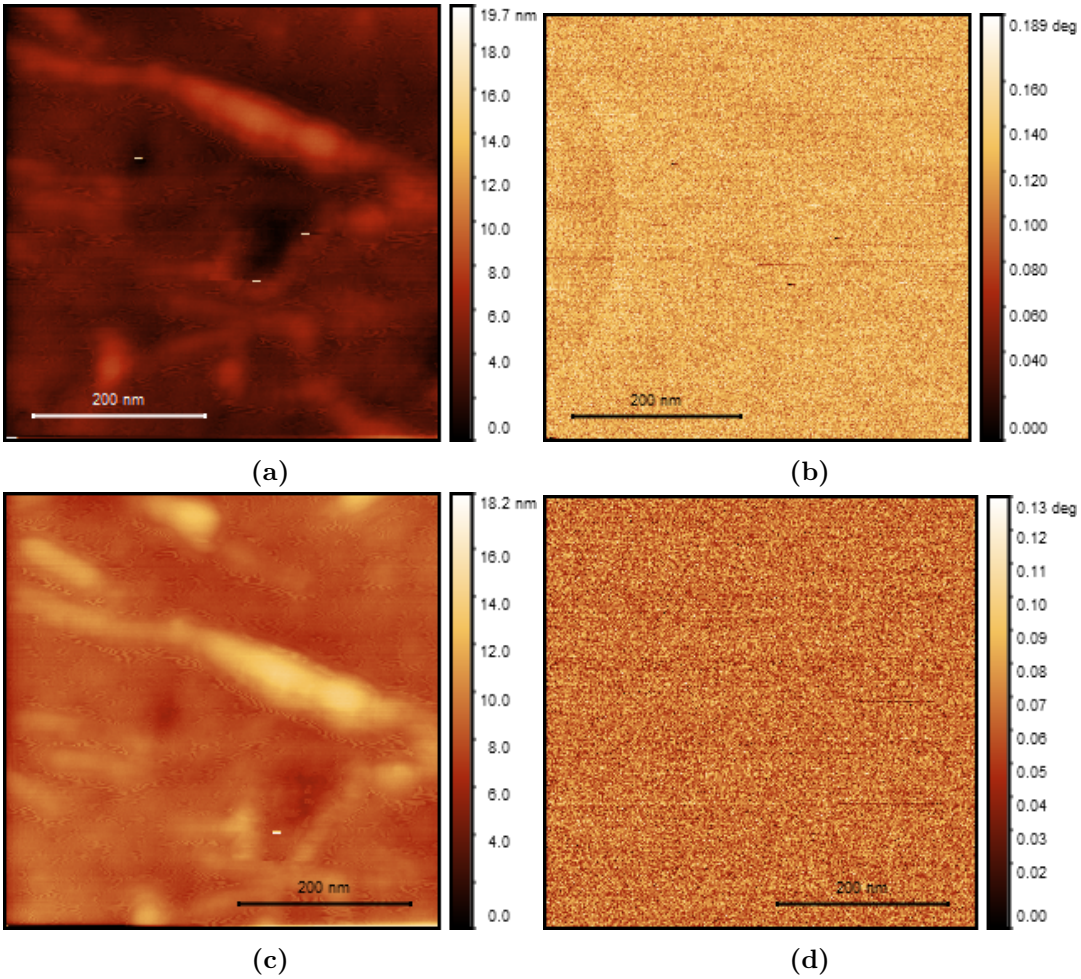

Figure E.6: a) ESFM height measurement of Mixed GFDFDFD and GFKFKFK at 20nm lift, -3 V. b) ESFM Phase measurement of Mixed GFDFDFD and GFKFKFK at 20nm lift, -3 V. c) ESFM height measurement of Mixed GFDFDFD and GFKFKFK at 20nm lift, 0 V. d) ESFM Phase measurement of Mixed GFDFDFD and GFKFKFK at 20nm lift, 0 V.

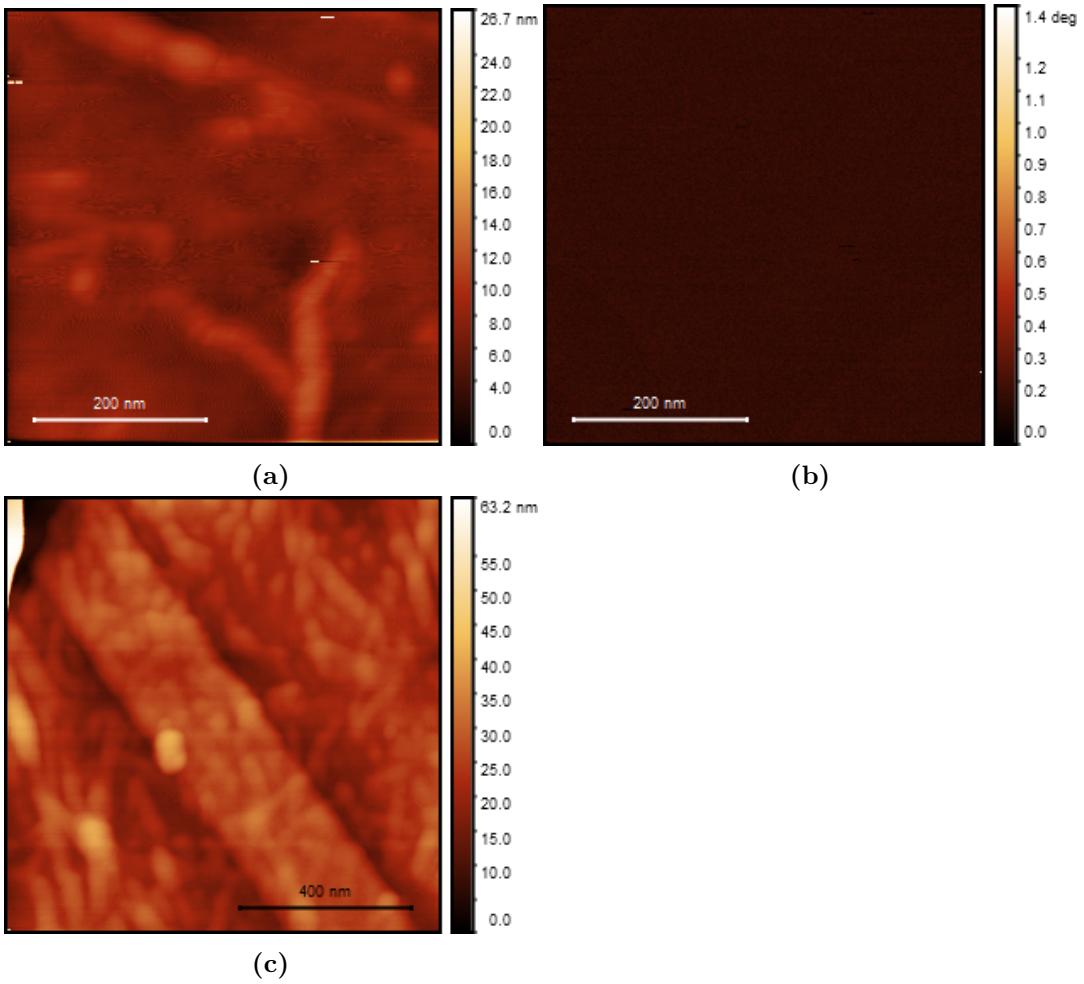

Figure E.7: a) ESFM height measurement of Mixed GFDFDFD and GFKFKFK at 20nm lift, 3 V. b) ESFM Phase measurement of Mixed GFDFDFD and GFKFKFK at 20nm lift, 3 V. c) ESFM height measurement of Mixed GFDFDFD and GFKFKFK Control at 20nm lift, 3 V.